A Study of the Optical and Electrical Properties of Conjugated Polymers for Use in Optoelectronic Applications

Thesis submitted in accordance with the requirements of
the University of Liverpool for the degree of Master in Philosophy
by
Sheng Lin

August 2014

Acknowledgement

I would like to express my thanks to my supervisor Dr M.Raja for her encouragement and guidance throughout the course of my work with the Organic Electronics Group.

I would also like thank Prof.William.Eccleston for his guidance on the theory and his tutorial. The past and present members of the Organic Electronics Group have made my study pleasant and enjoyable. I would like to thank all the group; namely Dr.D. Donaghy, Dr.R.J.Myers for their support and teaching me the skills required in the clean room.

Finally, I also wish to thank my family and friends, especially my parents, for their encouragement and support which has enabled me to complete this work.

Abstract

In this thesis, the characteristics of conjugated polymer based devices such as the Schottky barrier diode and thin film transistor are studied. A brief introduction of the charge transport mechanism and models is presented. In addition, a demonstration of dependency of mobility on the carrier concentration in disordered organic material explains the nature of charge transport in disordered material.

Various Schottky barrier diode structures have been explored. The electrical characteristics of the ring structure Schottky barrier diode has been studied in detail. Several parameters, such as doping density N_A, effective mobility μ, series and shunt resistances, are extracted from device current-voltage and capacitance-voltage characteristics. The air and bias stability of the ring structure Schottky diode have been investigated.

P3HT thin film transistors were fabricated with silicon dioxide as the dielectric layer. The output and transfer characteristics of the P3HT thin film transistor have been studied.

A vertical structure single layer solar cell was thought to have low efficiency. The P3HT single layer solar cell with ring structure was investigated. Compared to the P3HT vertical single layer solar cell, the efficiency of the energy conversion is higher. And the potential of using ring P3HT Schottky diode and P3HT thin-film transistor as photo detector has been explored. The light sensitivity of ring Schottky P3HT photo detector and P3Ht phototransistor have been evaluated.

All the devices were solution processed. The effect of changing the polymer solution concentration on device performance, stability and light sensitivity were investigated.

Contents

List of Figures

List of Tables

Chapter 1

Introduction

A brief introduction to the subject of device based on conjugated polymer is discussed in this chapter. The organisation of the thesis is also included in this chapter.

1.1 Introduction to conjugated polymers

Organic materials play an important role in industry, agriculture and even our daily life. In 1976, three scientists, H.Shirakawa, A.G.MacDiarmid and A.J.Heeger (Nobel prize in Chemistry, 2000) discovered conductive polymer, and reported over 7 orders of magnitude increase in conductivity of polyacetylene after doping with iodine.[1] The potential of organic materials in the field of electronics has triggered intensive research in material science field in order to improve their electrical characteristics and also in engineering field to develop devices using such materials as active layers. Organic electronics, which refers to those devices using organic material as the semiconductor layers, has been a popular research area for over 30 years. Organic electronic devices, such as organic light-emitting diodes(OLEDs)[2][3], organic field effect transistors (OFETs), and organic memory devices[4], have attracted considerable attention. Amongst them, OLEDs have been successfully commercialized[5]. Based on their material properties, the organic semiconductor can be divided into two main categories, namely small molecule and long molecule conjugated materials also known as polymer.

The polymer base devices are normally solution based, which provides advantages such as low processing costs and flexibility. However, the main drawback from such material includes the low mobility of charge carriers. Due to such attributes, the area of organic electronics that has matured is in the optoelectronic field.

Photovoltaic (PV) technology generates electricity directly from sunlight, which is a potential solution to the energy crisis and environment problem caused by fossil fuel. The research in this field is aimed at reducing the fabrication cost and power consumption during large scale manufacturing. The polymer semiconductors show great promise owing to low-temperature and solution processing.

Organic light detectors convert light into an electrical signal. Some interesting advantages of this type of device are ease of integration with other optical and electrical components, flexibility and large area.

The research work presented in this thesis is mainly concerned with fabrication and characterization of device with Poly(3-hexylthiophene) (P3HT). The aim is to investigate the interfaces between the polymer/metal and polymer/dielectric, and the optical and electrical characteristics of the devices based on P3HT. In addition, the potential of using such material in organic photovoltaic and light detector is explored using different device configurations.

1.2 Thesis organization

- Chapter 2 gives an brief introduction to conjugated polymer material and its development and background in optoelectronic field. The focus is the important charge transport models proposed for description of organic semiconductors.

- Chapter 3 covers the fabrication and characterization of organic thin film transistors. The bottom gate structure is used in the device fabrication. The output and transfer characteristics of devices are characterized and analysed. The experimental results are validated using the disordered transistor model. The effect of varying the concentration of P3HT on transistor characteristics/performance is also presented here.

- Chapter 4 focuses on the Schottky barrier diode, exploring three different structures such as vertical, lateral, and ring. The electrical properties of the Schottky barrier diode are studied in detail. The current-voltage characteristics are analysed using different approaches. The parameters extracted such as ideality factor, barrier height, series resistance and shunt resistance are compared using different approaches. In addition, the capacitance-voltage characteristics are also analysed with respect to changes in the frequency. The parameters extracted from the reverse characteristics include the dopant concentration and built-in potential.

- Chapter 5 is primarily concerned with the optical characteristics of a polymer based device such as organic Schottky diode and organic thin film transistor. The efficiency of a lateral single layer solar cell is evaluated. The responsivity of the ring structure diode for use as a photo diode is investigated with the aid of the current-voltage characteristics obtained under dark and illumination conditions. The photocurrent generation mechanism is also discussed briefly. Finally the air-instability of the ring structure Schottky diode is also investigated with varying concentration of P3HT.

- Chapter 6 summarises all the results presented in the thesis, and also includes some future work recommendations.

1.3 Contributions

This thesis consists of the following contributions:

- P3HT based vertical Schottky diodes were fabricated with various materials (such as silver, gold, indium tin oxide) as back contact. The current-voltage characteristics of gold, palladium and indium tin oxide prove that those materials can be used as the ohmic contact for a P3HT diode since their work functions are close to the highest occupied molecular orbital (HOMO) level of P3HT. The work function of silver is low enough to form an effective potential barrier at the silver/P3HT interface, and it can not be used as ohmic contact.

- A lateral structured Schottky barrier device was fabricated, and the gap size between the contacts was examined using Atomic Force Microscopy (AFM). Subsequently, due to performance issues, a variant of the lateral structure was proposed, referred in this

thesis as the ring structured Schottky barrier diode. The fabrication process for such an alternative structure is much simpler, with stable performances.

- The effect of alternating the P3HT/xylene solution concentration on Schottky diode electrical, optical properties and stability of performance has been demonstrated.
- Several methods have been used to obtain the important parameters of the organic Schottky diode such as ideality factor η, potential barrier ϕ_b, and series resistance R_s.
- The efficiency of the single layer ring structure P3HT solar cell was investigated. The best obtained efficiency is superior compared to those of a vertical single layer OPV device.
- The performance of the single layer ring diode using P3HT was evaluated. The detectivity and responsivity of the photodiode to the visible light was extracted quantitatively. Comparing to some recent literature results, these results are similar. The air instability of the ring structure diode is also studied with changes in concentration of the P3HT/xylene solution.
- Organic thin film transistors using P3HT with BGBC (bottom gate bottom source/drain contact) and BGTC (bottom gate and top source/drain contact) structures were fabricated and characterized. The effect of varying the P3HT/xylene concentration is also presented. Key parameters such as effective field-effect mobility, threshold voltage and sub-threshold slope are extracted. The parameters are subsequently used in validating the experimental data with the organic transistor model.

References

[1] H. Shirakawa, E. J. Louis, A. G. MacDiarmid, C. K. Chiang and A. J. Heeger, "Synthesis of electrically conducting organic polymers: halogen derivatives of polyacetylene, (CH)x," Journal of the Chemical Society, Chemical Communications, no. 16, pp. 578-580, 1977.

[2] J. H. Burroughes, D. D. C. Bradley, A. R. Brown, R. N. Marks, K. Mackay, R. H. Friend, P. L. Burns, A. B. Holmes, "Light-emitting diodes based on conjugated polymers," Nature, vol. 347, pp. 539-541, 1990.

[3] A. C. Grimsdale, K. L. Chan, R. E. Martin, P. G. Jokisz , A. B. Holmes, "Synthesis of light-emitting conjugated polymers for applications in electroluminescent devices," Chemical Reviews, vol. 109, pp. 897-1091, 2009.

[4] S. Mller, C. Perlov, W. Jackson, C. Taussig, S. R. Forrest, "A polymer/semiconductor write-once read-many-times memory," Nature, vol. 426, pp. 166-169, 2003.

[5] L. Dou, J. You, Z. Hong, Z. Xu, G. Li, R. A. Street, and Y. Yang, "25th Anniversary Article: A Decade of Organic/Polymeric Photovoltaic Research," Advanced Materials, vol. 25, no. 46, pp. 6642-6671, 2013.

Chapter 2

Review of conducting polymers

Organic π-conjugated polymer is an emerging material due to the potential to realise large area and flexible optoelectronic devices using cost effective deposition methods such as printing, spraying and spin-coating[1]. The charge transport mechanisms and definition of the distribution function and density of states models are introduced. The dependency of mobility on the carrier concentration is also demonstrated. Finally, the applications of polymer devices and their developments are covered.

2.1 Introduction

Devices based on organic semiconductors are already widely commercialized. For display and lighting applications they are employed as light emitting diodes or transistors, and they compete with conventional solar cell for renewable energy application. As a result, interest in the science behind this novel class of materials has risen among researchers. For instance, the optoelectronic properties of organic semiconductors differ from those of conventional semiconductors in many aspects. A core problem to improve the device performance is the understanding of the mechanisms related to charge transport.

2.2 Distribution function for occupancy of the carriers and models for the density of states

The probability of charge carriers occupying an empty state in a certain system can be described in terms of the probability distribution function. The Fermi Dirac (FD) statistics, in general, describes the relationship between the probability of occupancy of carriers on the energy states and the energy. The FD distribution is as given below:

$$f(E) = \frac{1}{1 + exp(\frac{E-E_F}{k_B T})} \tag{2.1}$$

Here, T is the absolute temperature, k_B is the Boltzmann constant, and E_F is the energy level, known as the Fermi level, where the probability of the states being occupied by carriers are halved. In most cases, this relationship between the probability function and energy levels is approximated in the form of the Maxwell Boltzmann distribution given as:

$$f(E) = \begin{cases} exp(-\frac{E-E_F}{k_B T}), & if \quad E > E_F \\ 1 & if \quad E \leq E_F \end{cases} \tag{2.2}$$

where E is the energy of the states and E_F is the Fermi level of the semiconductor.

In organic materials, the HOMO (highest occupied molecule orbital) and LUMO (lowest unoccupied molecular orbital) are the two significant energy levels. In order to understand the physical meaning behind the terms HOMO and LUMO, it should be clear that polymer materials are made of molecule subunits. Organic semiconductors are carbon-hydrogen (CH) molecules with a backbone of carbon atoms. The strong bonds that form the molecular backbone arise from sp^2 hybridized atomic orbitals of adjacent carbon atoms that overlap, yielding a bonding and antibonding molecular orbitals, also known as σ and σ^* orbitals respectively. The remaining atomic P_z orbitals overlap to a lesser degree, so that the resulting molecular π and π^* orbitals are less binding or antibinding, thus forming the frontier orbitals of the molecule. In the ground states, all the bonding orbitals are fully occupied, the HOMO,

is filled with two electrons, which are from LUMO. For instance, when a molecule absorbs a photon, an electron will be promoted from the HOMO to LUMO.

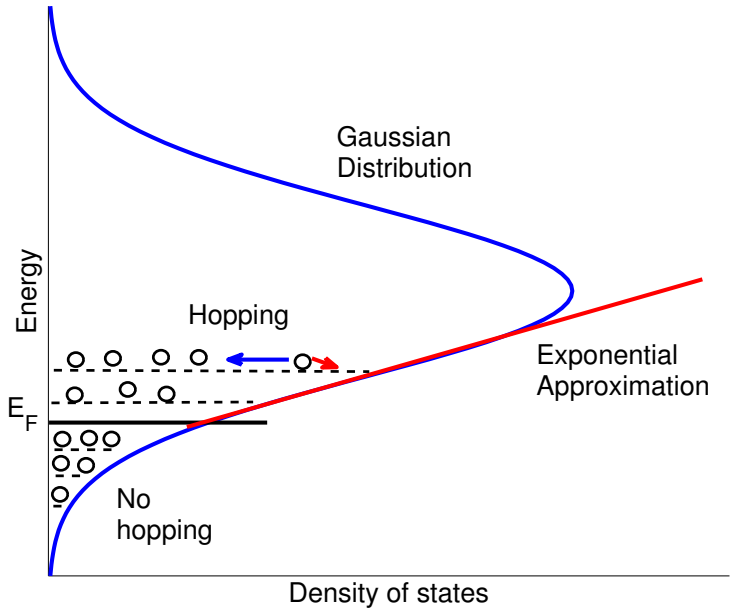

Figure 2.1: Demonstration of Gaussian distribution of states.

In disordered organic material, a distribution function is used to describe the energy state distribution. The density of states (DOS) in organic materials described using a Gaussian distribution of energy sites $N_G(E)$ is given as:

$$N_G(E) = \frac{N_T}{\sqrt{2\pi}E_\sigma} exp(-\frac{(E-E_\mu)^2}{2E_\sigma^2}) \tag{2.3}$$

where N_T is the concentration of the states (m^{-3}), E_σ is the standard deviation, and its variance is E_σ^2, E_μ is where the energy deviation is at a maximum. In disordered organic semiconductors, at low carrier concentrations, the Gaussian distribution can be approximated to an exponential,, as shown in *Figure.*(2.1). Therefore the exponential DOS $N_{ex}(E)$ is as given in *Equation*(2.4), because the majority of the carrier hopping occurs at the band tail[19].

$$N_{ex}(E) = \frac{N_T}{k_B T_0} exp(\frac{E}{k_B T_c}) \tag{2.4}$$

Here k_B is the Boltzmann constant, and T_c is the characteristic temperature describing the distribution of the traps.

2.2.1 Significance of Meyer Neldel Energy in density of states

The Meyer Neldel rule (MNR) is an experimental relation observed among many different semiconducting materials which includes single-crystal, polycrystalline, and amorphous. Although it is a commonly observed phenomenon, the origin of MNR in inorganic and organic semiconductors is still under constant discussion. Several processes, with a thermally activated behaviour, co-existing simultaneously can lead to the MNR.

The existence of MNE can be explained by fundamental parameters such as the current, bulk conductivity, diffusion and other physical parameters. Elementary quantities like the charge carrier mobility are used to understand the concept of Meyer Nedel energy (MNE). However, justification of MNE for the charge carrier mobility is still under discussion. Also those technical detail during the sample fabrication processing may affect the Meyer Nedel energy.

2.3 Conjugated polymer transport mechanism

Unlike inorganic material, the atoms in organic materials are covalently bonded; the organic long conjugated molecule materials or polymers are individual molecule semiconductors. Within a molecule, the P_z atomic orbitals of a carbon atom overlap to form π conjugation molecular orbitals and the π electrons are delocalized within the conjugated backbone. Interactions between the molecules are formed through the Van der Waals force and aromatic $\pi - \pi$ interactions.

The energy difference between the highest occupied molecule orbital (HOMO) and the lowest unoccupied molecule orbital (LUMO) determines the bandgap of the material, which corresponds to valence band and conduction band in inorganic material. The material with relatively higher HOMO level can be easily p-doped and transport is due to holes.

A semiconducting polymer is not a perfect conjugated system, because its twisted and kinked chains and chemical defects cause breaks in conjugation. Because of their spatial and energetically disordered configuration, these systems have no translation symmetry. The concept of band conduction by free charges does not apply. Instead, localized states are formed and a different theoretical approach is required. In order to contribute to the charge transport, the charge carrier must hop between these localized states (inter-or-intra chain transitions). This is usually thought to be the main cause of low carrier mobility.

2.3.1 Charge hopping model

For disordered organic semiconductor materials, the charge transport does not follow the classical band transport as in inorganic materials, but rather a hopping transport mechanism. Several such mechanisms have been proposed in the literature.

Miller Abraham hopping model

Bassler proposed in 1993, a charge transport model for disordered organic systems. He assumed that electron-phonon coupling is sufficiently weak so that the polaronic effect can be neglected, and the hopping rate can described by the Miller-Abrahams as described in *Equation*(2.5) and *Equation*(2.6)[17].

$$\nu_{i-j} = \nu_0 exp(-2\gamma\alpha\frac{R_{ij}}{\alpha}) \times exp(-(\frac{\varepsilon_j - \varepsilon_i}{k_B T})), for \varepsilon_j > \varepsilon_i \tag{2.5}$$

$$\nu_{i-j} = \nu_0 exp(-2\gamma\alpha\frac{R_{ij}}{\alpha}) \times 1, for \varepsilon_j > \varepsilon_i \tag{2.6}$$

where $\frac{R_{ij}}{\alpha}$ is the relative jump distance between sites i and j, ε_i and ε_j are the respective energy potentials of state, α is the lattice constant, γ is the inverse localization radius related to the electron coupling matrix element between adjacent sites, and ν_0 is a frequency factor for the attempt-to-hop frequency.

Variable range hopping model

The variable range hopping (VRH) mechanism is thought to occur in systems where the thermal energy, $k_B T$, is less than the energy variation between successive states. The charge carrier hops between localized states, randomly distributed in space, and energetically distributed according to the DOS function. In most of the calculations the DOS is assumed to be Gaussian, for lack of better knowledge. From this point onwards this assumption is made and known as the Gaussian disorder model, unless otherwise mentioned. There is no phase memory between hops, and therefore "continuum band "like transport is excluded. This condition stems from the long distance between sites that dictate a slow transfer rate where compared to the inverse phase coherence(dephasing) time. The hopping rate between sites is the same as in the Miller Abrahams model. Energies of adjacent sites are uncorrelated. The expression for the conductivity as a function of the temperature and carrier concentration is given in terms of exponentail DOS in thermal equilibrium as:

$$\sigma \propto \frac{N_T}{k_B T_c} exp(\frac{E}{k_B T_c}) \tag{2.7}$$

Here N_T is the total number of states per unit volume, and T_c is the characteristic temperature describing the distribution of the traps. Charge carriers are thermally activated and tunnel between localised states. The distance of hops depends on the activation energy of the charge carriers. If the activation energy is high, the hopping distance is short; if the activation energy is low, the hooping distance is long, as shown in *Figure*(2.1).

2.3.2 Charge Transport in Conjugated Polymers

An ideal device model is assumed here to demonstrate the significance of the Universal Mobility Law (UML) in disordered material. Two electrodes with length x are placed horizontally on a substrate with a fixed spacing y, a semiconductor film with thickness z is sandwiched by those two electrodes. The diagram *Figure*(2.2) defines the coordinate system. M represents the metal electrode, and S for the semiconductor.

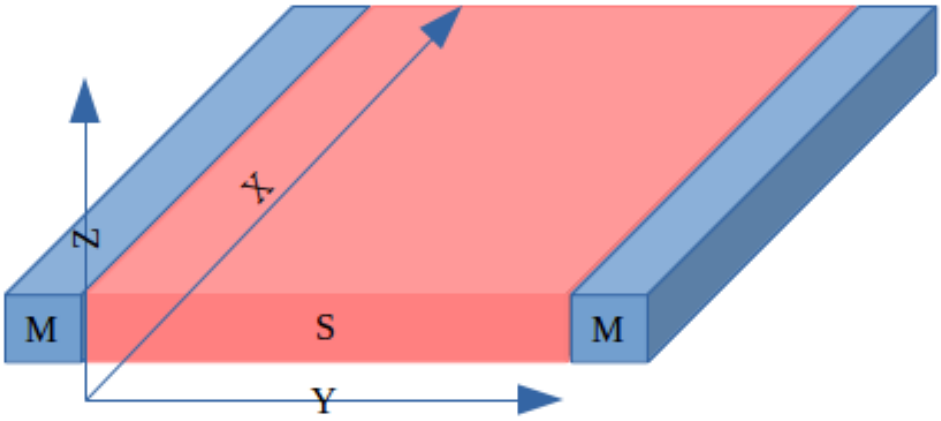

Figure 2.2: Cross-sectional diagram of an ideal device's coordinates system.

The current density at a certain point inside the semicondutor film can be expressed as *Equation*(2.8):

$$J = nq\mu F_y \tag{2.8}$$

Where J is the current density, n is the charge carrier concentration, μ is the drift mobility and F_y is the electrical field strength along the direction of y. Here, the effective mobility is not approximated to the drift one, but rather a numerical result obtained from electrical measurement of the neutral region, given by *Equation*(2.9).

$$\mu_{eff} = K_{UML} n^m \tag{2.9}$$

where K_{UML} is a constant in the Universal Mobility Law, and m is the exponent dependent on the properties of the semiconductor and the characteristics temperature T_c associated with the distribution of the traps. Combining *Equation*(2.8) and *Equation*(2.9), the expression for the current density can be modified into *Equation*(2.10)

$$J = K_{UML} n^{m+1} q F_y \tag{2.10}$$

Compared to the disordered semiconductor, the concept of the mobility is more useful in crystalline material where the carriers are considered to concentrate on the single energy level i.e. the conduction band, .

$$J = \mu_0 N_c exp(-\frac{E_C - E_F}{k_B T}) q F_y \tag{2.11}$$

Here N_c is the effective density of states in the conduction band edge E_C. For the disordered material, the conduction mechanism is different from the conventional materials. In the disordered system, the 'banding' dose not occur and the hopping process plays a significant role[2], as the polymer chain length varies and the sites contributed to charge transport is distributed energetically. Therefore, the Gaussian distribution can be used for the description of Density of states. As shown in *Figure*(2.1), the hopping mostly occurs in the tail of Gaussian DOS, the DOS is approximated to the exponential distribution. The exponential distribution is used as density of states function, the Maxwell-Boltzmann function is used to estimate the Fermi-Dirac statistics above the Fermi level E_F. The carrier concentration can be seen as integrating the product of the Maxwell-Boltzmann equation and the exponential density of states from E_F to ∞.

$$n(E) = \int_{E_F}^{\infty} \frac{N(0)}{k_B T_c} exp(\frac{E}{k_B T_c}) exp(-\frac{E - E_F}{k_B T}) d(E) \tag{2.12}$$

where E_F is the fermi energy level, T is the room temperature i.e. $300K$, T_c is the characteristics temperature of a trap distribution in disordered material, and E is the localized energy level. $N(0)$ is the number of states per volume at $E = 0$. The characteristic temperature which describe the distribution of the traps T_c and carriers T_0, can be expressed as $\frac{1}{T_0} = \frac{1}{T} - \frac{1}{T_c}$. Subsequently, the carrier concentration equation can be modified into *Equation*(2.13).

$$n(E) = \int_{E_F}^{\infty} \frac{N(0)}{k_B T_c} exp(\frac{E_F}{k_B T}) exp(-\frac{E}{k_B T_0}) d(E) \tag{2.13}$$

With further reorganizing and integrating of *Equation*(2.13), the carrier concentration equation can be expressed as below:

$$n(E) = \frac{T_0 N(0)}{T_c} exp(\frac{E_F}{k_B T_c}) \tag{2.14}$$

In order to find the net charge carriers concentration per unit area, *Equation*(2.14) is differentiated and then integrated between appropriate limits. Two assumptions have been made, those depend on the relationship between the Fermi level $E_F$and minimum transport level. Firstly, if the Fermi level E_F is above the minimum transport Energy level E_T, then, the carrier concentration equation is given as *Equation*(2.15):

$$n(E) = \frac{T_0 N(0)}{T_c} exp(\frac{E_F}{k_B T_c}) \tag{2.15}$$

Substituting the charge carrier concentration expression into the *Equation*(2.8), the current density equation can be represented in the following form.

$$J = n(E) = \frac{T_0 N(0)}{T_c} exp(\frac{E_F}{k_B T_c}) q\mu F_y \tag{2.16}$$

Corresponding to *Equation*(2.11), and assuming that the carrier concentration at the energy level E_T is N_T, then the current density can be expressed as in the following equation:

$$J = \mu q F_y N_T exp(\frac{E_F - E_T}{k_B T}) \tag{2.17}$$

In order to make the two current density model look similar, *Equation*(2.17) is rearranged into the following format:

$$J = \mu q F_y N_T exp(-\frac{E_T}{k_B T}) exp(\frac{E_F}{k_B T_C})^{\frac{T_C}{T}} \tag{2.18}$$

Comparing *Equation*(2.17) and *Equation*(2.18):

$$N_T exp(-\frac{E_T}{k_B T}) exp(\frac{E_F}{k_B T_C})^{\frac{T_C}{T}} = \frac{T_0 N(0)}{T_c} exp(\frac{E_F}{k_B T_c}) \tag{2.19}$$

Thus,

$$J = \mu F_y q \frac{N_T exp(-\frac{E_T}{k_B T})}{\frac{T_0 N(0)}{T_c}} exp(\frac{E_F}{k_B T_c})^{\frac{T_c}{T}-1} \frac{T_0 N(0)}{T_c} exp(\frac{E_F}{k_B T_c}) \tag{2.20}$$

Corresponding the current density model in same form of *Equation*(2.17), the universal mobility law can be presented in an alternative way, which is temperature related.

$$\mu_{eff} = \mu \frac{N_T exp(-\frac{E_T}{k_B T})}{\frac{T_0 N(0)}{T_c}} exp(\frac{E_F}{k_B T_c})^{\frac{T_c}{T}-1} \tag{2.21}$$

$$m = \frac{T_c}{T} - 1 \tag{2.22}$$

where N_T is the effective density of states, and E_T is the transport level in the disordered material. If minimum transport energy level E_T is above the Fermi level E_F, the lower condition for the integral is E_T, and the carrier concentration should be changed as below.

$$n(E) = \frac{T_0 N(0)}{T_c} exp(\frac{E_F}{k_B T}) exp(-\frac{E_T}{k_B T_0}) \tag{2.23}$$

Using the same method above, the current density model can be derived in two different forms:

$$J = \mu q F_y \frac{T_0 N(0)}{T_c} exp(\frac{E_F}{k_B T}) exp(-\frac{E_T}{k_B T_0}) \tag{2.24}$$

Or:

$$J = \mu q F_y N_T exp(-\frac{E_T - E_F}{k_B T}) \tag{2.25}$$

Furthermore, since the different forms represent the same quantity for the current density:

$$J = \mu F_y q \frac{N_T}{\frac{T_0 N(0)}{T_c}} exp(\frac{E_F}{k_B T_0})^{\frac{T_0}{T}-1} \frac{T_0 N(0)}{T_c} exp(\frac{E_F}{k_B T}) exp(-\frac{E_T}{k_B T_0}) \tag{2.26}$$

$$\mu_e f f = \mu \frac{N_T}{\frac{T_0 N(0)}{T_c}} exp(\frac{E_F}{k_B T_0})^{\frac{T_0}{T}-1} \tag{2.27}$$

$$m = \frac{T_0}{T} - 1 \tag{2.28}$$

The above derivation of current density for the second condition is based on the method used in the previous condition. The model is presented under the assumption of the equivalence of E_C and E_T, which both notation has got identical physical meaning of the lowest transport energy level for the majority charge carriers in the semiconductor. In order to understand basic conduction processes in the band tails of highly disordered organic materials, a Schottky diode is a good illustration of these processes consists of a film of the semiconductor between two electrodes of differing work function. One of the contacts is rectifying, the other is nominally ohmic. The forward current rises rapidly due to the flow of majority carriers into the rectifying contact and at higher applied voltages, in the forward direction and additional applied potential falls across the neutral region which is ideally ohmic. Based on this similar method, the model for OTFT is also developed, as shown in *Equation*(3.10) and *Equation*(3.11).

2.4 Charge photo-generation

In polymeric semiconductors, a neutral excited state also known as an exciton, is a bound electron-hole pair, formed upon photon absorption[20].Tightly bound Frenkel excitons (electron-hole pairs) have been observed in organic material, with binding energy of around $0.3eV$, whereas the Wannier exciton believed to exist in inorganic material, has a comparable binding energy to thermal energy at room temperature of $26meV$[21]. Another distinction between the organic and inorganic material is the mobility. The mobility in organic material is known to be lower due to difficulties in charge carriers hopping from one molecule to the adjacent molecule.

Concurrent phenomena that exciton dissociation (photo-generation) must compete against, are radiative decay, exciton diffusion, and exciton quenching. Regarding diffusion, the exciton diffuses by hopping according to a generalized Forster mechanism, which involves a large-range electro-static force, the typical diffusion lengths are in the range of $10nm$. Regarding exciton quenching, a non-exhaustive list of possible quenching paths includes: non-radiative decay to ground state; inter-system crossing, which is a singlet to triplet exciton conversion; singlet singlet (singlet-triplet) annihilation, with the generation of a ground state and of a higher excited singlet state; singlet-charge annihilation.

2.4.1 Photogeneration due to oxygen traps

It is widely believed that oxygen can act as traps for electrons in the HOMO level of the organic material and thereby lead to a higher concentration of free holes in the LUMO. In this sense, oxygen can act as a dopant that favours p-type conductivity. However, the oxygen traps can also act as exciton dissociation sites and therefore generate free charge carriers in the presence of excitons. After a certain period, three scenarios may occur. Firstly, the electron from a just dissociated exciton combines with a hole that comes from a different exciton. Both excitons are dissociated, but only two free charges are produced,and the others recombine. Secondly, one of the recombination partners is associated with an exciton. This means that the dissociation procedure yields one free charge only. Thirdly, none of the recombination partners belongs to an exciton. Two free charges are eliminated. The photo-generation due to the presence of the traps is not sufficient since the recombination of free charges.

2.4.2 Electrode/Semiconductor interface

The theory of the Semiconductor/Metal contact was developed by Mott, Schottky and others. The charge injection from the metal electrode into the semiconductor is explained in detail in Chapter 4. Excitons can be separated with the aid of internal field within a diffusion region ($\sim 20nm$). The charge separation occurs at the polymer/metal rectifying contact due to

internal electric field. Photo-excited electrons from the HOMO level of the electron acceptor encounter a barrier before they are collected by the rectifying contact. The current-voltage characteristic of a Schottky barrier diode under illumination is described by:

$$I = I_s \left[exp(\frac{qV}{\eta k_B T}) - 1 \right] - I_{ph} \tag{2.29}$$

Here, I_s is the reverse saturation current, η is the ideality factor, and I_{ph} is the photo-generated current. However, the efficiency of exciton separation at the Schottky contact is quite low due to recombination of excited charges. One of the main advantages of the Schottky barrier device is high speed.

2.4.3 Donor/Acceptor interface

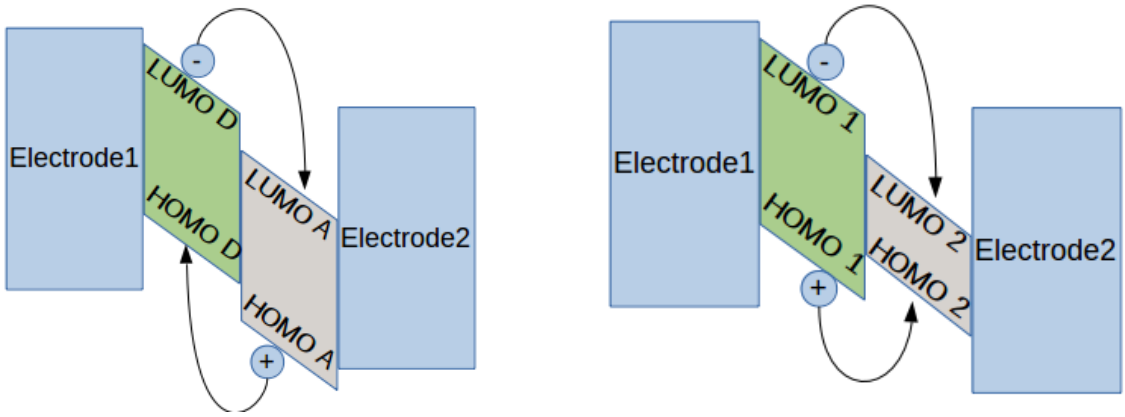

(a) An interface of D/A materials, where exciton can be separated and collected by electrodes on both sides respectively.

(b) An interface of two different materials, where the dissociated charge carriers from exciton transfer and recombine again soon.

Figure 2.3: Energy band diagram of the interface between a donor (D) and acceptor (A) semiconductor materials.

The interface formed by an electron donor material and an electron acceptor material could be a more efficient approach to generate free charge carriers. At first glance, the concept of the donor/acceptor interface is very similar to the P/N junction for silicon devices. For the silicon P/N junction, before the p-type material and n-type material form contact, the positions of Fermi levels in P/N material are different due to the dopant types. After the contact is made, the electrons in the n-type material will diffuse to p-type material, and the holes will diffuse in the opposite direction. The diffusion and drift driven by the built in potential of charge carriers bend the Fermi levels on the both sides, the system reaches the equilibrium finally. However, the mechanism behind D/A interface is different. The positions of the HOMO and LUMO of two materials determine the bending direction of the

energy level, such as an interface as shown in the $Figure(2.3)(a)$ contributes to dissociation of excitons, while, at the interface like $Figure(2.3)(b)$, there are no net exciton splitting. It should be noted that the $Figure(2.3)(a)$ has some energy level offset, due to the nature of semiconductors, one of which is n-type and the other is p-type.

This device with bilayer donor/acceptor interface was thought to be more efficient than the Schottky-barrier type device. The photocurrent generation does not depend on the nature of the electrode work function. Many theoretical reports have shown that in bilayer organic solar cell ($OSCs$), theoretically, the open circuit voltage V_{oc} is linearly related to the difference between the HOMO level of the donor material and the LUMO level of the acceptor material, and it does not depend much on the work function of the electrodes. It should also be noted that the V_{oc} loss of 0.3V is empirical, and potentially the loss could be greater or smaller. [22]

$$V_{oc} = \frac{(|E_{HOMO,D}| - |E_{LUMO,A}| - 0.3eV)}{q} \tag{2.30}$$

Here, $E_{HOMO,D}$ is the HOMO energy level of the donor material, and $E_{LUMO,A}$ is the LUMO energy level of the acceptor material.

However, efficient photo-generation requires that the photo-excitation occurs within a diffusion length from the bilayer D/A interface, and the dissociation of excitons is with the aid of the internal electric field near the D/A interface, as shown in $Figure.(2.4)(a)$. The required small film thickness still limits the power conversion efficiency. In order to overcome this problem, the acceptor and donor materials are blended into a single film between two electrodes, which is referred to bulk heterojunction. It can be assumed that there are bi-continuous D/A interfaces linked together, as shown in $Figure.(2.4)(b)$, which can overcome the limitation of film thickness due to the exciton diffusion length. Bulk heterojunction was proposed in 1990s [23], so far, it is believed to be the most effective structure for organic photovoltaic devices. Unlike the organic photovoltaics (OPVs), dark currents play a key role in determining the overall performance of a photodetector, suppressing charge injection phenomena is generally accounted as a preferable way to reduce dark current. For instance, a high enough Schottky barrier at a semiconductor/metal interface can significantly suppress charge injection phenomena. While, as shown in $Figure.(2.4)(b)$, in the D/A bulk heterojunction device, the donor and acceptor materials possibly present at the same metal/semiconductor interface, which always makes such energy barrier small and ill-defined. Therefore, vertical phase segregation is applied to avoid the energy barrier at metal/semiconductor interface being ill-defined. For example, as shown in $Figure.(2.4)(c)$, using chemical method controls the concentration of donor material decreasing from Electrode1 side to Electrode2 side, while acceptor material changes in another direction. Another approach is shown in $Figure.(2.4)(d)$, applying Electron Blocking Layer (EBL) and Hole Blocking Layer at the anode and cathode sides respectively preventing charges injecting into the semiconductor.

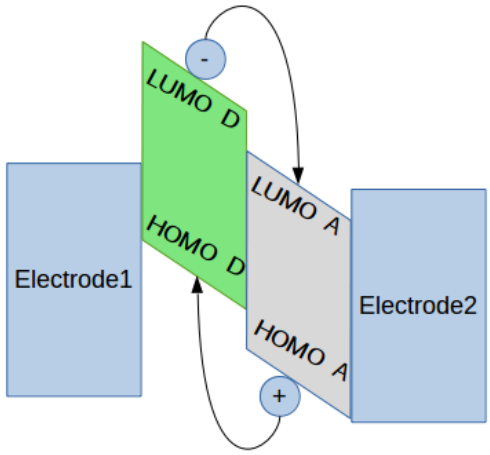

(a) A generic D/A planar-heterojunction

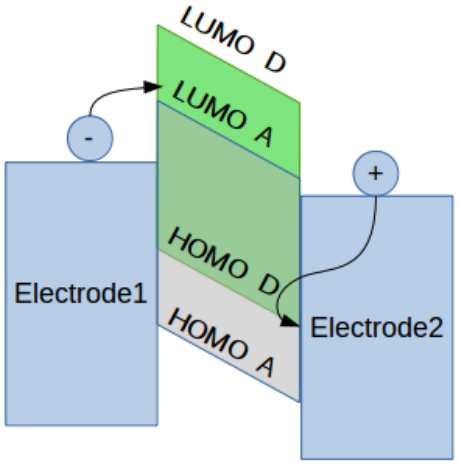

(b) A generic D/A bulk-heterojunction

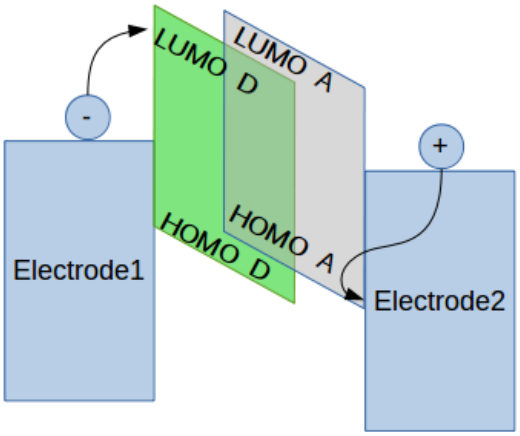

(c) A vertically segregated D/A bulk-heterojunction

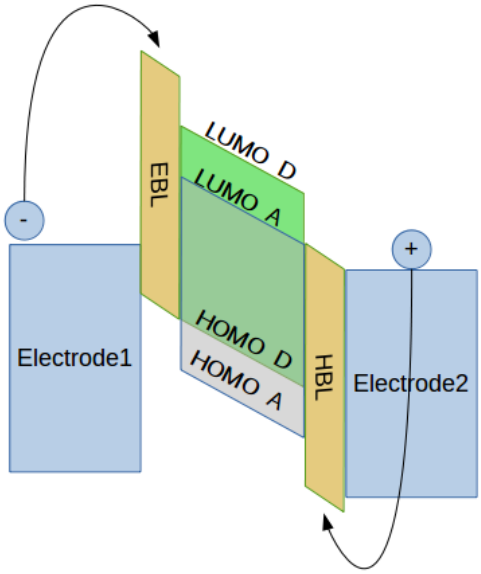

(d) A device provided with dedicated injection blocking layers.

Figure 2.4: Energy band diagram representing charge separation phenomena at various interfaces.

2.5 Applications Development

Since 1976, Heeger, and MacDirarmid and Shirakawa discovered conducting polymers [2], which initiated extensive and systematic research referring to its properties and application [3]. With its progress in performance in recent years, the development of devices based on semiconductor polymer is dramatic, including organic photovoltaic cells (OPVs), organic light-emitting diodes (OLEDs), organic field effect transistor (OTFTs) and complementary logic circuits. Here, two applications will be briefly reviewed.

2.5.1 Organic photovoltaic device

Photovoltaic (PV) technology, which generates electricity directly from sunlight, is a promising solution of renewable energy. PV now covers 2.6% of overall electricity demand in Europe. The annual PV installation in the world first exceeded $1GW$ in 2003, and by the end of 2012 world cumulative installed PV capacity had surpassed $100GW$[4]. Intensive research in this area focuses on seeking high efficiency solar cell with reduced fabrication cost and less environmental issues. Currently, the commercial market of PVs is dominated by inorganic based devices. However, the polymer semiconductor is a promising alternative to inorganic material due to low cost, low weight, and flexibility.

Unlike in inorganic photovoltaic devices, the hopping mechanism is the dominant charge transport mechanism in polymeric semiconductor. The charge mobility is significantly lower than the mobility of inorganic materials such as crystalline Si. In addition, the low dielectric constant ($\varepsilon_s \approx 2-4$), results in tightly bounded Frenkel excitons (electron-hole pairs). The binding energy of the Frenkel exciton is in the range of $0.3-1eV$, whereas the binding energy of Wannier excitons (free electron-hole pairs at room temperature) in inorganic semiconductor is comparable to the thermal energy at room temperature of $25meV$. Those two factors make the OPVs working principal different from the conventional PV device. The simplified work mechanism of the OPVs is comprised of four steps: firstly, photo absorption and exciton generation, secondly, exciton diffusion, thirdly, charge separation, finally, charge collection.

The simplest form of organic photovoltaic device is a single layer structure, which consists of a single polymer semiconductor layer. However, the properties of the single layer organic solar cell are strongly dependent on the work-function and nature of electrodes, and the fill factor (FF) is significantly limited by the large series resistance of the device. Normally, based on the literature summary, for single layer OPV, the efficiency dose not exceed 0.1%, by contrast, single layer crystalline Si PV efficiency can reach 24%. In order to improve the OPV efficiency, Tang proposed a two-layer organic photovoltaic cell [5]. In this double layer structure, the interface of two organic layers was shown to be responsible for the photo generation current rather than the metal/semiconductor interface. The independence of photo-current generation on the electric field yields a significant enhancement in both fill factor and photovoltaic efficiency. Subsequently, the power conversion efficiency of $\approx 1\%$ and high fill factor of 65%, has been achieved in two-layer OPV, compared to single layer OPVs. However,the device using a bi-layer structure demonstrated low efficiency of power conversion, because the lifetime of the exciton is very short and its diffusion length is shown to be only $\approx 10nm$. This means that the active layer must be very thin in order to avoid exciton recombination. However, such thin film ($\approx 20nm$) is insufficient for effective light absorption; for most polymer semiconductor the film thickness should be more than $100nm$ in order to absorb most of the light. To overcome this problem, the bulk-heterojunction (BHJ) structure made from a solution of p-type and n-type materials was invented by Sariciftci and Heeger

in 1992 [6][7][8]. The blending of the donor and acceptor can overcome the recombination problem of thick polymer film. This local fields aids dissociation of excitons diffusing to the interface. Indeed charge separation is much more efficient at the donor-acceptor interface than at the electrode interface.

Material and Device structure	Method	J_{sc} and V_{oc}	FF	Efficiency (%)	Ref
CuPc/PV Vertical Planar Heterojunction	Vacuum Evaporation	$2.3 \pm 0.1 mA/cm^2$ $450 \pm 20 mV$	0.65 ± 0.03	0.95	[5]
Me-PTC/H_2Pc Vertical Bulk Heterojunction	Vacuum Evaporation	$2.14 mA/cm^2$ $0.51V$	0.48	0.7	[10][11]
HBC-PHC_{12} /Perylene Vertical Bulk Heterojunction	Solution processing and spun-coating	$33.5 \mu A/cm^2$ $0.69V$	0.4	2	[12]
MDMO-PPV/PCBM Vertical Bulk Heterojunction	Solution processing and spun-coating	$5.25 mA/cm^2$ $0.82V$	0.61	2.5	[14]
P3HT/PCBM Vertical Bulk Heterojunction	Solution processing and spun-coating	$14.1 mA/cm^2$ $0.65V$	0.6	5.5	[15]
P3HT/PCBM Vertical Bulk Heterojunction using TiO_x interfacial layer	Solution processing and spun-coating	$10 mA/cm^2$ $0.611V$	0.62	3.78	[16]

Table 2.1: Some important milestones in the development of organic and polymeric photovoltaic device

In the last two decades, there has been a steady improvement in OPV power conversion efficiencies. The increase in power conversion efficiency (PCE) to 10% is regarded as an important threshold for widespread development. For efficiency $< 10\%$, the cost of installation is typically too expensive for widespread energy production, even if the solar cells and modules are inexpensive. Some industrial research institutions have already announced the achievement of non-transparent OPVs efficiency reaching 12% and the transparent device reaching the efficiency record 7.2% with a 40% light transparency[18]. Three important parameters determine the PCE of a solar cell: the open-circuit voltage (V_{oc}), short-circuit

current density (J_{sc}) and fill-factor(FF). The maximum power generated in the external circuit is the product of the three: $P_{max} = I_{sc}V_{oc}FF$.

2.5.2 Organic photodetector

The operation mechanism behind the organic photo detector is similar to the organic solar cell. The photodetector can classified by spectral regions, ranging from ultra violet to near infra-red (NIR) light. A successful photo detector requires not only low dark current but also high photo current. Several parameters are essential in evaluating the performance of a photodetector, which are summarised in $Table(2.2)$.

Parameter	units	comments
Responsivity	A/W	sensitivity
Spectral Response Range	nm	range of detectable wavelength
Normalized Detectivity	$Jones$	sensitivity
Linear dynamic range	dB	
Response time	s	the time of rising to 63.2% of the final state
Quantum efficiency	%	the number ratio of photo-excited excitons and charge carriers to the incident photon

Table 2.2: Parameters of organic photodetector

References

[1] H. L. Dong, H. F. Zhu, Q. Meng, X. Gong and W. P. Hu, "Organic photoresponse materials and devices"Chemical Society Review, vol. 41, no. 5, pp. 1754-1808, 2012.

[2] H. Shirakawa, E. J. Louis, A. G. MacDiarmid, C. K. Chiang and A. J. Heeger, "Synthesis of electrically conducting organic polymers: halogen derivatives of polyacetylene, (CH)x,"Journal of the Chemical Society, Chemical Communications, no. 16, pp. 578-580, 1977.

[3] X. G. Zhao, X. W. Zhan, "Electron transporting semiconducting polymers in organic electronics,"Chemical Society Review, vol. 40, no. 7, pp. 3728-3743, 2011.

[4] G. Masson, M. Latour, M. Rekinger, I. T. Theologitis and M. Pap, "Global Market Outlook for Photovoltaics 20132017", European Photovoltaic Industry Association, 2013.

[5] C. W. Tang, "Two layer organic photovoltaic cell,"Applied Physics Letters, vol. 48, no. 2, pp. 183, 1986.

[6] A. J. Heeger, N. S. Sariciftci, "Conjugated polymer-acceptor heterojunctions; diodes, photodiodes, and photovoltaic cells,"U.S. Patent 5331183 A, 19 July 1994.

[7] G. Yu, J. Gao, J. C. Hummelen, F. Wudl and A. J. Heeger, "Polymer Photovoltaic Cells: Enhanced Efficiencies via a Network of Internal Donor-Acceptor Heterojunctions,"Science, vol. 270, pp. 1789-1791, 1995.

[8] J. J. M. Halls, C. A. Walsh, N. C. Greenham, E. A. Marseglia, R. H. Friend, S. C. Moratti, and A. B. Holmes, "Efficient photodiodes from interpenetrating polymer networks,"Nature, vol 376, pp. 498-500, 2002.

[9] C. W. Tang and S. A. VanSlyke, "Organic electroluminescent diodes,"Applied Physics Letters, vol 51, no. 12, pp. 913, 1987.

[10] M. Hiramoto, H. Fujiwara and M. Yokoyama, "Threelayered organic solar cell with a photoactive interlayer of codeposited pigments,"Applied Physics Letters, vol. 58, no. 10, pp. 1062-1064, 1991.

[11] M. Hiromoto, H. Fujiwara and M. Yokoyama, "Organic solar cell based on multistep charge separation system,"Applied Physics Letters, vol. 61, no. 21, pp. 2580-2582, 1992.

[12] L. Schmidt-Mende, A. Fechtenkötter, K. Müllen, E. Moons, R. H. Friend, and J. D. MacKenzie,"Self-Organized Discotic Liquid Crystals for High-Efficiency Organic Photovoltaics,"Science, vol. 293, pp. 1119-1122, 2001.

[13] G. Yu, K. Pakbaz, and A. J. Heeger, "Semiconducting polymer diodes: Large size, low cost photodetectors with excellent visibleultraviolet sensitivity,"Applied Physics Letters, vol. 64, pp. 3422, 1994.

[14] S. E. Sean, B. J. Christoph, S. N. Serdar, P. Franz, F. Thomas, and H. C. Jan, "2.5 % efficient organic plastic solar cells ,"Applied Physics Letters, vol. 78, no. 6, pp. 841-843, 2001.

[15] X. H. Yang, A. Uddin, "Effect of thermal annealing on P3HT:PCBM bulk-heterojunction organic solar cell: A critical review", Renewable and Sustainable Energy Reviews, vol. 30, pp. 324-336, 2014.

[16] K. Foe, G. Namkoong, M. Samson, E. M. Younes, I. Nam, and T. M. Abdel-Fattah1, "Stability of High Band Gap P3HT:PCBM Organic Solar Cells Using TiOx Interfacial Layer,"International Journal of Photoenergy, Vol. 2014, 2014.

[17] H. Bässler, and A. Köhler, "Charge transport in organic semiconductors,"Topics in Current Chemistry, vol. 312, pp. 1-65, 2012.

[18] Heliatek reaches efficiency record with 40% transparent organic solar cells, $http : //www.heliatek.com/newscenter/latest_news/heliatek - erzielt - effizienzrekord - mit - 40 - transparenten - organischen - solarzellen/$

[19] N. Sedghi, D. Donaghy, M. Raja, S. Badriya, S. J. Higgins, W. Eccleston, "Experimental observation of the density of localized trapping levels in organic semiconductors", Journal of Non-crystal Solids, vol. 352, pp. 1641-1643, 2006.

[20] K. J. Baeg, M. Binda, D. Natali, M. Caironi, and Y. Y. Noh, "Organic Light Detectors: Photodiodes and Phototransistors,"Advanced Materials, vol. 25, no. 31, pp. 4267-4295, 2013.

[21] L. Dou, J. You, Z. Hong, Z. Xu, G. Li, R. A. Street, and Y. Yang, "25th Anniversary Article: A Decade of Organic/Polymeric Photovoltaic Research,"Advanced Materials, vol. 25, no. 46, pp. 6642-6671, 2013.

[22] B. Y. Qi,J. Z. Wang, "Open-circuit voltage in organic solar cells,"Journal of Material Chemistry, vol. 22, pp. 24315-24325, 2012.

[23] J. J. M. Halls, C. A. Walsh, N. C. Greenham, E. A. Marseglia, R. H. Friend, S. C. Moratti and A. B. Holmes, "Efficient photodiodes from interpenetrating polymer networks Nature,", vol. 376, pp. 498-500, 2002.

Chapter 3

Organic Thin Film Transistors

This chapter explores the characteristics of P3HT Thin Film Transistors (TFTs) with low-K gate dielectrics (SiO_2). The OTFTs with bottom gate structure were fabricated. The devices were characterized in non-vacuum conditions. In addition, the influence of the solution concentration is investigated so as to optimize the performance of the devices.

3.1 Introduction

The organic thin film transistor (OTFT) has gained considerable popularity in the application of low cost, and flexible substrate devices such as RFID tags, and displays.[1] However, due to low mobility, large contact resistance and poor ambient and bias stabilities, polymers are not thought to be an alternative to conventional material such as amorphous silicon (a-Si:H). Nonetheless, its unique characteristics such as solution processing, and transparency, underlines the interest in the polymer device in spite of the limitations. The deposition of the polymer thin film in the liquid phase means that the device can be fabricated cost-effectively in large scale. Also with the possibility for integration of organic electrode material, organic dielectric and transparent flexible substrates (i.e. polyethylene naphthalate (PEN) and polyethylene terephthalate (PET)), makes it more attractive over conventional material. This chapter focuses on the study of P3HT OTFT. The structure diagram of P3HT is shown in *Figure.*(3.1). And with the aid of the output and transfer characteristics, useful parameters are extracted and subsequently used it to fit the developed organic models. Moreover the effect of variation of the P3HT concentration on device performance is also examined.

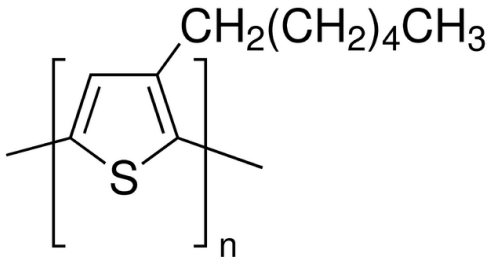

Figure 3.1: Diagram of the structure of poly(3-hexylthiophene) (P3HT)

3.2 Fundamental theory of the organic thin film transistor

3.2.1 OTFT architecture

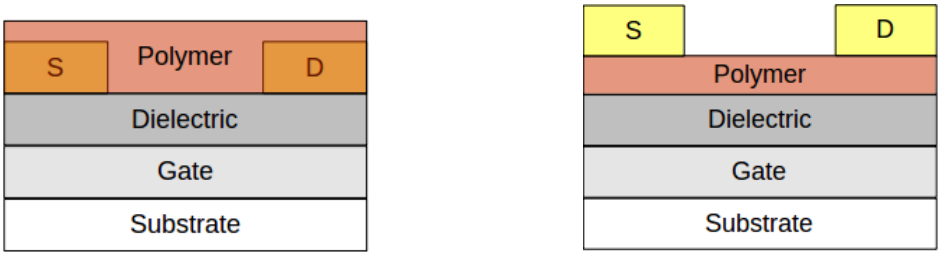

(a) BGBC (b) BGTC

Figure 3.2: Schematics of two types of OTFT structures mentioned in thesis

The three main types of OTFT structures are, BGBC (bottom gate with bottom source/drain contact) and BGTC (bottom gate with top source/drain contact), as shown in *Figure*(3.2). All the structures have their own advantages and limitations. The BGBC structure has an advantage in device fabrication, the polymer thin film can be deposited at the last stage. However, this structure also has some limitations such as high contact resistance. The BGTC structure was thought to give a lower contact resistance in comparison. The top contacts are normally formed by thermal evaporation using a shadow mask whose gap definition is not less than $10\mu m$. The photo lithography normally can not be applied in this case due to potential damage to the polymer thin film from the chemical involved (photoresist, developer, etch solution and even deionized water). In addition, with the BGTC device there is a requirement for vertical current flow through the bulk of the device, from the channel to the contacts, which is film thickness dependent.[2][3] The top gate device has the advantage of self-encapsulation by an insulator layer to reduce device air instability. All three types of architecture have been commonly applied for active matrix organic light emitting diode (AMOLED) displays. BGBC and BGTC type devices have been fabricated and characterised in this work.

3.2.2 Fabrication procedure

Thermal evaporation of metal and patterning of source/drain contacts

All the metal contacts on the device are formed through thermal evaporation. There are two major solutions to form the channel between the source/drain contacts. Firstly, during the thermal evaporation, a shadow mask is applied on the top sample to form the channel directly, which yields the minimum achievable channel length in the order of $10\mu m$. Secondly, the photolithography method is used to pattern the sample prior to thermal evaporation. Normally, the sample is spun-coated with positive photoresist(HPR 504) followed by a soft-bake and exposure through the mask under UV light. The sample is then dipped into developer to remove unwanted parts of photo-resist. Then, the sample is loaded into thermal evaporator to deposit the metal contact layer. After thermal evaporation, the sample is immersed into acetone or Microstrip 2001 to remove remaining photoresist layers and the metal attached onto them, which is known as the lift-off procedure. Microstrip 2001 can remove photoresist more effectively, however due to health and safety considerations, acetone is used as the photoresist remover in this work.

Solution processing of polymer film

One of the most attractive features of organic devices is the potential for low cost and large area manufacturing using the solution based processes. Spin-coating, drop-casting, zone casting and printing are the mostly widely used methods. In this work, spin-coating is applied

as the polymer thin film deposition method. The thickness of the film can be controlled by volume of the solution, spin-speed and duration. The detail of solution processing (such as solvent selection, heating temperature, post-deposition bake/annealing) depends on the polymer properties. Drop casting is another commonly used method, which is even more straight forward. The uniformity of the thin film depends on the evaporation of solvent and film thickness which is generally difficult to control. In other word, the repeatability of the spin-coating method is much better, in comparison to drop casting.

3.3 Characteristics of the OTFT

3.3.1 Output Characteristics

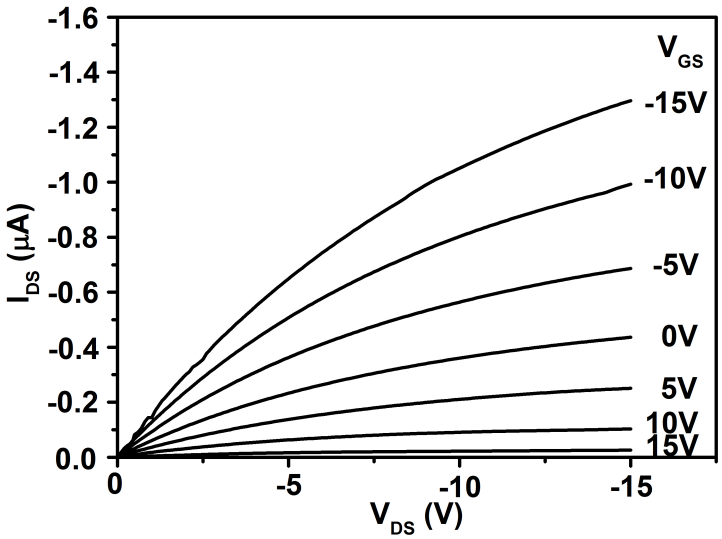

Figure 3.3: Output characteristics of a BGTC OTFT, Spun-coated P3HT film is used as the semiconductor, $50nm$ SiO_2 as dielectric, Palladium as the drain/source contact. The concentration of the P3HT/xylene solution is $1mg/mL$. The channel width and length of the OTFT was $2000\mu m/60\mu m$.

Figure(3.3) shows a typical output characteristics of P3H OTFT measured in ambient conditions. The output current through the channel between the source and drain can be modulated by gate voltage. Unlike the silicon field effect device, OTFTs normally have intrinsic semiconductor, therefore, the OTFTs always work in accumulation mode instead of the inversion mode. Theoretically, for a p-channel device, when the gate-source voltage is positive, the device is in the depleted mode, the charge carriers in the channel have been depleted forming a high channel resistance, and the device is in the off condition. Applying a negative gate-source voltage across dielectric, a sheet of mobile charge carriers accumulated

at the polymer/insulator interface. This forms a low resistance conducting channel, as shown in $Figure(3.4)(a)$, and the device is in the on condition. With a low drain-source voltage bias, those holes accumulated in the channel are driven by drain voltage with respect to the source V_D to drift forming the drain current I_D. The channel current I_D is controlled by both gate voltage and drain voltage. With the drain-source voltage increasing, the voltage difference between gate and drain has been lowered, the carrier concentration near the drain electrode is reduced, as shown in $Figure(3.4)(b)$; the current I_D increases linearly with the voltage V_{DS} which can be approximated as in $Equation(3.1)$.

$$I_D = \frac{W}{L}\mu_{eff}C_0\left[(V_G - V_{th}) - \frac{V_D}{2}\right]V_D \tag{3.1}$$

Here, I_D is the drain current, V_D is the drain voltage, V_{th} is the threshold voltage, μ_{eff} is the effective mobility, C_0 is the gate capacitance, and W/L is the length/width ratio of the OTFT channel.

With further increase in the drain voltage close to the boundary condition$V_D \geq (V_G - V_{th})$, the charge carriers close to drain electrode have been completely depleted, the drain source current I_D starts to saturate due to the pinching-off of the channel, as shown in$Figure(3.4)(c)$ and $Figure(3.4)(d)$; the I_D do not change significantly with V_D, which can be approximated as $Equation(3.2)$

$$I_D = \frac{W\mu_{eff}C_0}{2L}(V_G - V_{th})^2 \tag{3.2}$$

As shown in $Figure(3.4)d$, the pinch-off does not move towards the sources as it does in standard FETs, which is due to the TFT does not have a reverse biased junction at the drain, it has an ohmic contact.

The modulation of the drain current with gate voltage in saturation can be described by the transconductance g_m:

$$g_D = \left.\frac{\partial I_D}{\partial V_D}\right|_{V_G=constant} \tag{3.3}$$

In the linear region, I_D follows the $Equation(3.1)$ and thus,

$$g_m = \mu_{lin}C_0\frac{W}{L}V_D \tag{3.4}$$

In the saturation region, g_m is obtained by differentiating :

$$g_m = \mu_{sat}C_0\frac{W}{L}(V_G - V_{th}) = \sqrt{2\mu_{sat}C_0\frac{W}{L}I_{Dsat}} \tag{3.5}$$

The equation can be rearranged into

$$\sqrt{I_D} = \sqrt{\frac{W}{2L}\mu_{sat}C_0}(V_G - V_{th}) \tag{3.6}$$

$$g_m = \mu_{sat} C_0 \frac{W}{L}(V_G - V_{th}) \tag{3.7}$$

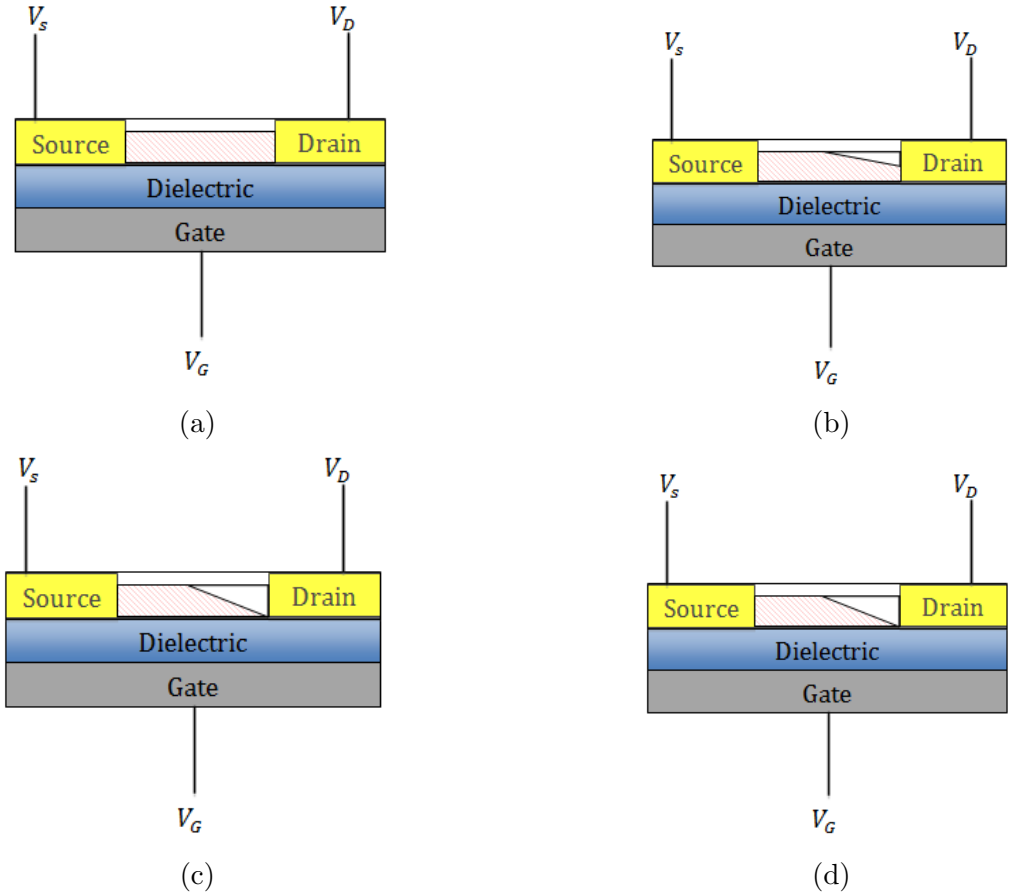

Figure 3.4: Demonstration of P3HT TFT in different drain/ gate biasing conditions

Several device parameters are used in evaluating the performance of OTFTs; namely mobility μ that describes the drift velocity of charge carriers flow driven by the channel electrical field, threshold voltage V_{th} that is the essential gate-source voltage required to induce mobile charges at the insulator/polymer interface in order to form the channel. The value of the threshold voltage can be obtained from the intercept of the plot of $I_{DS}^{1/2}$ against V_{GS} as $Figure 3.7(b)$. For the threshold voltage, ideally, the V_{th} should be zero. However, nonzero V_{th} is common in practical devices. For p-channel OTFT, if deep traps are present at the insulator/polymer interface, the channel is conductive only until all those deep traps are filled. In this case, the threshold voltage whould have a negative value. Conversely, devices can exhibit a positive V_{th} due to contamination of the polymer film by unintentional doping by air/moisture and impurities produced during fabrication, at the interface[7]. The channel conductance g_D in the linear region is defined as,

$$g_D = \frac{\partial I_D}{\partial V_D}\Big|_{V_G = constant} \tag{3.8}$$

For small values of V_D, it is possible to assume $V_D^2/2$ to zero in *Equation*(3.1). The channel conductance is then expressed as,

$$g_D = \mu C_0 \frac{W}{L}(V_G - V_{th}) \tag{3.9}$$

From the plot of channel conductance g_D against gate voltage V_G, the field effect mobility and threshold voltage can thus be calculated from the slope and intercept respectively.

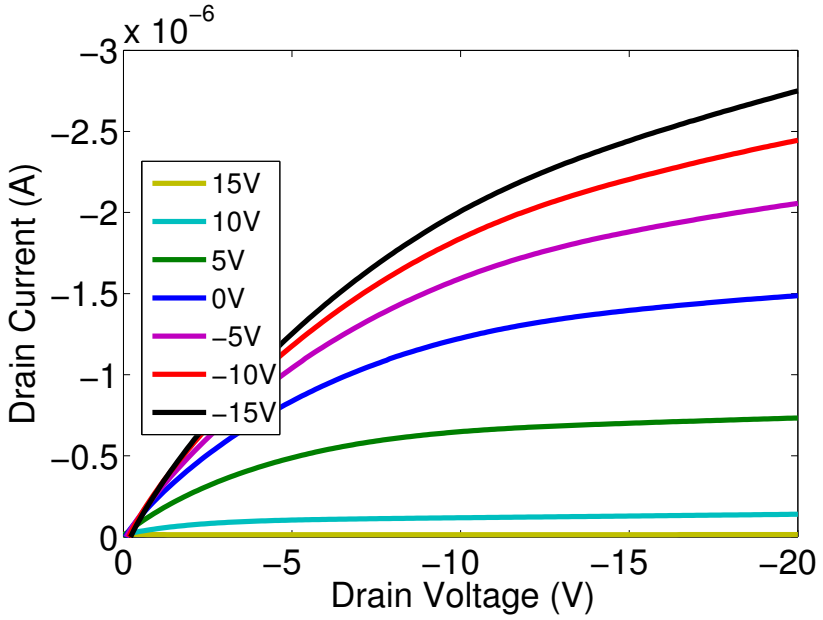

Figure 3.5: Output characteristics of P3HT based (BGBC) TFT, $W/L = 150$, 50nm SiO_2 as dielectric, P3HT/Xylene solution1mg/mL

Although the charge transport mechanism of conjugated polymer is different from conventional thin film transistor, the polymer TFT yields a similar TFT characteristics. The output characteristics of P3HT OTFTs as presented in *Figure*(3.3) and *Figure*(3.5), the device is normally on; a positive gate voltage is necessary to turn the device off. Therefore, a reverse voltage is needed to deplete the bulk of the polymer film. This part can be examined by capacitance-voltage characteristics of the P3HT based Metal Insulator Semiconductor (MIS), it is clearly indicated that the flat band voltage is positive, i.e. an accumulation layer exists at the polymer/dielectric interface even at zero gate voltage.

3.3.2 Disordered Transistor Model

For the disordered semiconductors material, the effective mobility varies significantly with the carrier concentration. Therefore, the universal mobility law should be applied in the analytical model for organic thin film transistor. In this thesis, the analytical model proposed

in [10] is used to analyse the organic thin film transistor results. In the linear region, the drain current equation is given as *Equation*(3.10)

$$I = \frac{W}{L}\frac{K_{UML}C_o^{2m+1}}{(2m+1)(2m+2)(2\varepsilon_0\varepsilon_s k_B T_c)^m}\left[(V_G - V_{th})^{2m+2} - (V_G - V_{th} - V_D)^{2m+2}\right] \tag{3.10}$$

The drain current in saturation region is given as *Equation*(3.11)

$$I = \frac{W}{L}\frac{K_{UML}C_o^{2m+1}}{(2m+1)(2m+2)(2\varepsilon_0\varepsilon_s k_B T_c)^m}\left[(V_G - V_{th})^{2m+2}\right] \tag{3.11}$$

and the power exponent m is related to the distribution of traps,

$$m = \frac{T_c}{T} - 1 \tag{3.12}$$

Where C_o is gate oxide capacitance per unit area, K_{UML} is the constant in universal mobility law, W/L is the width/length ratio of the thin film transistor channel, T_c is the characteristic temperature representing the distribution of the traps, m is the power exponent in universal mobility law, I is the drain current, V_G, V_D and V_{th} are the gate voltage, drain voltage and the threshold voltage, respectively. This analytical model can also be applied to the conventional material device. When $T_c = T$, the *Equation*(3.10), (3.11) are the same as the standard FET models, which can be given as *Equation*(3.13), (3.14).

$$I = \frac{W}{L}\frac{K_{UML}C_o}{2}\left[(2V_G - V_{th})V_D - V_D^2\right] \tag{3.13}$$

$$I = \frac{W}{L}\frac{K_{UML}C_o}{2}\left[(V_G - V_{th})^2\right] \tag{3.14}$$

With differencing and taking the logarithmic on the both side of *Equation*(3.11), the essential parameters for experimental results analysis can be obtained.

$$log(\frac{dI}{dV_G}) = log(\frac{W}{L}\frac{K_{UML}C_o^{2m+1}}{(2m+1)(2\varepsilon_0\varepsilon_s k_B T_c)^m}) + (2m+1)log(V_G - V_T) \tag{3.15}$$

Using this *Equation*(3.15), the power exponent m and the constant K_{UML} can be obtained from the slope and intercept of the *Figure*(3.10), respectively. The effective mobility can be expressed in terms of materials parameters K_{UML} and T_c, as in *Equation*(3.16).

$$\mu = \frac{K_{UML}C_o^{2m}}{(2m+1)(m+1)(2\varepsilon_0\varepsilon_s k_B T_c)^m} \tag{3.16}$$

Or in another format as in *Equation*(3.17).

$$\mu = \frac{K_{UML}C_o^{2(T_c/T-1)}}{(2T_c/T-1)(T_c/T)(2\varepsilon_0\varepsilon_s k_B T_c)^{(T_c/T-1)}} \tag{3.17}$$

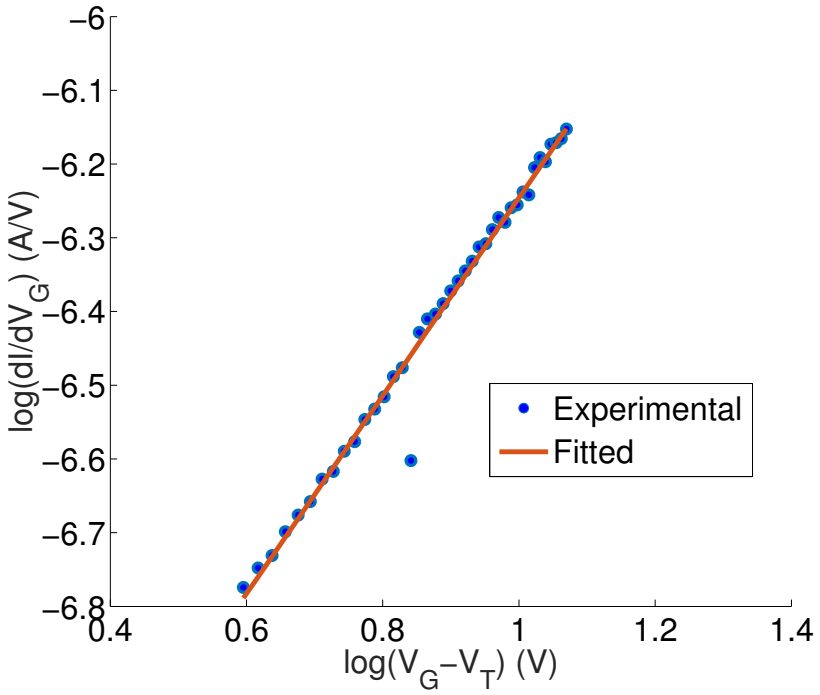

Figure 3.6: Plot of $log(dI/dV_G)$ against $log(V_G - V_T)$ for P3HT organic thin film transistor measured at $V_D = -20V$ at room temperature $T = 300K$. The blue dot is the experimental data, the red line is the fitted result.

The experimental results presented in figures from $Figures$(3.6) to (3.8) were obtained from BGBC P3HT thin-film transistor. The P3HT solution of concentration $0.5mg/mL$ was spun-coated onto the device. From $Figure.$(3.6), the value m was found to be 0.17, based on the $Equation$(3.12), the characteristic temperature for trap distribution was found to be $351K$, and the corresponding Meyer-Neldel energy is $30.7meV$. The Value of K_{UML} was also found to be 2.29×10^{-11} (SI Units). With those data extracted from the Figure above, this analytical model can be compared to the standard one. The validation of the experimental and simulation results using the standard and disordered models are presented in $Figure.$(3.7) and $Figure.$(3.8), for $V_D = -20V$. As seen from this figure, a significant divergence of the experimental data from the standard model results can be observed, which is the difference between the conduction modes. In the disordered model, the current is dominated by the drift mechanism even at low voltages, while, in the standard model, the current is dominated by diffusion mechanism at low voltages, and followed by drift mechanism at higher voltages. The disordered model appears to describe better the operation of the P3HT thin film transistor.

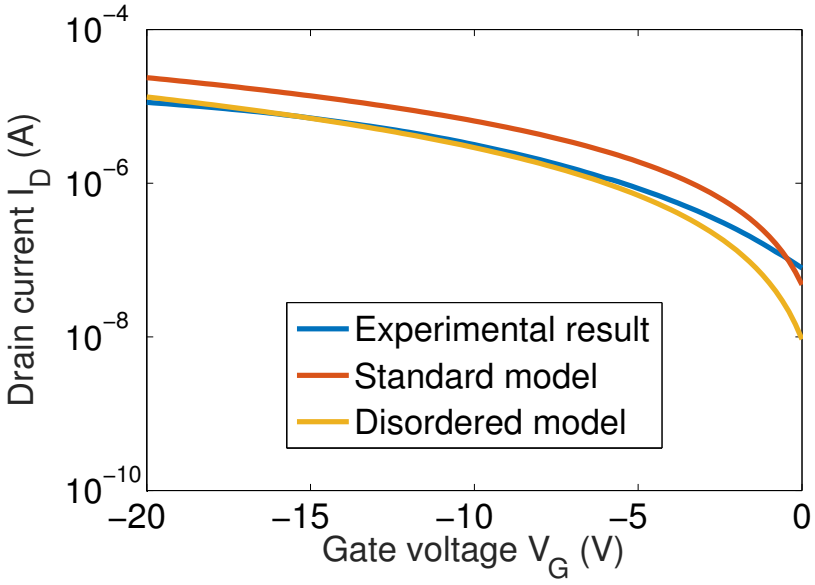

Figure 3.7: Sub-threshold plot of the P3HT TFT. The blue is experimental data, yellow is the disorder model result and red is the standard model results.

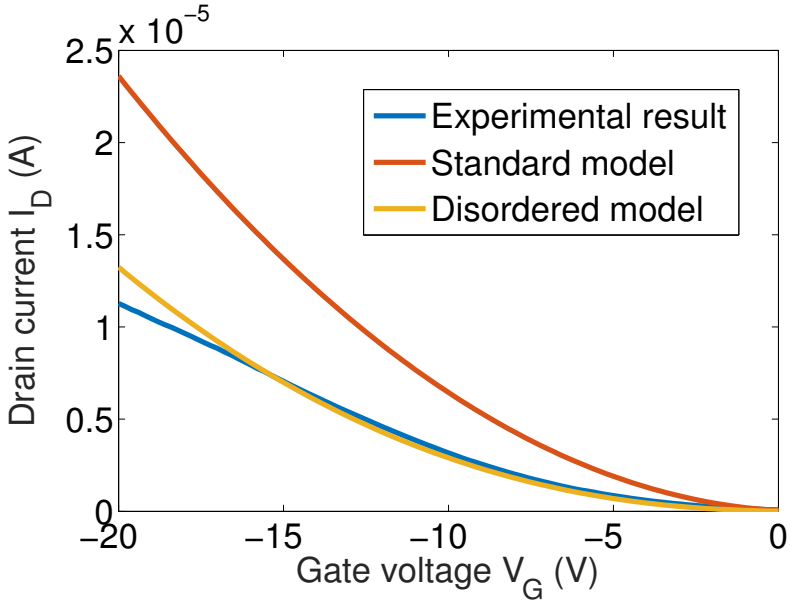

Figure 3.8: Sub-threshold plot of the P3HT TFT. The blue is experimental data, yellow is the disorder model results and red is the standard model results.

3.3.3 Transfer Characteristics

The transfer characteristics of the P3HT based BGBC TFT is shown in *Figure*(3.9). For $V_D = -20V$, the gate voltage sweep started from $+20V$ towards forward direction, and the drain current decreases and then stays roughly constant. This region is indicated as *Region*(c). The positive gate voltage depletes the holes from the interface and the dopant ions move towards the oxide/semiconductor interface. In *Region*(b), which is known as the sub-threshold region, the change in the gate voltage towards forward direction results in a sharp rise in the drain current. In the *Region*(a), the drain current gradually saturates with further increase on the gate voltage. A high ratio of the on state drain current to the off state is key for good circuit operation. The on/off ratio yielded by the device shown in *Figure.*(3.9) is 1.6×10^3.

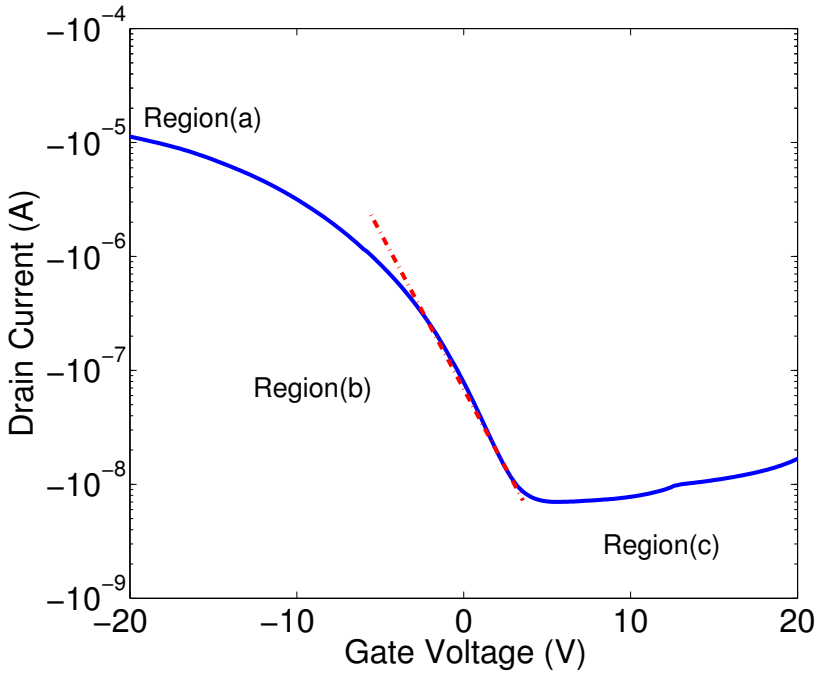

Figure 3.9: Sub-threshold plot of BGBC P3HT TFT with with gate voltage sweep from $-20V$ to $20V$ for the drain voltage $V_D = -20V$.The W/L ratio is 150, and the thickness of silicon dioxide is $50nm$. The concentration of polymer solution spin coated on the sample is $0.5mg/ml$, the solvent is xylene. The on/off ratio is 1.6×10^3.

Compared to other similar P3HT TFT results in the literature, higher on/off ratio has been reached of about 10^6 [4]. The better performance comes from the use of hexamethyldisilazene (HMDS) to modify the oxide/polymer surface. During the fabrication of organic thin film transistor, the dielectric surface is exposed to the air, which results in existence of Si-OH bond and water on the surface. In the 1990s, the method using hexamethyldisilazene to modify the SiO_2 substrate was proposed, which aimed at forming an hydrophobic layer

upon the dielectric surface. This surface modification significantly reduces the dielectric suface conductivity and improves mobility. Such chemicals are normally called self-assembled monolayers (SAM), which are molecular assemblies formed spontaneously on surfaces by adsorption and are organized into more or less large ordered domains.

The threshold voltage defines the transition point where charge transport changes from diffusion to drift. If negative charges are present in the gate oxide they will induce an accumulation layer and this must be removed prior forming an inversion layer. Assuming there is no work function difference, the applied voltage appears across the oxide and the semiconductor:

$$V_G = V_i + \psi_s \tag{3.18}$$

Where V_i is the voltage across the oxide and ψ_s is the potential to induce accumulation or inversion.

The threshold voltage V_{th} and mobility μ_{sat} can be estimated from the intercept and slope of the plots of both g_m against V_G and $\sqrt{I_D}$ against V_G as shown in $Figure$(3.10). Based on the experimental results presented in $Figure$(3.10), the mobility μ and threshold voltage V_{th} were found approximately to be $5.2 \times 10^{-3} cm^2 V^{-1} s^{-1}$ and $0.94V$ respectively. The on/off ratio estimated from $Figure$(3.9) is around 10^3. Normally, the device prepared in ambient air exhibts a very low on/off ratios of $10 - 100$. The steps to acheive the high on/off current ratio in P3HT TFTs are, firstly, reducing the chemical residual, and secondly, increasing thickness of the dielectric layer to reduce the leakage current.

A sub-threshold swing S of can be estimated from the plot of V_G against the drain current I_D in $Figure$(3.9). The parameter is used to describe the essential gate voltage needed to induce drain current change of one order of magnitude. The value of sub-threshold swing determines how sharply the device can be turned on/off. The theoretical minimum value of S is $60mV/dec$, when in the room temperature condition ($T = 300K$). While, the experimental S obtained from $Figure$(3.9) is $4.64V/dec$.

$$S = \frac{\partial V_G}{\partial (log_{10} I_D)}\bigg|_{V_D = constant} \tag{3.19}$$

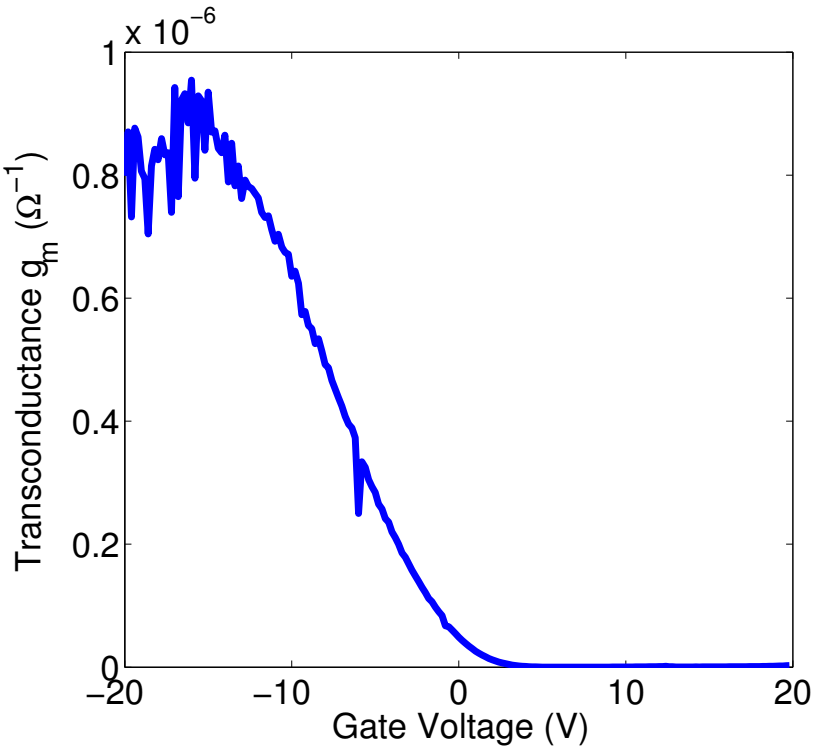

(a)

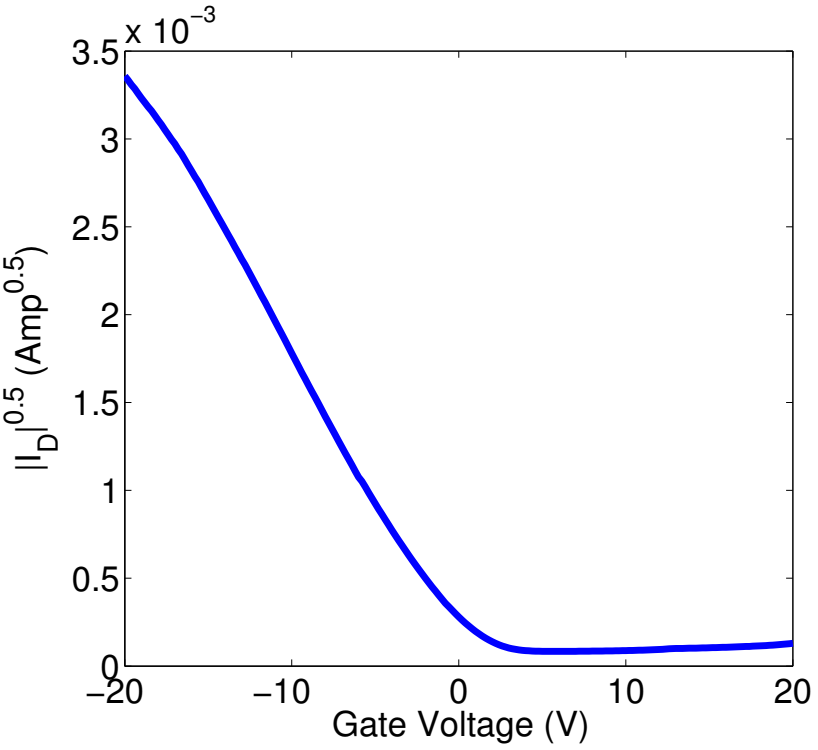

(b)

Figure 3.10: (a)Plot of transconductance g_m against gate voltage V_G yields the mobility and threshold voltage. (b) Plot of $\sqrt{|I_D|}$ against gate voltage V_G

3.3.4 Metal/polymer contacts

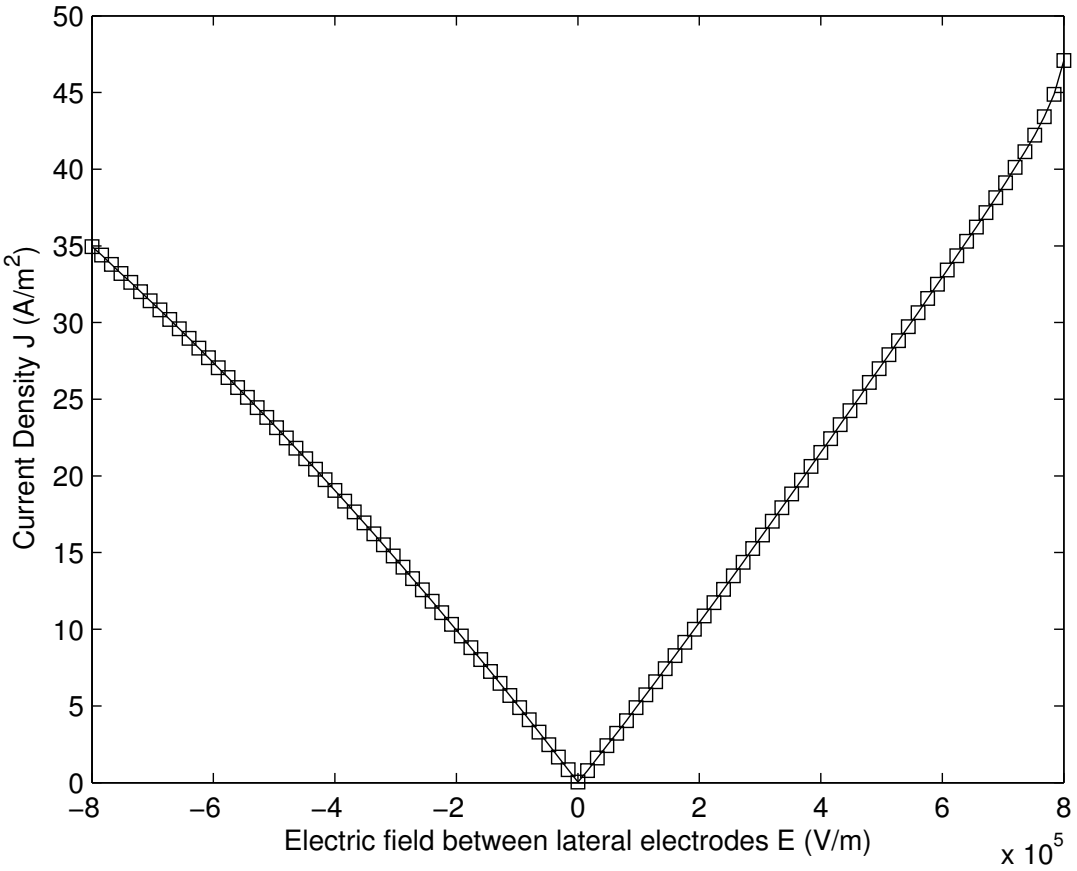

Figure 3.11: Linear plot of the current density against electric field between lateral gold-P3HT-gold structure, the conductivity estimated from the slope, was $3.78 \times 10^{-8}\Omega^{-1}m^{-1}$.

The electric field against current density characteristic of Au/P3HT/Au device is as shown in $Figure(3.11)$. The polymer material applied are not undoped, the polarity of charge carriers injected from the source metal contact determines whether the device a p-channel one or n-channel one. For instance, if the work function of the contact metal is close to the LUMO level, the electrons will be more easily injected (giving n-channel operation), and conversely, if it is closer to HOMO level, holes will be preferentially injected, giving p-channel behaviour. Gold is widely used as a contact metal in OTFTs, and its work function is normally quoted as $\sim 5.1 - 5.2eV$, which is very close to the HOMO level of P3HT. However, it was found that exposing the gold contact to air and contact with organic solvent will reduce the work function to $\sim 4.5eV$.

3.3.5 Influence of solution concentration on the device characteristics

All P3HT TFT are solution processed, therefore the concentration of solution that is spin-coated onto the sample has an influence on device performance. One of the most obvious effects is the thickness of the polymer. Increasing mobility μ with increasing P3HT layer thickness was found for thin layers in bottom-gate transistors on silicon substrates. The higher mobility may result from interfacial strain, thin layers/monolayers are poorly ordered whereas the presence of a highly ordered bulk in thicker films causes an ordering effect in the interfacial layer[8]. All the output and transfer characteristics of BGBC P3HT thin-film transistors with P3HT solution concentration varying from $3mg/mL$ to $0.5mg/ml$, are presented in figures from $Figures$(3.12) to (3.15).

Sample	Specification (mg/ml)	$V_{th}(V)$	on/off ratio	SS$(V/decade)$
TFT17	3	33.71	24.8	12.02
TFT18	2	13.02	79.1	8.65
TFT21	1	7.63	277	6.59
TFT23	0.5	0.94	1.6×10^3	4.64

Table 3.1: Parameters extracted from the spun-coated P3HT TFTs with different concentration of the solution.

The on/off ratio shows a strong dependency on the film thickness [9]:

$$\frac{I_{on}}{I_{off}} = \frac{\mu}{\sigma} \frac{C_0^2}{qN_A z_p^2} V_D^2 \tag{3.20}$$

Where I_{on}/I_{off} is the on/off ratio of the drain current, σ is the conductivity of the polymer film, z_p is the thickness of the polymer film, C_0 is the gate insulator capacitance, N_A is the dopant concentration. The polymer film thickness of the devices have not been measured during the experiment, there is no direct experimental result support for $Equation$(3.21). Based on the TFT results summarised from various devices in $Table$(3.1), with the polymer solution concentration decreasing, the on/off ratio increases significantly. In addition, it is widely believed that the thickness of a spin-coated polymer film is determined by the selection of solvent, time and speed of spin-coating, and the concentration of the solution. Therefore, the experimental results presented in $Table$(3.1) may support $Equation$(3.21) indirectly. Based on experimental results shown in $Figure$(3.12) to $Figure$(3.15), the mobilities of P3HT based TFT with thicker films may not be accurately obtained from the experiment due to absence of saturated drain current in the transfer I-V curves, therefore, no conclusion about the mobility dependence can be made.

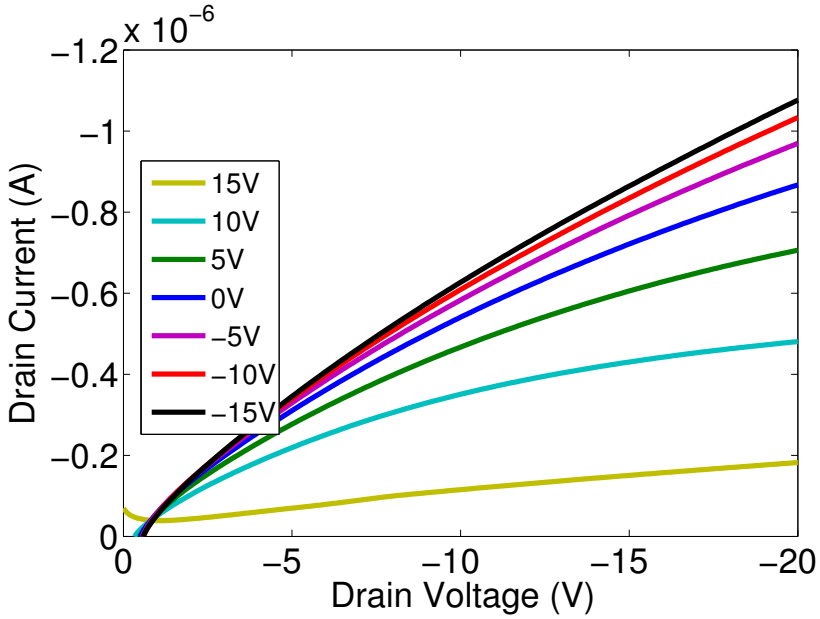

(a) Output Characteristics

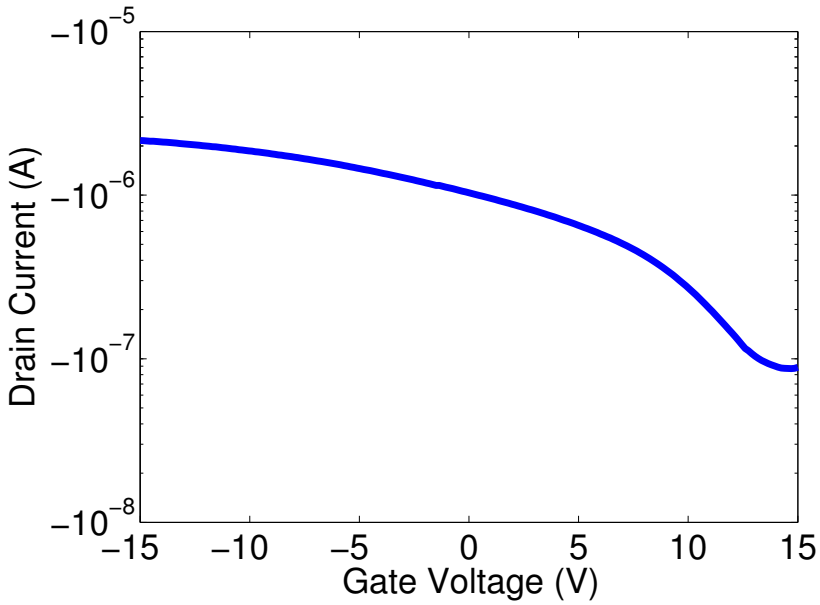

(b) Transfer Characteristics at $V_D = -20V$

Figure 3.12: The P3HT based TFT, the device structure is BGBC (bottom gate bottom contact), $W/L = 150$, and $50nm$ silicon dioxide is used as gate dielectric. The polymer solution of concentration $3mg\ /mL$ was spin-coated onto the device.

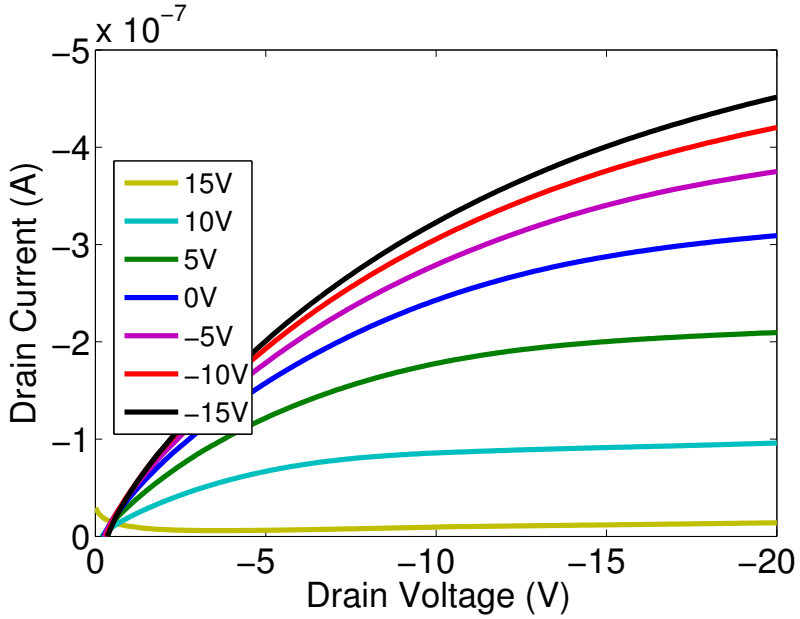

(a) Output characteristics

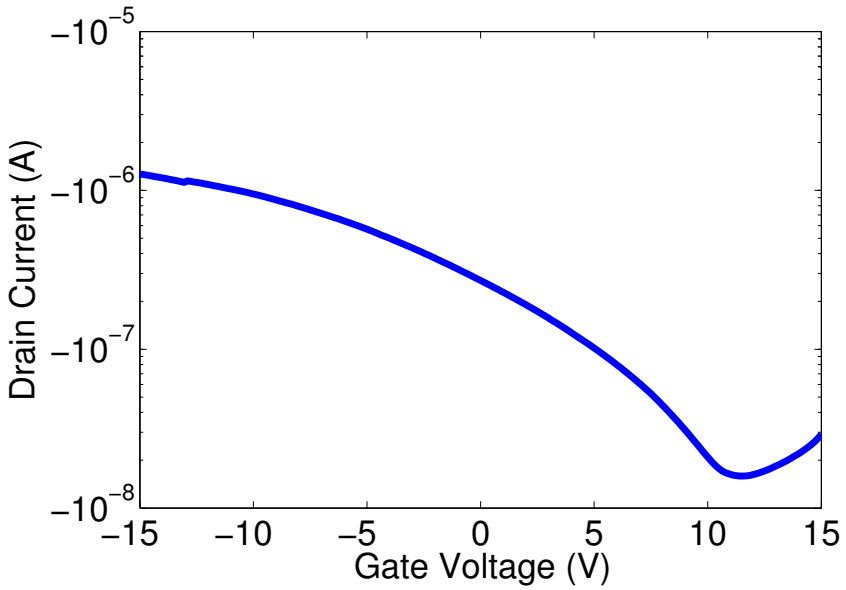

(b) Transfer Characteristics at $V_D = -20V$

Figure 3.13: The P3HT based TFT, the device structure is BGBC (bottom gate bottom contact), $W/L = 150$, and $50nm$ silicon dioxide is used as gate dielectric. The polymer solution of concentration $2mg\ /mL$ was spin-coated onto the device.

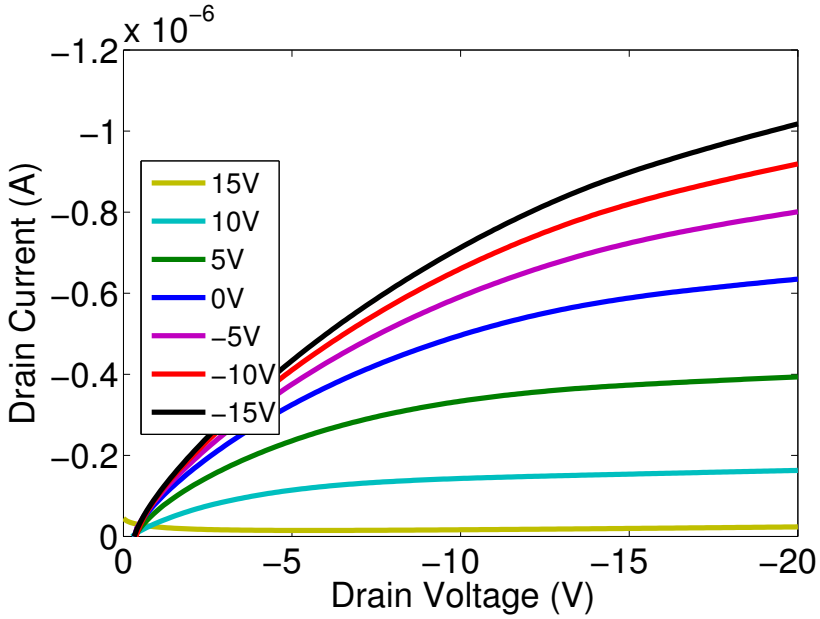

(a) Output Characteristics

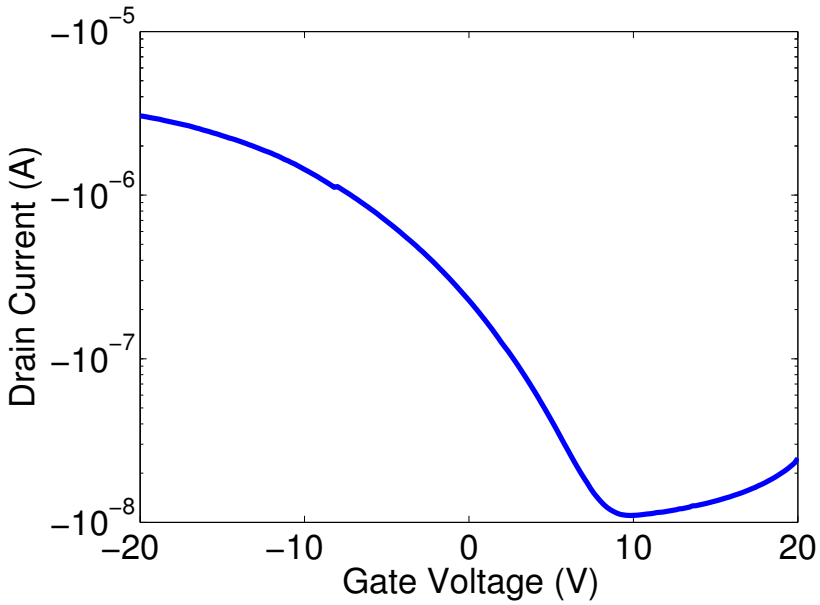

(b) Transfer Characteristics at $V_D = -20V$

Figure 3.14: The P3HT based TFT, the device structure is BGBC (bottom gate bottom contact), $W/L = 150$, and $50nm$ silicon dioxide is used as gate dielectric. The polymer solution of concentration $1mg\ /mL$ was spin-coated onto the device.

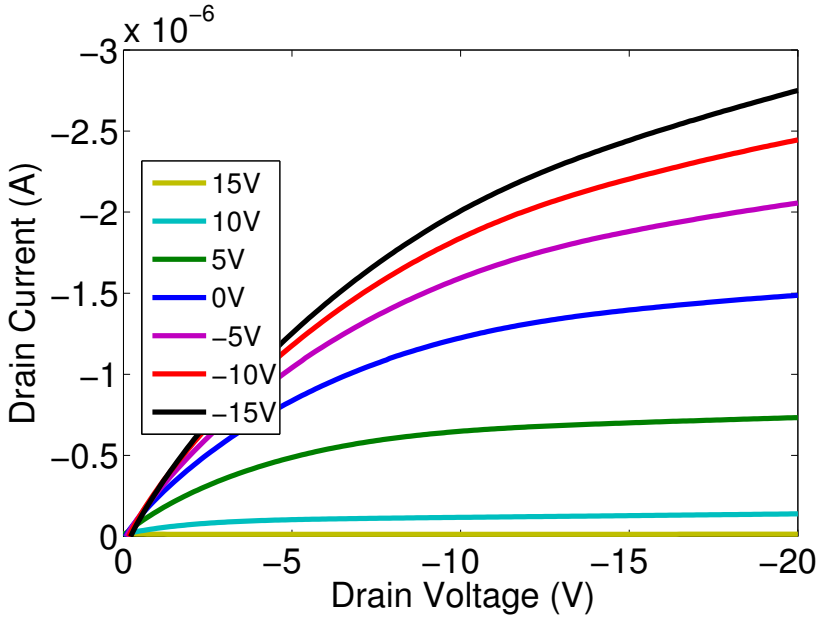

(a) Output characteristics

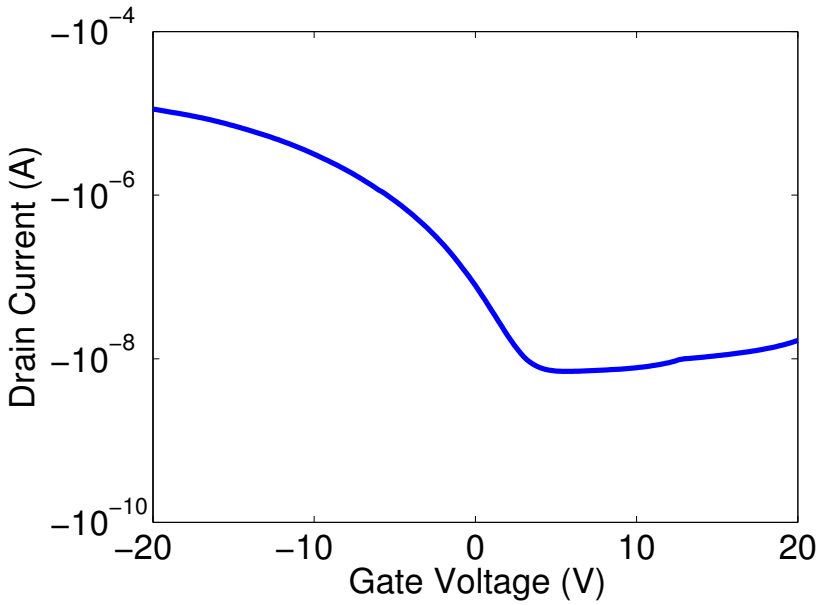

(b) Transfer Characteristics at $V_D = -20V$

Figure 3.15: The P3HT based TFT, the device structure is BGBC (bottom gate bottom contact), $W/L = 150$, and $50nm$ silicon dioxide is used as gate dielectric. The polymer solution of concentration $0.5mg\ /mL$ was spin-coated onto the device.

3.4 Conclusion

The thin film transistors using P3HT were fabricated with BGBC and BGTC configurations. The mobility and threshold voltage obtained from the transconductance and channel conductance plots were different. The mobility extracted from the transconductance was higher than that from channel conductance, while the threshold voltage was viceversa. The channel conductance is obtained in the linear region where the drain field dependency is small and significantly affected by the polymer bulk conductivity unlike the transconductance plots obtained in the saturation region. The effect of the solution concentration has been investigated, the low polymer solution concentration gives a better OTFT performance.

References

[1] S. D. Brotherton, Introduction to Thin Film Transistor, Spinger publishing, 2013.

[2] L. Mariucci, D. Simeone, S. Cipolloni, L. Maiolo, A. Pecora, G. Fortunato, S. Brotherton and C. R. Newman, "Introduction to organic thin film transistors and design of n-channel organic semiconductors," Chemistry of Materials, vol. 16, pp. 4436-4451, 2004.

[3] T. J. Richards, and H. Sirringhaus, "Analysis of the contact resistance in staggered, top-gate organic field-effect transistors,"Journal of Applied Physics, vol. 102, no. 9, pp. 094510, 2007.

[4] H. Sirringhaus, N. Tessler, and R. H. Friend, "Integrated optoelectronic devices based on conjugated polymers,"Science, vol. 280, pp. 1741-1744, 1998.

[5] S. K. Park, T. N. Jackson, J. E. Anthony, D. A. Mourey(2007) "High mobility solution processed 6,13-bis(triisopropyl-silylethynyl) pentacene organic thin film transistors,"Applied Physics Letters, vol. 91, no. 6, pp. 063514, 2007.

[6] T. Sekitani, and T. Someya, "Stretchable and foldable displays using organic transistors with high mechanical stability,"SID Symposium Digest of Technical Papers, vol. 42, no. 1, pp. 276-279, 2011.

[7] C. R. Newman, et al., "Introduction to organic thin film transistors and design of n-channel organic semiconductors,"Chemistry of Materials, vol. 16, pp.4436-4451, 2004.

[8] H. G. O. Sandberg, G. L. Frey, M. N. Shkunov, H. Sirringhaus, R. H. Friend, "Ultrathin regioregular poly(3-hexyl thiophene) field-effect transistors,"Langmuir, vol. 18, no. 26, pp. 10176-10182, 2002.

[9] A. R. Brown, C. P. Jarrett,D. M. de Leeuw and M. Matters, "Field-effect transistors made from solution-processed organic semiconductors,"Synthetic Metals, vol. 88, no. 1, pp. 37-55, 1997.

[10] M. Raja, W. Eccleston, "Analytical device models for disordered organic Schottky diodes and thin-film transistors for circuit simulation,"IET Circuits, Device&Systems, vol. 6, iss. 2, pp. 122-129, 2011.

Chapter 4

Organic Schottky Diode

This chapter focus on the theory and characteristics of P3HT Schottky diodes. Charge transport across the metal-semiconductor junction is discussed, including image force lowering of the Schottky barrier. Forward and reverse current voltage characteristics of P3HT Schottky diode are analysed, as well as the capacitance-voltage characteristics. The effect of varying device structure (including vertical, lateral and ring) and methods of semiconductor formation (spin-coating and drop casting) are also discussed.

4.1 Introduction

The organic Schottky diode has drawn considerable attention from the researchers working in the optoelectronics field. It also has the potential to play an important role in future organic circuits and to be an alternative to the metal/inorganic semiconductor junction device. A typical Schottky organic diode consists of an organic semiconductor film sandwiched between two different types of metal electrodes. Highly regioregular poly-3-hexyl-thiophene (P3HT) is well known as one of the most promising materials for application in organic photodiode and solar cell. P3HT has been intensively studied, and field-effective mobility of the order of $0.1cm^2/Vs$ has been reported[17]. To form a Schottky barrier with a p-type polymer, a low work function metal (i.e. aluminium) is used as the Schottky metal electrode. The other electrode-semiconductor interface, is an ohmic contact, which must have negligible junction resistance compared to the rectifying contact; the metal work-function should be close to the HOMO of the organic semiconductor.

The main focus of this chapter is to investigate the influence of the metal/semiconductor device structure on the its performance and stability and understand the spread of depletion region in complex device structure. Three different device structures are used including the vertical, lateral, and lateral ring structures. The vertical structure has been intensively used for decades for- investigation of metal/semiconductor characteristics in both organic/inorganic field. Lateral structures are contributed by two researchers- Dr R.Meyers and Dr.D.Donaghy in the Organic Electronics group at the University of Liverpool and is achieved by an undercut method in photoresist lift-off. The novel ring structure is a variant based on the lateral structure. The device fabrication procedures are presented in detail in this chapter. The current-voltage and capacitance-voltage characteristics of the ring structured P3HT diodes are obtained and analysed for extraction of several important parameters, such as shunt and series resistance, ideality factor, acceptor concentration, built-in potential and potential barrier height.

4.2 Theory of the metal-semiconductor contact

With a low-work function metal contacting with p-type semiconductor, a potential barrier is formed at the semiconductor-metal interface due to the difference in work function between the metal and the semiconductor[1]. The barrier is responsible for controlling the current as well as its capacitance behaviour. *Figure*(4.1) is the energy level diagram of semiconductor-metal contact before contact and after contact.

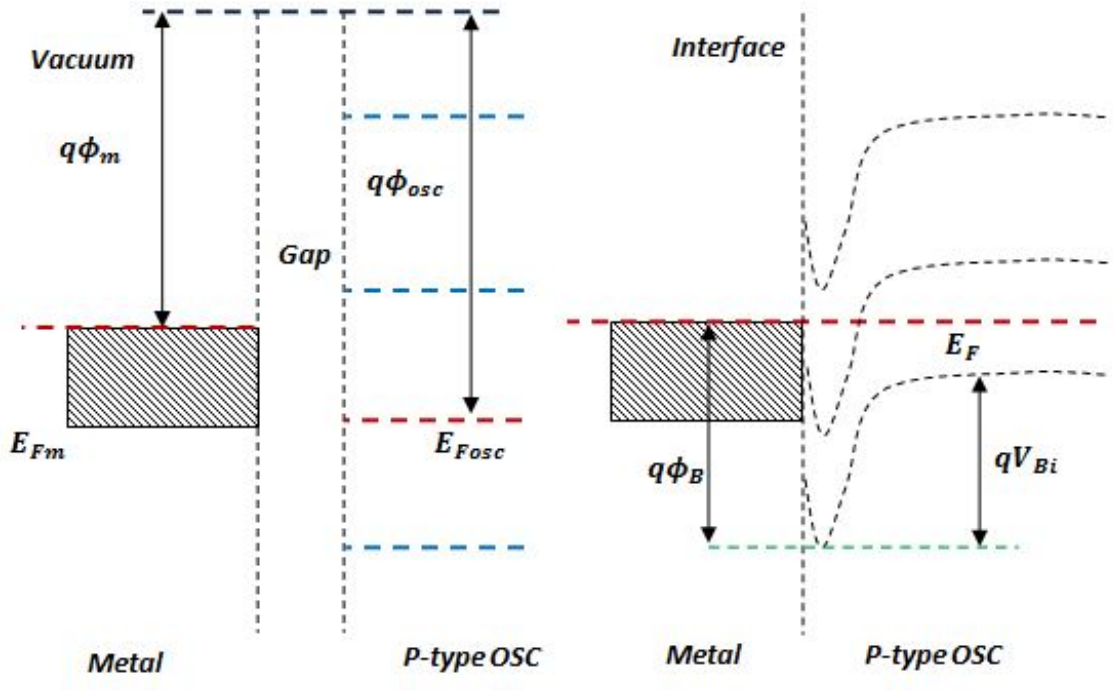

Figure 4.1: Energy level diagram of P-type semiconductor and low work function metal before contact (left hand-side) and after contact(right hand-side). $q\phi_m$ is the work-function of metal,E_F is the Fermi-level after contact,V_{bi} the built-in potential and ϕ_B is the barrier height of the junction.

For a p-type polymer semiconductor in contact with a low work function metal like aluminium, the electron flow flow the metal into semiconductor, an increasing positive charge is built up on the metal side, an equal and opposite charge must exist in the semiconductor depletion region. The energy level bend upwards, the electrons flowing from metal to semiconductor will face a potential barrier which must be overcome for charge carrier flow.

An energy level diagram of a low function metal in contact with p-type semiconductor at different bias condition is presented in $Figure(4.2)$. W_{D3}, W_{D2} and W_{D1} represent the depletion region width for reverse, zero and forward bias, respectively. A forward bias can decrease the width of depletion region, the potential barrier height is also lowered with the peak of barrier moving from the metal/semiconductor interface. Applying a reverse bias causes an opposite changes in all three aspects.

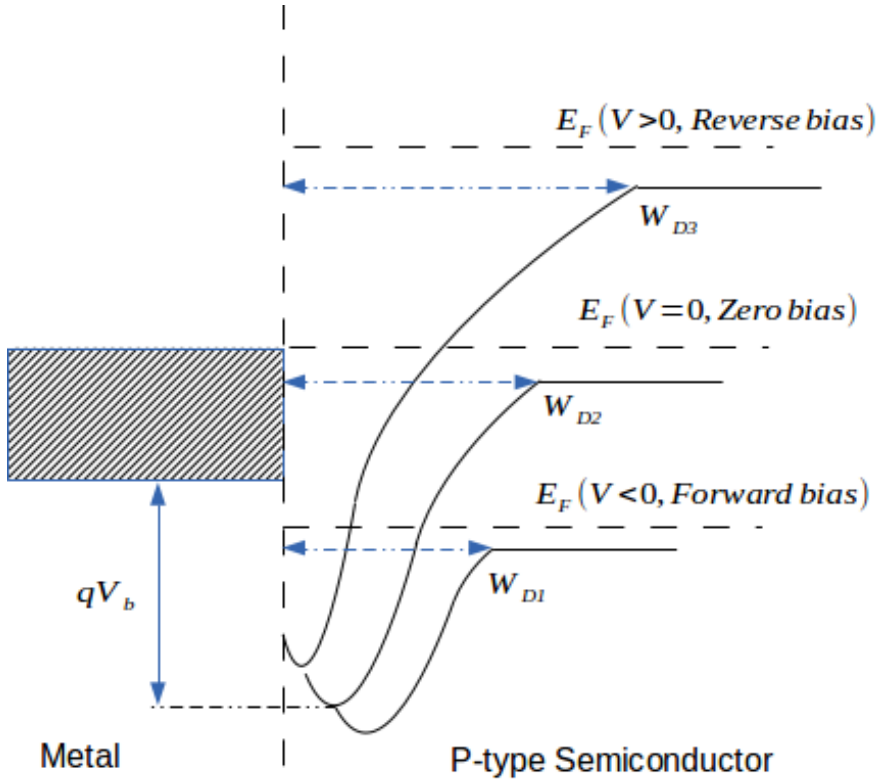

Figure 4.2: Energy level diagram of a metal in contact with a p type semiconductor under three different bias conditions.

Forward bias

With the forward bias, all the energy levels have been raised, the numbers of carriers with enough energy to overcome such a barrier increases exponentially, as predicted from *Equation*(4.1)

$$p = N'(0)k_B T_0 exp(-\frac{E_F}{k_B T_c}) \tag{4.1}$$

Where p is hole concentration, $N'(0)$ is the rate of change of energy distribution of carrier, k_B is the Boltzmann constant, T_0 is the characteristic temperature describing the carrier distribution, T_c is the characteristic temperature describing the distribution of the traps. In this condition, it is widely believed that the charge transport is dominated by the diffusion of charge carriers. As the total amount of carrier has an exponential relationship with increasing energy as in *Equation*(4.1) The forward current density flow across the semiconductor/metal contact is given as *Equation*(4.2),

$$J_F = J_0 exp(\frac{qV}{\eta k_B T}) \tag{4.2}$$

where q is the electron charge, η is the ideality factor, V_{app} is the applied voltage, T is the absolute temperature, and J_0 is the reverse saturation current density given as *Equation*(4.3).

$$J_0 = A^* T^2 exp[\frac{-q\phi_B}{k_B T}] \tag{4.3}$$

where A^* is the Richardson constant and ϕ_b is the potential barrier height. The current is related to the applied voltage V_{app} and is given by Maxwell Boltzmann relationship applied to the quasi Fermi level. A quasi Fermi level E_F is used to determine the carrier density at the peak of the potential barrier, as shown in *Equation*(4.1). Based on the exponential distribution model for density of states (DOS) and Maxwell Boltzmann approximation, the forward current density can be expressed as:

$$J_F \propto exp(\frac{qV_{app}}{k_B T_0}) \tag{4.4}$$

The value of T_0 can extracted from the current-voltage characteristics plot. In addition, the relationship between the characteristic temperature of the distribution of carriers and traps, is given as *Equation*(4.5):

$$\frac{1}{T_0} = \frac{1}{T} - \frac{1}{T_c} \tag{4.5}$$

The corresponding characteristic temperature of distribution of traps and Meyer Neldel Energy can be obtained the using above equation.

Reverse bias

The calculation of diode current density depends on the simple approximation that its value depends of the deficit in the density of electrons at the peak of the barrier imposed by presence on the depletion region field which sweeps away carreiers from this point. The value of this deficit is obtained by extending the quasi Fermi level to this point. The quasi fermi level is particularly useful when the densities of electrons and/or holes are out of equilibrium. At the peak of the barrier the electrons, which are assumed here to be majority carrier, is close to zero because they experience the force of their image field. They then waterfall into the metal. The electron quasi Fermi level however remains constant. Thermodynamically the electron generation rate, at the peak, may be assumed to be proportional to the concentration deficit $n_{virtual}$ at the peak. The current density in the reverse direction can be obtained from:

$$J_R \propto exp(\frac{q\Delta\phi}{k_B T}) \tag{4.6}$$

Here, Thus, an equation for the current density can be obtained when the image force lowering is taken into account, the detailed derivation of *Equation*(4.7) is presented in Appendix B, which is given as below:

$$J_R = J_0 exp[\frac{q}{k_B T}(\frac{q^3 N_A (V - V_{bi} - \frac{k_B T}{q})}{8\pi^2 \varepsilon_0^3 \varepsilon_s^3})^{\frac{1}{4}}] \tag{4.7}$$

Here, J_R is the reverse current density, n_A the dopant concentration, V_{bi} the built-in potential, ε_0 permittivity of free space and ε_s dielectric constant of the semiconductor.

4.3 P3HT Schottky diode with a vertical structure

The Schottky diode with a vertical structure is the most common device for metal semiconductor contact characteristic analysis. The gap size between two electrodes is controlled by the thickness of semiconductor film as shown in $Figure(4.3)$. In order to avoiding the device being easily punched through by probe during measurement, a thick polymer film is essential for successful device fabrication.

4.3.1 Fabrication of P3HT based vertical structure Schottky barrier diode

The schematic of the vertical structure diode is shown in $Figure(4.3)$. The substrate with ohmic metal layer which includes either indium-tin oxide (ITO), silver (Ag) and Palladium (Pd) is throughout rinsed by the acetone, propanol and de-ionized water to remove any dirt on the substrate, and dried in the furnace. P3HT is then dissolved in xylene and followed by heating and stirring to make sure that the polymer is fully dissolved. Fully mixed solvent of organic semiconductor is drop cast onto the sample followed by heating or annealing of the sample. The reason why xylene is chosen as the solvent is that xylene has got a slower evaporation rate compared to chloroform and tetralin. A slow slovent evaporation rate will contribute to the uniformity of polymer film. Typically thickness of the drop-cast P3HT layer is approximately 10 μm. Then, 200nm aluminium (Al) contacts are formed using shadow mask evaporation. The device area of vertical diode is $3.14 \times 10^{-6} m^2$.

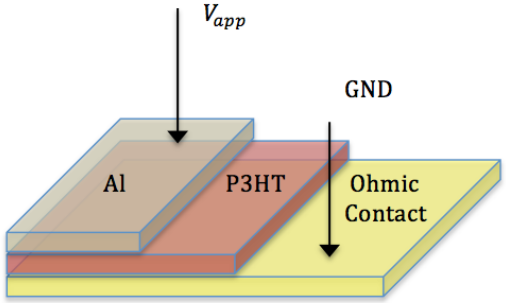

Figure 4.3: Structure of a vertical organic Schottky diode. The glass is used as substrate, top Al electrode is used as the Schottky contact, various materials are used as Ohmic contact such as ITO, Ag, Pd. The drop-cast of polymer film has a typical thickness of 10μm.

The performance of the device is strongly dependent on morphology and quality of the polymer film. Although, the spin-coating can give a more uniform polymer film, the polymer

film with thickness around $100nm$ can easily cause a short circuit between the two electrodes. Apart from the quality of the polymer film, the work functions of the electrodes are also important factors. The energy level diagram of metal/semiconductor/metal device with different back contacts is illustrated in the $Figure(4.4)$.

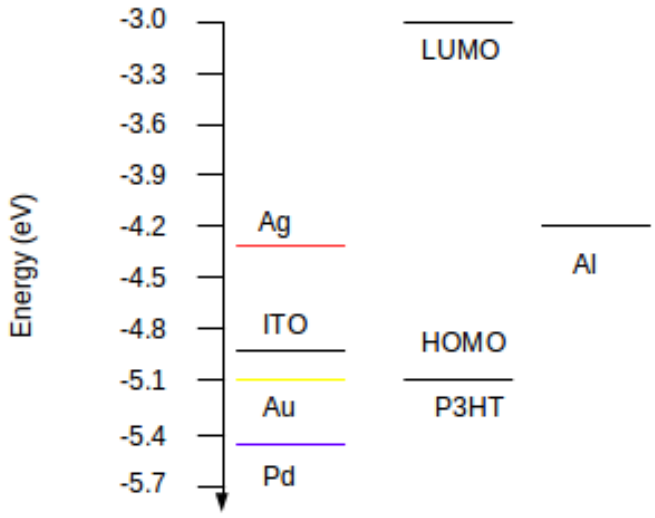

Figure 4.4: Energy level diagram of the materials studied (under non-equilibrium conditions).

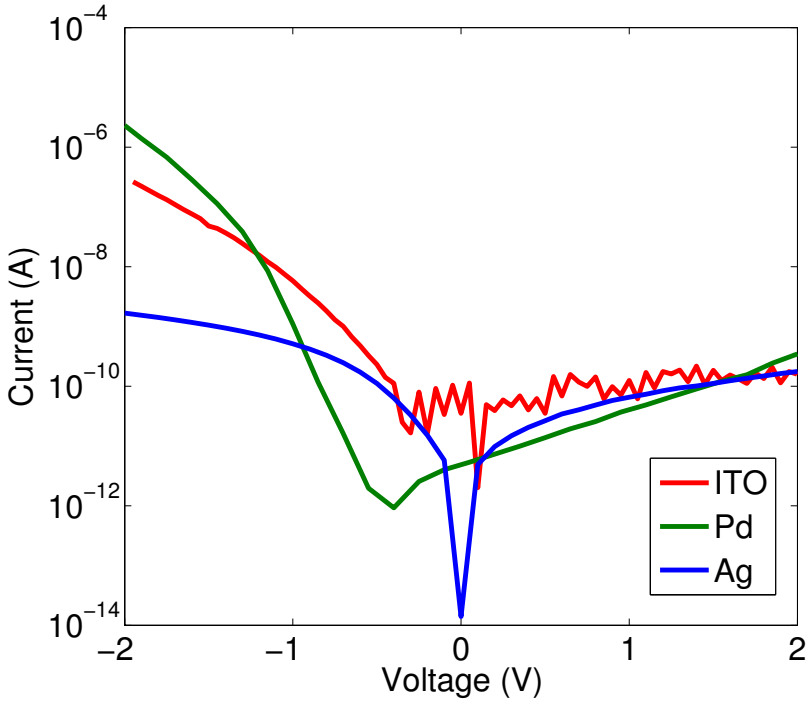

Figure 4.5: Current-Voltage characteristics of the metal/semiconductor/metal device that use indium tin oxide, palladium and silver as the back contact. The top contact is aluminium.

The current-voltage characteristics of metal/semiconductor/metal devices with different back contacts are presented in *Figure*(4.5). The current-voltage characteristics of Ag/P3HT/Al device shows that Ag contact is inferior as a ohmic contact compared to the other electrode material. The saturation current level in both bias direction are close. The main reason is that the work function of the silver is too low, even so close to the aluminium, which means the device has a potential barrier at the semiconductor/back contact interface.

4.4 P3HT Lateral Schottky diode experimental results

The performance of the vertical structured diode is strongly dependent on the film morphology, which is difficult to control due to variability in the drying conditions. In addition, the need for using a transparent indium-tin oxide electrode for optoelectronic applications, narrows the selection of the electrode material to be used. Therefore, the self-aligned lateral structure Schottky diode is proposed. The design and fabrication technique is mainly contributed by two research fellows in the Organic Electronic group, Dr.D.Donaghy and Dr.R.J.Myers. The main novelty in this design is in using the undercut technique which is widely used in lift-off metal patterning, to form a small gap with sub micron size between two electrodes, which is then filled with semiconductor. The cross-section diagram of the lateral structured diode is shown in *Figure*(4.6). The detailed fabrication procedure is presented in

the Appendix C. One of the advantages of using the lateral configuration is that the polymer film can be spin-coated onto the substrate, which can form a uniform coherent film with a good thickness control.

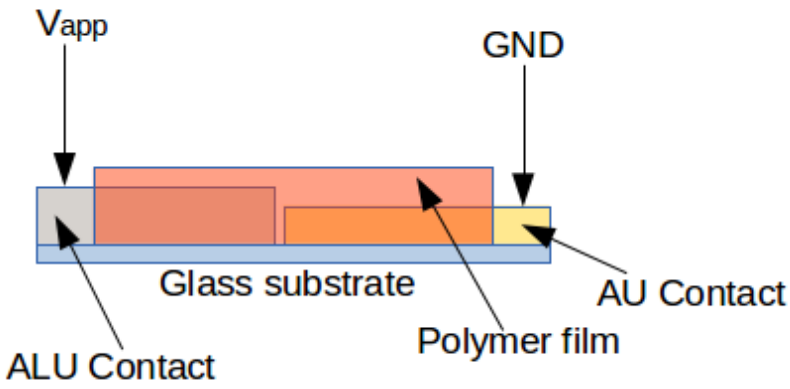

Figure 4.6: The cross-section diagram of a lateral structure Schottky barrier diode.

4.4.1 Results and analysis

Figure(4.7) (left)(middle) and *Figure*(4.7) (right) show the 3D/2D Atomic Force Microscopy (AFM) image of the active area representing the gap between the metal contacts, taken before the deposition of polymer film. The device area of the lateral diode is $4 \times 10^{-11} m^2$. The lateral structure Schottky barrier diode has some significant improvement, such that possibility of short circuit between the two electrodes is eliminated, and the quality of the polymer film is improved. In addition, the semiconductor film can be exposed to light if the Schottky barrier diode is used as a photodiode. Compared to the current-voltage characteristics obtained for the vertical device with gold back contact, the forward current of the lateral structure device is lower due to higher series resistance. This is thought to be due to the large neutral region and thinner semiconductor film. *Figure*(4.8) and *Figure*(4.9) present the current-voltage characteristic of the lateral structure Schottky diode in semi-logarithmic and linear. The on/off ratio is approximately 10^4. During the measurement, some of the results were unrepeatable and the hysteresis observed was large.

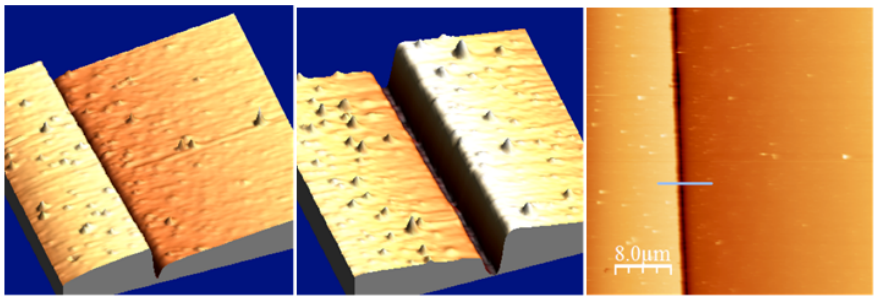

Figure 4.7: (Left) 3D plot of AFM image of Al/Au edge. (Middle) 3D plot of AFM image of Au/Al edge. (Right) 2D plot of device gap area, represented by the dark color.

Figures(4.10) and (4.11) demonstrate the air-stability of device with the aid of the current-voltage characteristics up to 120*hours*, when the sample is stored under normal ambient conditions. As observed from these results, the on-current decreased by more than one order of magnitude. The large hysteresis and poor air-stability of the lateral structured diode may due to that the complicated fabrication procedures left too much chemical residuals on the device surface and the sample surface was not smooth enough. Therefore, the modification about the device's fabrication procedure and structure must be done to produce stable P3HT Schottky diode with better air and bias stability.

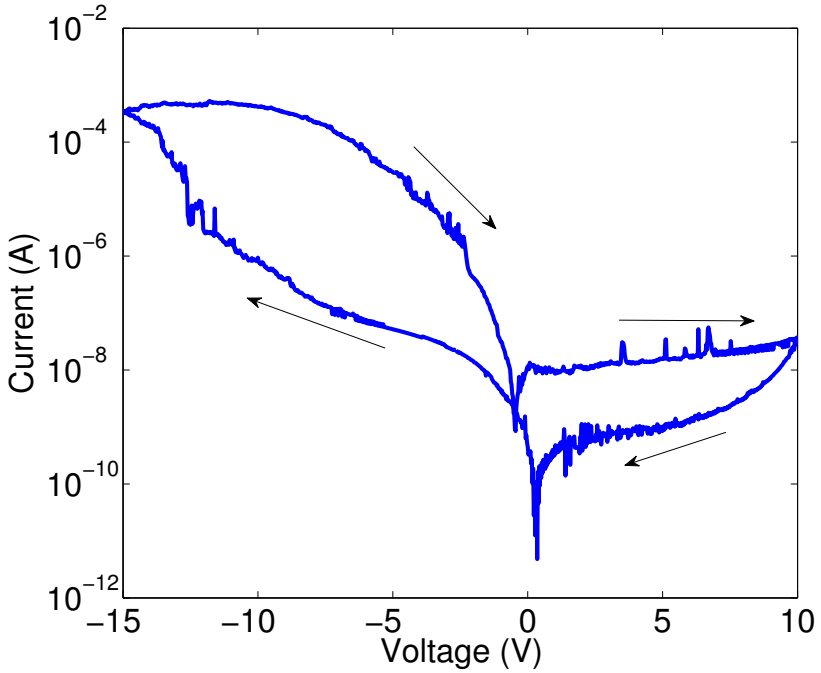

Figure 4.8: Current-Voltage characteristics of the lateral structured P3HT Schottky diode. The concentration of the solution spun-coated on diode is $1mg/mL$.

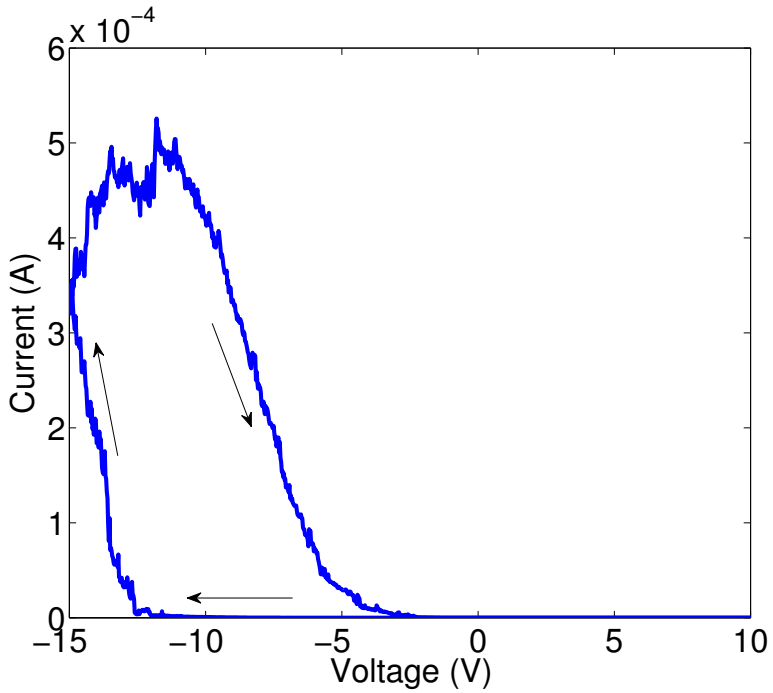

Figure 4.9: Current-Voltage characteristics of the lateral structured P3HT Schottky diode. The concentration of the solution spun-coated on diode is $1mg/mL$.

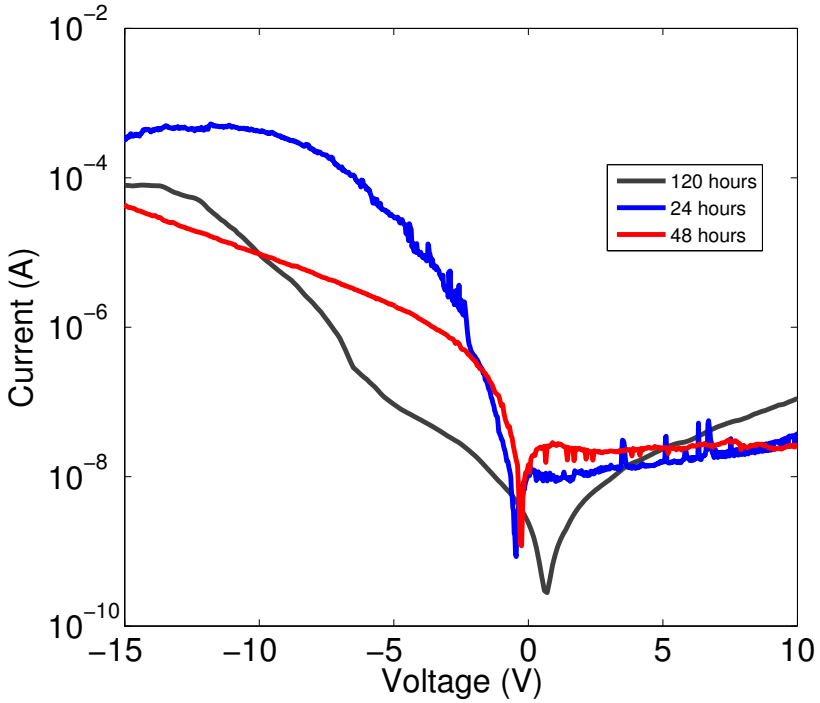

Figure 4.10: Air-instability analysis of the lateral Al/P3HT/Au Schottky diode after 120 hours.

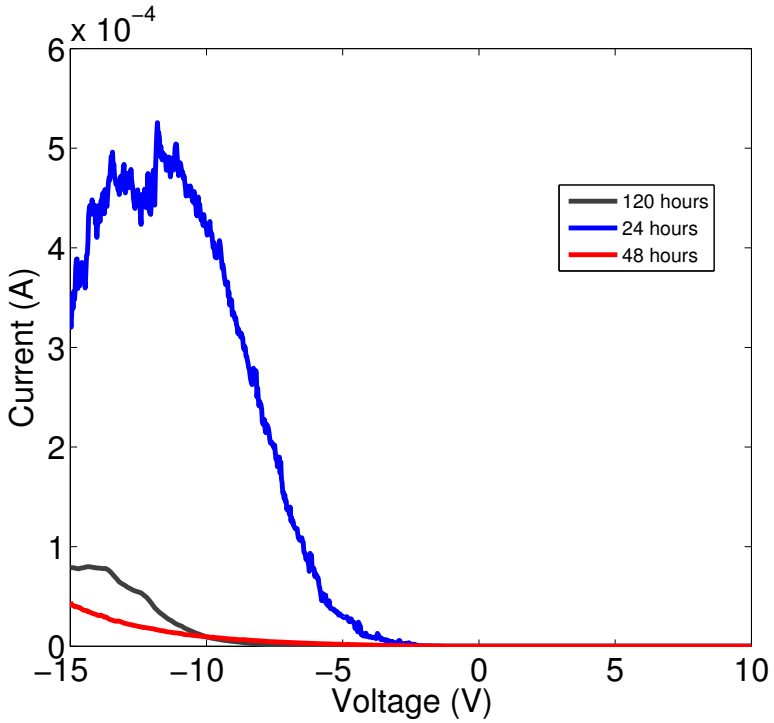

Figure 4.11: Air-instability analysis of the lateral Al/P3HT/Au Schottky diode after 120 hours.

4.5 P3HT Schottky diode with a ring structure experimental results

The self-aligned lateral structure is modified to develop the ring structure as shown in *Figure*(4.12). The main motivation of this modification is to improve the stability of the device and increase the lifetime of the device. Regarding the fabrication aspects, some processing steps such as the gold patterning and gold etch have been eliminated to reduce the chemical residual introduced on the device. The area of the substrate also has been reduced to give a more uniform film of the photoresist and polymer. The formation of the gap is still the same mechanism as the lateral Schottky diode. Similarly, the polymer also exists in the small gap between the electrodes and overlaps on top of the device.

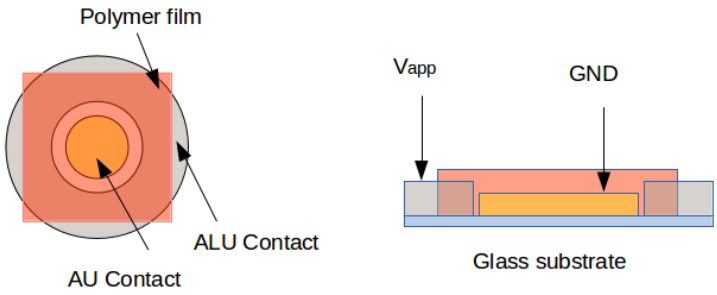

Figure 4.12: (Left-side), top view structure of ring Schottky diode. (Right-side), cross-section view of ring Schottky diode.

4.5.1 Forward current-voltage characteristics

Figure(4.13) shows the current-voltage characteristics of the ring SBD. If the Schottky diode is an ideal one, the current density should increase exponentially with applied voltage; in other words, the forward region current-voltage characteristics plot in semi-logarithm format should be a straight line. For a non-ideal device, a significant series resistance exists especially for polymer semiconductor. The applied voltage across the diode can be divided into two portions, one is the potential drop across the depletion region, and the other is the potential drop across the neutral region that extends with forward bias voltage increment, as in *Figure*.(4.13). The parameter ideality factor η is a measure of conformity of the diode to pure thermionic emission model. For ideal device, the ideality factor $\eta = 1$. The ideality factor can be extracted from the steepest part of the forward semi-logarithmic current-voltage characteristics plot, under low bias region using *Equation*(4.8).

$$\frac{1}{\eta} = \frac{k_B T}{q} \frac{d(V)}{d(lnI)} \tag{4.8}$$

Here, V is the voltage across the diode, I is the current, k_B is the Boltzmann constant and T is the room temperature.

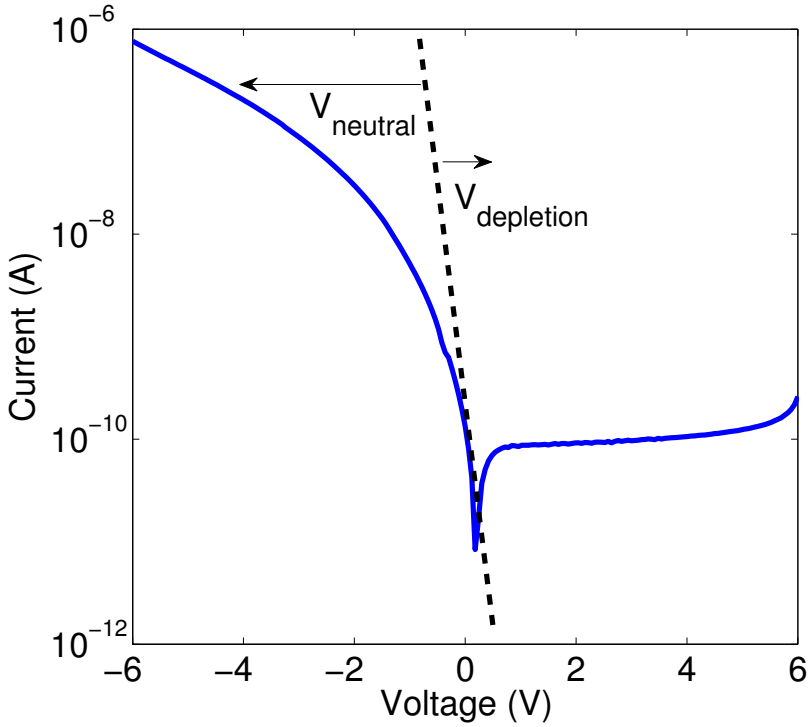

Figure 4.13: Current-voltage characteristics of the ring Schottky diode. The solution comprised of $1mg/1mL$ of P3HT/xylene. Illustration of the voltage across the depletion region, $V_{depletion}$, and across the neutral region, $V_{neutral}$, on a semi-logarithmic current-voltage characteristics of the Schottky diode.

4.5.2 Series resistance and shunt resistance

Based on the equivalent circuit shown in the *Figure*(4.14), the series resistance can be seen as the sum of the contact resistance between the metal and semiconductor and the bulk resistance of the semiconductor neutral region. The shunt resistance can be seen as the sum of bulk resistance of the gap region between the two electrodes. During device operation, the efficiency of a device (such as solar cell) is reduced by dissipation of power through such internal resistance. Both resistances significantly influence the device performance such as fill-factor photovoltaic device. Cheung's function and Norde's methods are now used here to extract these parameters.

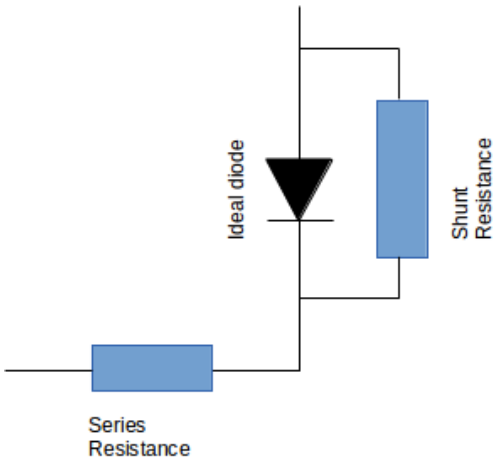

Figure 4.14: The equivalent circuit with shunt resistance and series resistance.

The equation for the current-voltage characteristics can be rewritten in terms of $V_D = V - IR_s$, where V_D is the voltage across the diode, V is the total voltage across the equivalent circuit, and R_s is the series resistance. The following equation can be obtained:

$$V = R_s I + \eta\phi_b + (\eta\frac{k_B T}{q})ln(\frac{I}{AA^*T^2}) \tag{4.9}$$

Where R is the series resistance, η is the ideality factor, ϕ_b is the barrier height, A^* is the Richardson constant ($A^* = 4\pi qm^*k^2/h^3 = 120A/cm^2K$), A is the device active area, k_B is the Boltzmann constant, q is the elementary electronic charge, T is absolute temperature. Differentiating the equation with respect to I:

$$\frac{d(V)}{d(ln(I))} = R_s I + \eta\frac{k_B T}{q} \tag{4.10}$$

As shown in $Figure.(4.15)(a)$, a plot of $\frac{dV}{d(ln(I))}$ vs I gives R_s as the slope and $\eta\frac{k_B T}{q}$ as the intercept of y-axis. In order to obtain the barrier height of the diode, a function $H(I)$ is defined as $Equation(4.11)$:

$$H(I) = V - \eta(\frac{k_B T}{q})ln(\frac{I}{AA^*T^2}) \tag{4.11}$$

Then a linear plot of $H(I)$ against I gives series resistance R_s as slope and $\eta\phi_b$ as the intercept to y-axis, as shown in $Figure.(4.15)(b)$.

$$H(I) = IR_s + \eta\phi_b \tag{4.12}$$

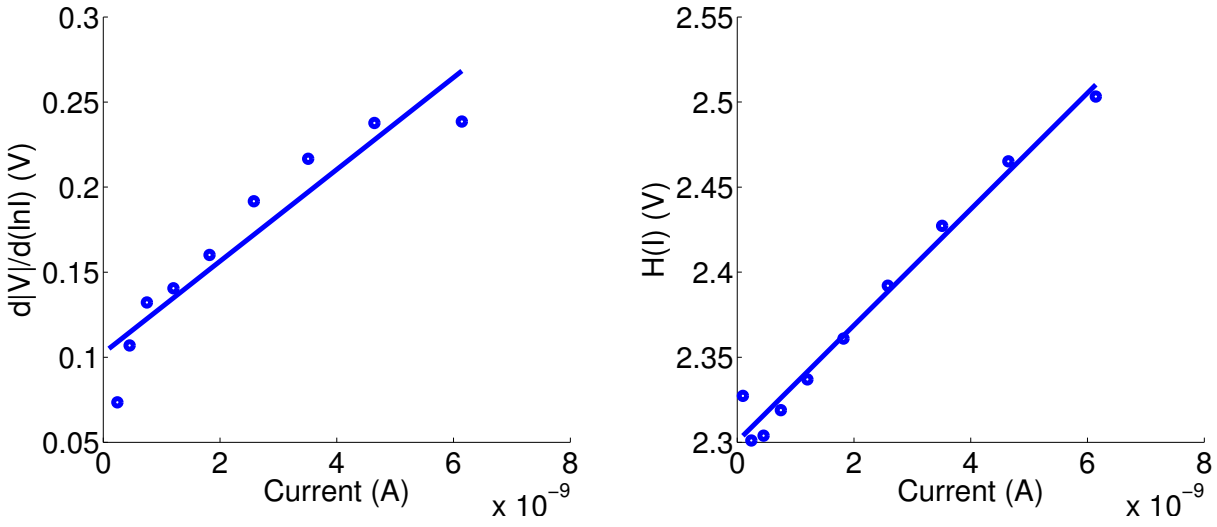

(a) (b)

Figure 4.15: (a): $d|V|/d(lnI)$ against I characteristics of ring structure Au/P3HT/Al Schottky device. (b): H(I) against I characteristics of ring structure Au/P3HT/Al Schottky device.

Another approach that is widely used for series resistance analysis is defined as Norde's method. The following function $F(V)$ has been defined in the Norde's method, as shown in $Equatio(4.13)$:

$$F(V) = \frac{V}{2} - \frac{k_B T}{q} ln(\frac{I}{AA^* T^2}) \tag{4.13}$$

The effective Schottky barrier height ϕ_b is given by:

$$\phi_b = F(V_{min}) + \frac{V_{min}}{2} - \frac{k_B T}{q} \tag{4.14}$$

Here $F(V_{min})$ is the lowest point in the plot of $F(V)$ against voltage V, as shown in $Figure.(4.16)$, the corresponding voltage and current value are V_{min} and I_0.

$$R_s = \frac{k_B T}{q I_0} \tag{4.15}$$

With existence of a large series resistance, the straight line interval in logarithm current-voltage plot may be not large enough to give a reliable saturation current I_s, which is a limitation of standard approaches of extraction of potential barrier ϕ_b. The same as Cheung's function, rewritten the current-voltage characteristics equation in terms of $V_D = V - IR_s$.

$$I = I_s[exp(\frac{q(V - IR_s)}{k_B T} - 1)] \tag{4.16}$$

However, the Norde's method has the limitation that it is not suitable for non-ideal device and inaccurate for devices with ideality factor $\eta > 1.5$. Therefore, some modification must

be added to this method. Alternative approach known as Lien method, is based on plotting several Norde type functions. A new parameter γ is introduced, which is a dimensionless integer ranging from $\eta_{min}+1$ to $\eta_{max}+1$. η_{min} and η_{max} indicate the possible range of the ideality factor from 3 to 7, which is summarised from the recent literature with regard to P3HT Schottky diode.

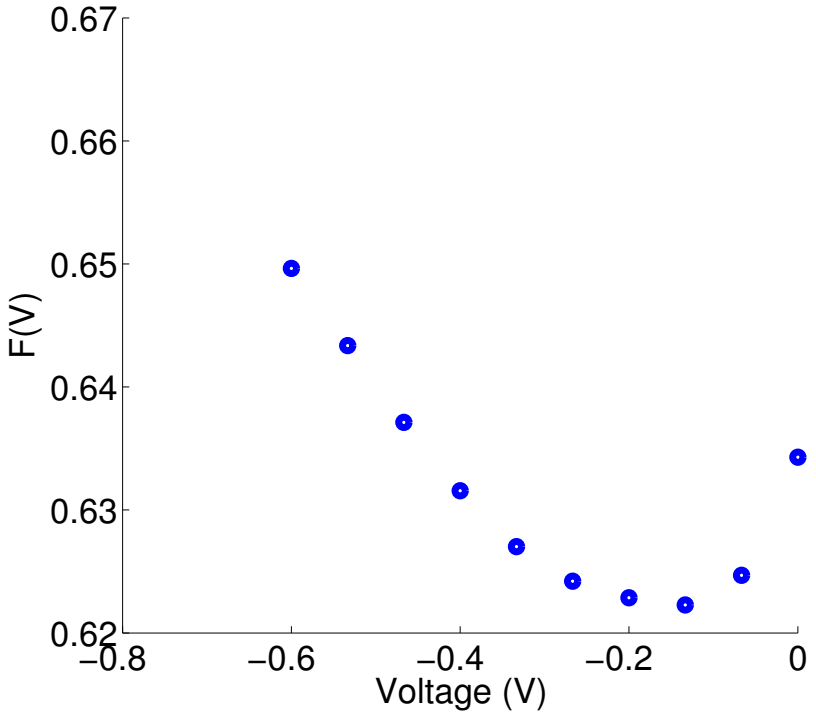

Figure 4.16: Norde plot of F(V,I) for P3HT-based Schottky diode with a ring structure, the minimum point of plot gives the barrier height ϕ_b and series resistance R_s.

$$G_\gamma = \frac{V}{\gamma} - \frac{k_B T}{q} ln(\frac{I}{A^* A T^2}) \tag{4.17}$$

Here, G_γ is a self-defined parameter in the Lien's method, which is given as $Equation(4.17)$. If $\gamma = 2$, $G_2(V,I) = F(V,I)$, the Norde plot is obtained. The effective barrier height ϕ_b and series resistance R_s are given by the following relation:

$$\phi_b = F(V_{min}) + \frac{V_{min}}{\gamma} - \frac{k_B T}{q} \tag{4.18}$$

and

$$R_s = \frac{k_B T(\gamma - n)}{q I_0} \tag{4.19}$$

The ideality facto η, the series resistance R_s and the barrier height ϕ_b extracted using Lien's method are listed in $Table.(4.1)$. Werner has proposed examining three different plots for the

determination of I_S, ϕ_b, η, and R_s from $I-V$ characteristics in his publication in 1988 [10]. In addition, the real diode can be modeled using the equivalent circuit shown in *Figure*.(4.12)

The relationship between the current I and the applied voltage V is given as *Equation*(4.20):

$$I = I_d + I_p = I_s(exp(\frac{q}{\eta k_B T}(V - IR_s) - 1)) + G_p(V - IR_s) \tag{4.20}$$

Here, I_d is the current through the ideal diode, and I_p is the current through the shunt resistance. The shunt conductance G_p is calculated from the reverse bias characteristics for large negative bias voltage $V_{reverse} > 25mV$, the parallel conductance G_P can be extracted by least square fit to the linear part of reverse current-voltage characteristics.

$$G_P = G_{reverse} = \frac{dI}{dV} \tag{4.21}$$

Based on the equivalent circuit of a real diode shown in *Figure*.(4.14) and definition of parallel conductance, the current-voltage characteristics can be corrected by removing the current through the parallel resistor $I_d = I - G_P V$. In addition, the correction used here does not affect the extraction of the series resistance R_S, ideality factor η and barrier height ϕ_b. Due to the large parallel resistance R_p, the shunt current plays a significant role on the reverse bias.

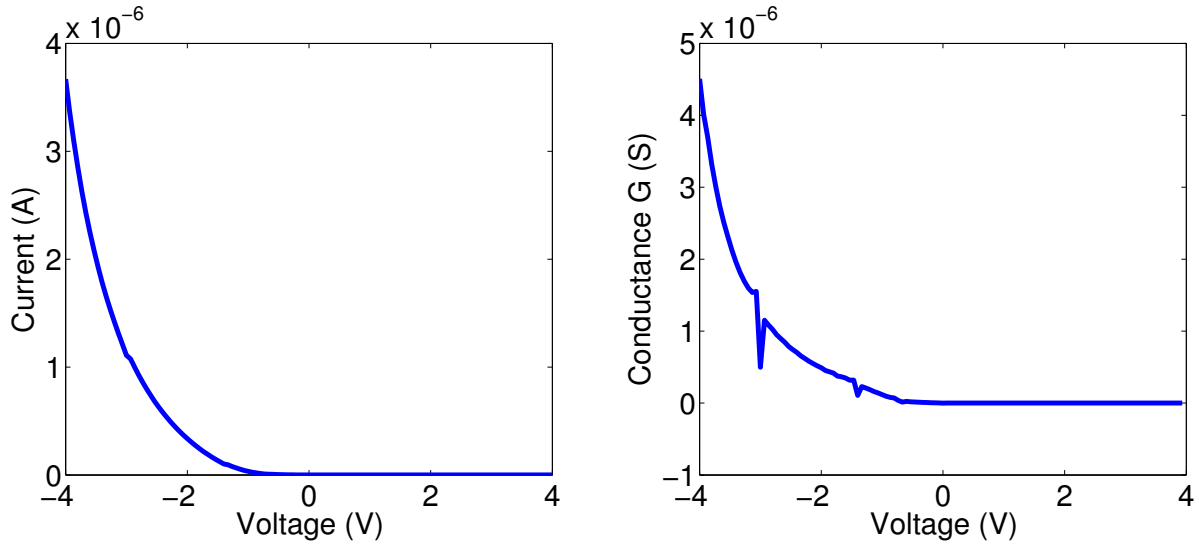

(a) (b)

Figure 4.17: Linear plot of conductance $G = dI_d/dV$ and diode current I_d against voltage V.

For $V > 3V$, the forward current varies linearly with applied voltage, and the conductance does not saturate within the voltage range $(3V - 4V)$. Under forward bias, *Equation*(4.22) shows that a plot of G/I_d versus conductance G, yields a slope $-\frac{\beta R_s}{n}$, and y-axis intercept $\frac{\beta}{\eta}$, x-axis intercept $\frac{1}{R_s}$, where $\beta = \frac{q}{k_B T}$, and η is the ideality factor of diode.

$$\frac{G}{I_d} = \frac{\beta}{\eta}(1 - GR_s) \tag{4.22}$$

Which is shown in *Figure.*(4.18) (Top Right).

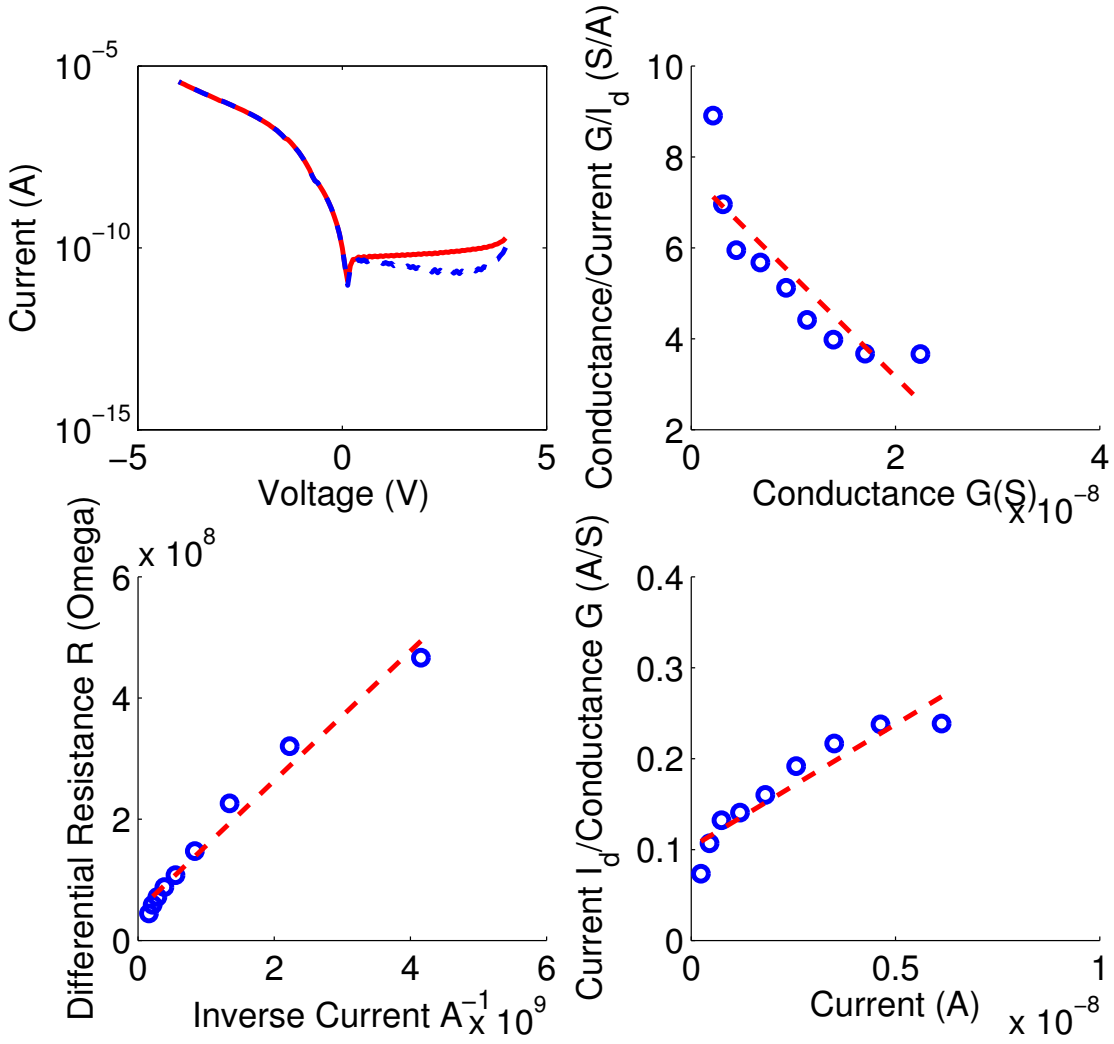

Figure 4.18: (Top-Left), Plot of current-voltage in semilog format, the red solid line is experimental data, and the blue dashed line is corrected data including shunt resistance. (Top-Right), corresponds to first equation in Werner's method yields series resistance R_s and ideality factor η from axis intercepts. (Bottom-Left), corresponds to *Equation*(4.23) in werner method yields R_s from y-axis intercept and η from the slope. (Bottom-Right), corresponds to third equation in Werner's method. All the parameters mentioned are listed in *Table*(4.1).

$$R_{dr} = \frac{\eta}{\beta I_d} + R_s \tag{4.23}$$

Where, R_{dr} is the differential resistance of diode, $R_{dr} = \frac{dV}{d(I - G_P V)}$. The plot with slope $\frac{\eta}{\beta}$ and y-axis intercept R_s is obtained.

$$\frac{dV}{dlnI_d} = R_s I_d + \frac{\eta}{\beta} \tag{4.24}$$

The plot of $\frac{dV}{dlnI_d}$ against I_d yields a straight line with slope R_s and y-axis intercept $\frac{\eta}{\beta}$. This plot is similar to the Cheung's method.

Methods	Ideality Factor η	Barrier Height $\phi_b(eV)$	Series Resistance $R_s(\Omega)$	Shunt Resistance $R_{sh}(\Omega)$
Standard Forward Method	3.24			
Standard Reverse Method		0.68		4.8×10^{10}
Cheung's Method	4	0.57	2.9×10^{7}	
Norde & Lien's Method	4	0.59	5.6×10^{7}	
Werner Method	5		2.9×10^{7}	4.8×10^{10}

Table 4.1: Direct determination of R_s, η,and ϕ_b using the standard and Norde methods. Lien *et al.* and Werner plots indicate that these methods do not directly yield the barrier height.

In summary, the values of ideality factor η, series resistance R_s, shunt resistance R_{sh} and barrier height ϕ_b were obtained from the current-voltage characteristics using 4 methods. An agreement can be seen on the extracted values for the series and shunt resistances using the different methods. The large series resistance is thought due to the large electrodes gap of ring structure diode, comparing to the vertical structure diode. In reverse bias, the current level is as low as $10^{-10}A$, the influence of series resistance is not significant, while in forwrd bias, the large series resistance will limit the forward saturation current.

4.5.3 Space charge limited currents in saturation region

Transport in organic systems is generally described by the model based on hopping between point-like localized states, which are disordered in space and energy [7][8], but the restrictions of this concept for the case of the transport occurring via the extended states within micro-regions, as in the conjugated polymers, was also discussed in the literature. For the metal/semiconductor/metal structure device, an ohmic contact is defined as an infinite reservoir of charge that is able to sustain a steady state space charge limited current in a device. With ohmic contacts, the current-voltage relation is linear at low bias up to a certain value since the electrical field due to the injected carrier is negligible compared to that due to applied voltage. The slope of a log-log plot of the current against voltage at low bias is then equal to 1, and the behaviour can be defined by Ohm's Law and definition of current density given as:

$$J_{Ohmic} = qp\mu\frac{V}{x} \tag{4.25}$$

where q is the electronic elementary charge, n the charge carrier concentration, μ the effective mobility, V the applied voltage and x the distance between two electrodes. The theory of space charge limited current (SCLC) between two electrodes with a constant mobility value and without the presence of trapping effects was introduced by Mott-Gurney[9] as given below.

$$J = \frac{9}{8}\mu\varepsilon_0\varepsilon_s\left(\frac{V^2}{x^3}\right) \tag{4.26}$$

Where ε_0 is the permittivity of free space, μ is the mobility, ε_s is the dielectric constant of the polymer, and x is the distance between two electrodes.

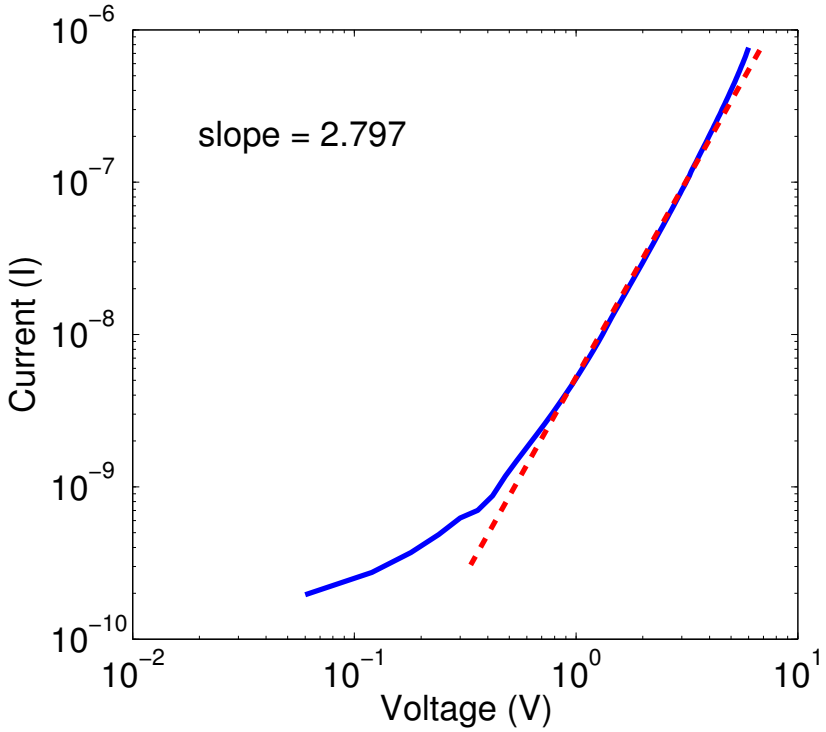

Figure 4.19: Logarithmic plot of the current against voltage (in the neutral region), for a ring Schottky diode. The slope is approximately 2.79 indicating SCLC to be dominated transport.

For the ring structured Schottky diode, the slope of the logarithmic plot of the current against voltage in neutral region as in *Figure*(4.19) is found to be approximately 2.797. This suggests SCLC to be the domainnated mechanism in the neutral region and possibly associated with the trapping of the carriers within the disordered grain boundaries.

4.5.4 Reverse current-voltage characteristics

In reverse bias, the depletion region widens restricting the path for current flow. With reverse bias voltage increasing, the depletion region expands towards the ohmic contact The potential barrier is formed by the combined effect of the built-in potential and image-charge

force. The current density is give as *Equation*(4.7). As shown in *Figure*(4.20), the plot of the logarithmic of the current density against the reverse bias $V^{0.25}$ gives $\frac{q}{K_B T}(\frac{q^3 N_A}{8\pi^2 \varepsilon_0^3 \varepsilon_s^3})^{0.25}$ as the slope, the dopant concentration N_A can be extracted from this slope. The intercept to y-axis, gives the reverse saturation current. Seen from the *Figure*(4.20), the dopant concentration was found to be $2.02 \times 10^{21} m^{-3}$.

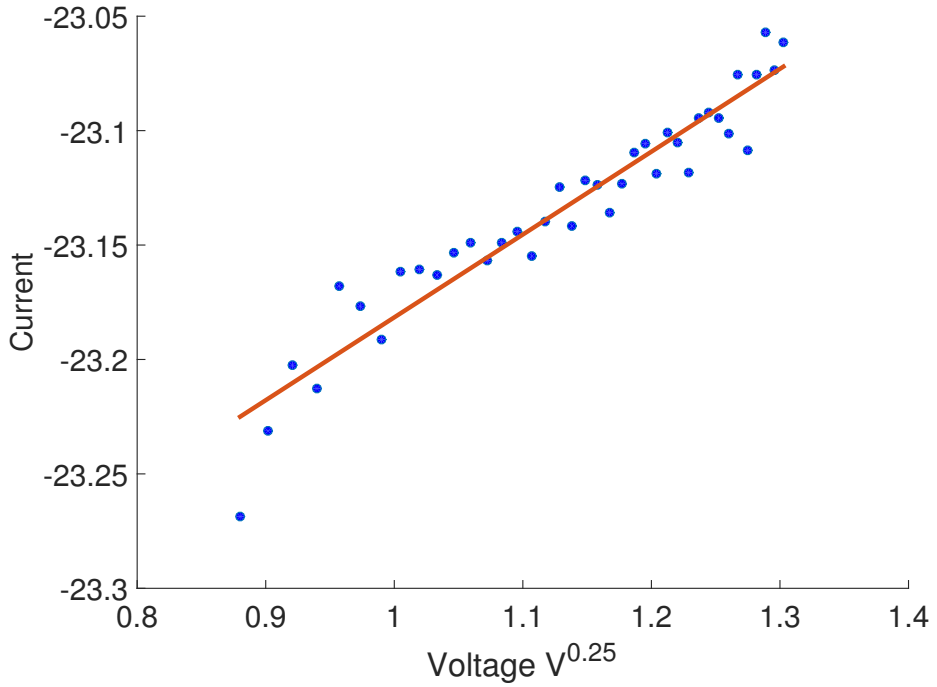

Figure 4.20: Natural logarithm of the reverse current $ln(I)$ against $|V|^{0.25}$. The above figure is one of the best fitted results based on P3HT diode.

4.5.5 Capacitance-Voltage characteristics and AC behaviour of device

The AC behaviour of a Schottky diode is dominated by the capacitance of the depletion region which forms at the Schottky contact. For organic Schottky diodes, the AC behaviour can be used to evaluate important device characteristics such as the doping density, built-in potential and even the interface states can be extracted from high frequency regime. The depletion layer of an ideal Schottky barrier formed in a p-type semiconductor contains a uniformly distributed, fixed space charge, Q_{sc} per unit area, arising from ionized acceptor impurities. When the voltage applied to the metal electrode is changed by a small increment, dV, the depletion width changes causing the capacitance C_d corresponding to the depletion region. *Figure*(4.21) shows an enhanced equivalent circuit of the diode.[11][16]

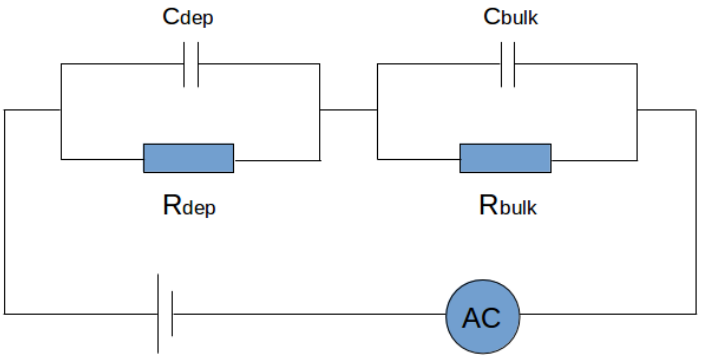

Figure 4.21: Equivalent circuit of the polymer schottky diode. C_{dep} and R_{dep} are due to the depletion region and C_{Bulk} and R_{Bulk} are due to the bulk of the polymer

With voltage applied on the electrodes, the width of depletion region and neutral region will be changed. The depletion region with a changing edge can be approximated to a variable parallel capacitor, which is in series with bulk resistor R_{BULK}. The expression for the capacitance can be expressed as follow:

$$C_{dep} = \frac{\varepsilon_0 \varepsilon_s A}{W_d} \tag{4.27}$$

Where C_{dep} is the depletion capacitance, ε_0 is permittivity of free space, ε_s is the relative permittivity of the material, W_d is the width of depletion region. Based on Gauss's Law, the relationship between depletion region field strength and charge enclosed in this region can be derived as below.

$$\varepsilon_0 \varepsilon_s F_{max} A = q N_A W_d A \tag{4.28}$$

Where maximum field strength within the depletion region F_{max} can be expressed as $F_{max} = \frac{qN_A W_d}{\varepsilon_0 \varepsilon_s}$. The relationship between the potential drop across the depletion region and depletion region width can be expressed as below.

$$V_C = \frac{F_{max} W_d}{2} \tag{4.29}$$

combined two expression together, the equation can be as below:

$$\frac{qN_A W_d}{\varepsilon_0 \varepsilon_s} = \frac{2V_C}{W_d} \tag{4.30}$$

$$W_d = \sqrt{\frac{2(V_{app} - V_{bi})\varepsilon_0 \varepsilon_s}{qN_A}} \tag{4.31}$$

After substituting the expression for depletion region width into the equation of parallel plates capacitor,

$$C_{dep} = |\frac{dQ_{sc}}{dV}| = \sqrt{\frac{q\varepsilon_s \varepsilon_0 A^2 N_A}{2(V_{app} - V_{bi})}} \tag{4.32}$$

$$\frac{1}{C_{dep}^2} = \frac{2(V_{app} - V_{bi})}{q\varepsilon_s\varepsilon_0 A^2 N_A} \tag{4.33}$$

The equation can be seen as the capacitance of the depletion region of the Schottky barrier diode. The carrier concentration can be obtained from the slope of $\frac{1}{C^2}$ versus voltage applied, the intercept of the plot gives the built-in voltage. With the V_{bi} determined from $1/C^2$ versus V_{app} by the $Equation(4.33)$, the barrier height was in turn obtained:

$$\phi_b = q[V_{bi} + \frac{k_B T}{q} ln(\frac{N_C}{N_A})] \tag{4.34}$$

Where N_C is the effective density of states in the conduction band. $Figure(4.22)$ shows a plot of A^2/C^2 against the applied voltage measured at $1KHz$. The doping density extracted here at low frequency is close to the value obtained through the reverse current-voltage characteristics shown in $Tabel(4.3)$.

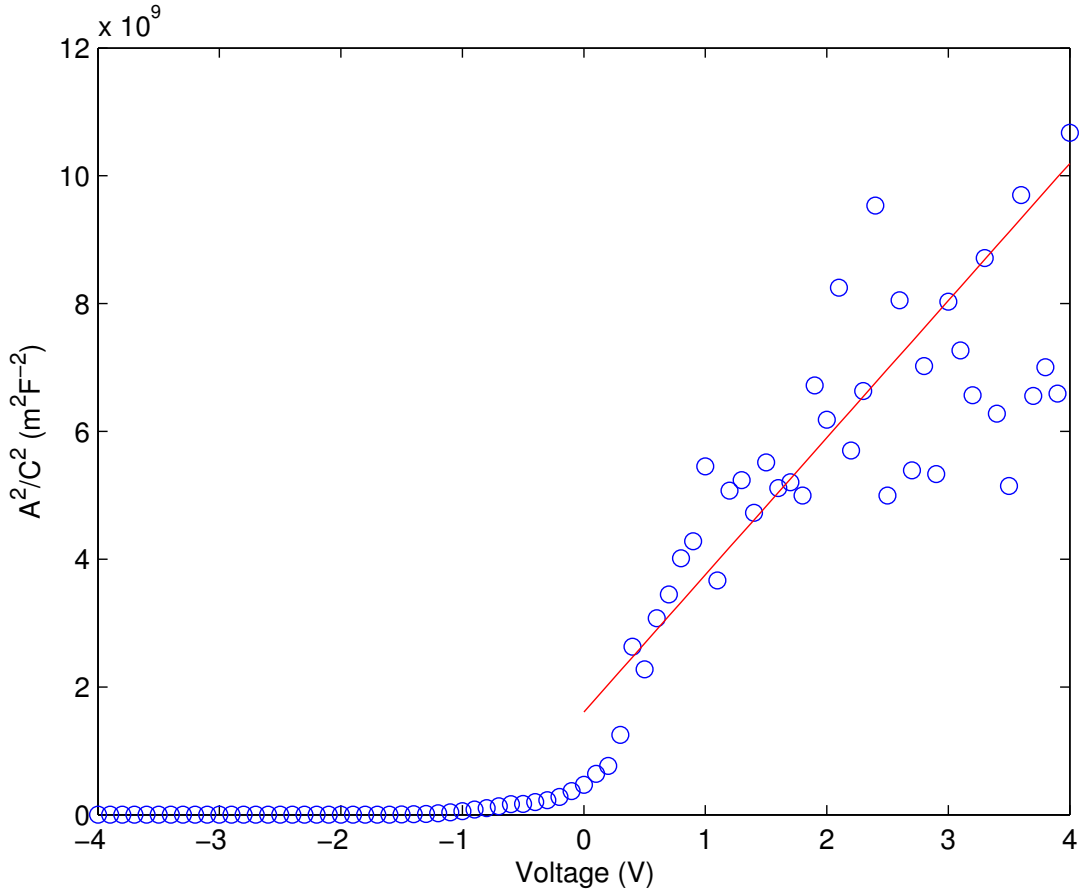

Figure 4.22: Plot of $\frac{A^2}{C^2}$ against applied voltageV_{app} for the ring structure Al/P3HT/Au diode measured at frequency $1kHz$, the built in potential can be estimated from the x-axis intercept, the doping density N_A can be extracted from the slope of linear fitted line.

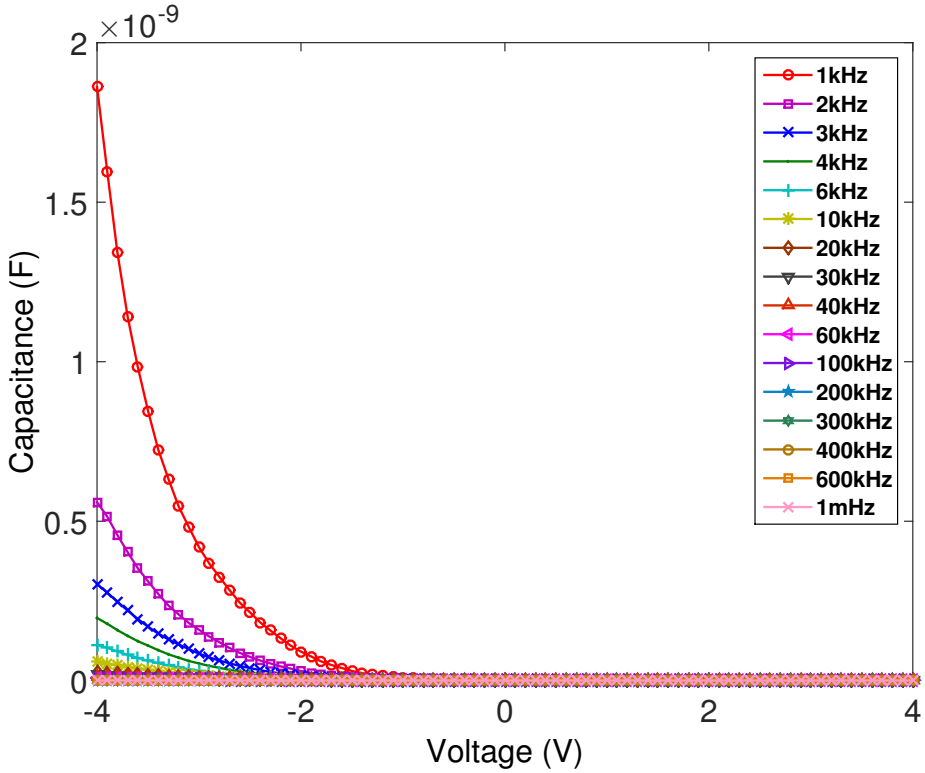

Figure 4.23: Capacitance against voltage characteristics measured at frequency ranging from $1kHz$ to $1MHz$.

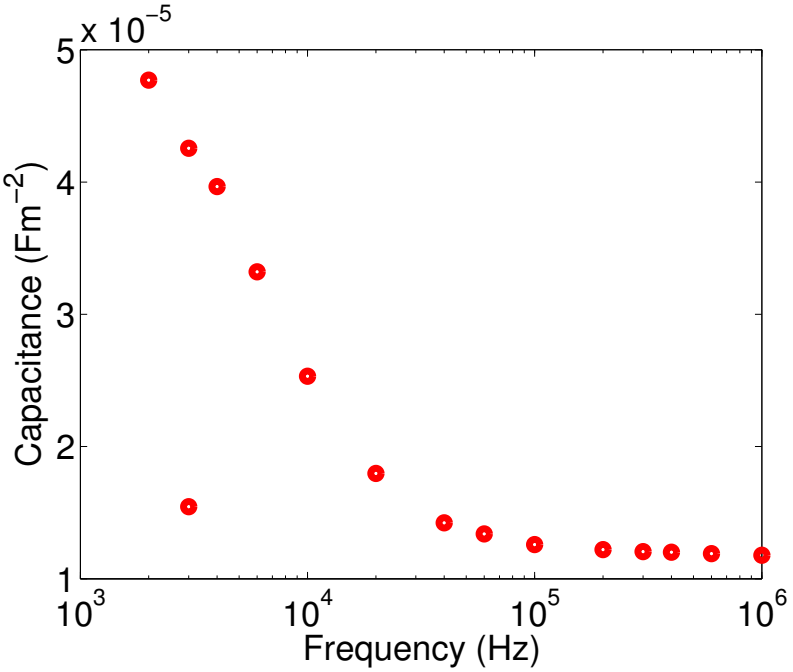

Figure 4.24: Variation of the capacitance (per unit area) against frequency (log) at reverse bias $V = 1V$.

The frequency dependency of the capacitance obtained experimental at low reverse bias ($V = 1V$) is shown in $Figure.(4.24)$. This result agrees with the basic physical explanation of diode capacitance, the capacitance should decrease with the rise of the signal frequency.

Theoretically, the doping density should be independent of the signal frequency, which is a parameter about the nature of polymer semiconductor. The doping density obtained at low frequency is close to the value obtained in the reverse current-voltage characteristics, which is shown in $Table.(4.3)$. The general dependency of extracted doping density value against the AC signal frequency is shown as $Figure.(4.25)$. With AC signal frequency increasing, the extracted doping density value increases. This phenomenon may result from two reasons. Firstly, at low frequency, the charge carriers are able to follow both the AC and DC signal and when a positive voltage is applied on aluminium; holes have enough time to deplete from the aluminium-polymer interface. However, at high frequencies the holes can only follow the DC signal. Their contribution to the capacitance is thus reduced. Secondly, seen from $Table.(4.1)$, the large series resistance may affect the correct doping density extraction from capacitance-voltage characteristics of the ring structure Schottky diode. The reliable value of doping density could only be obtained from reverse current-voltage characteristics of ring Schottky diode.

4.5.6 Stability analysis

Practical applications based on polymer are limited by their poor stability under normal ambient conditions, especially as these materials are sensitive to light and oxygen. The degradation process in air, due to the diffusion of oxygen and vapour into the organic layer, as well as oxidation of metal contacts, affects conductivity in organic semiconductors and leads to degradation of electrical parameters and overall device efficiency[15]. In this section, the working voltage range, air-stability and bias-stability of the ring Schottky diode will be examined with the aid of current-voltage characteristics of the device. Due to modification of the fabrication procedures, the stability of the device performance is improved significantly compared to lateral Schottky diode. Comparing *Figure*(4.8) with *Figure*(4.25), the hysteresis of the ring Schottky diode is much smaller. Based on DC measurements of the three types of Schottky diode, the working bias range is strongly dependent on the thickness of the polymer film. If the applied voltage exceeds an appropriate range, the device will be destroyed. For instance, the vertical diode with a typical film thickness of $10\mu m$ may tolerate the voltage in $15V$ to $-15V$ range, while, a spin-coated device that gives a thinner film has a much narrower voltage range, which can be seen from *Figure*(4.26) (6V to -6V) and *Figure*(4.27) (4V to -4V).

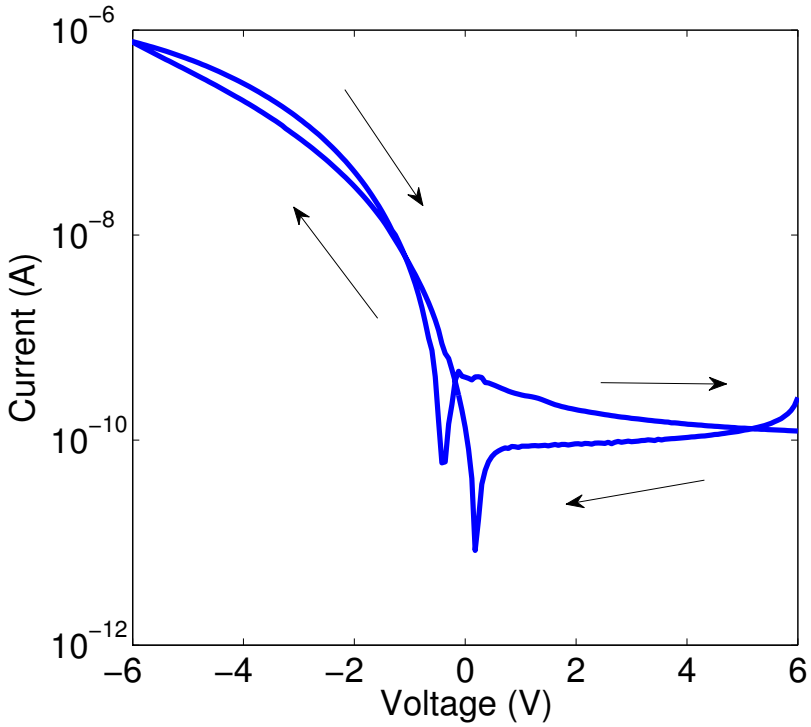

Figure 4.25: DC double sweep of Ring SBD, the arrows show the direction of DC voltage changing.

The air-instability analysis results of different ring SBD shown in *Figure*(4.26), *Figure*(4.27), *Table*(4.2) and *Table*(4.3) suggest that the doping density increases and mobility decreases when the device is exposed to oxygen. This is a typical phenomenon of a polymer device. In general, as the device continues to be exposed in air, the on-current reduces significantly by a factor of 5-10. The factor may depend on the thickness of the polymer film, whereby different polymer weight/solvent volume recipe can give different polymer thicknesses. A thicker polymer film is thought to have a self-passivation feature, which may protect the polymer film from oxidation. In comparison, the air-instability analysis of a lateral diode shown in *Figure*(4.9), some improvement can be seen, which may due to reduction on the chemical residuals and improved uniformity of sample. The effect of oxygen and moisture on the polymer charge transport mechanism needs further investigation. Based on the Universal Mobility Law, given as $\mu = K_{UML}p^m$, an increase in the doping density, results in increase in effective mobility, assuming every dopant results in a free carrier.

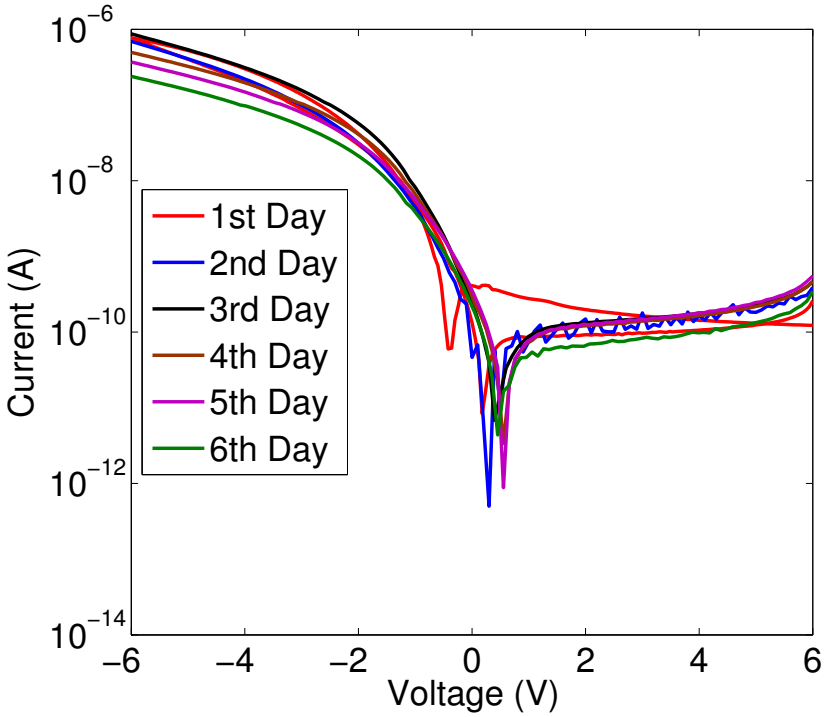

Figure 4.26: Current-voltage characteristic of a ring Schottky diode within 6 days. The sample was stored and characterized in air environment. The concentration of solution of P3HT/xylene was $1mg/ml$.

Comparing *Figure*(4.26) with *Figure*(4.27), the ring Schottky diode spun-coated with a higher P3HT concentration solution has a better air stability.

Day	1	2	3	4	5	6
Rectification	$\sim 10^3$	$\sim 10^3$	$\sim 10^3$	$\sim 10^3$	$\sim 10^3$	$\sim 10^3$
factor η	4.5	5.0	5.4	7.8	8.4	5.8
$T_0(K)$	1350	1500	1620	2340	2520	1740
$T_c(K)$	385.7	375	368.2	344.1	340.5	362.5
Meyer Neldel Energy (meV)	33.3	32.3	31.8	29.7	29.4	31.3
Doping density N_A (m^{-3})	2.3×10^{20}	1.1×10^{22}	5.0×10^{21}	1.2×10^{22}	2.0×10^{22}	5.2×10^{21}

Table 4.2: Parameters extracted from $1mg/mL$ Ring SBD using standard methods

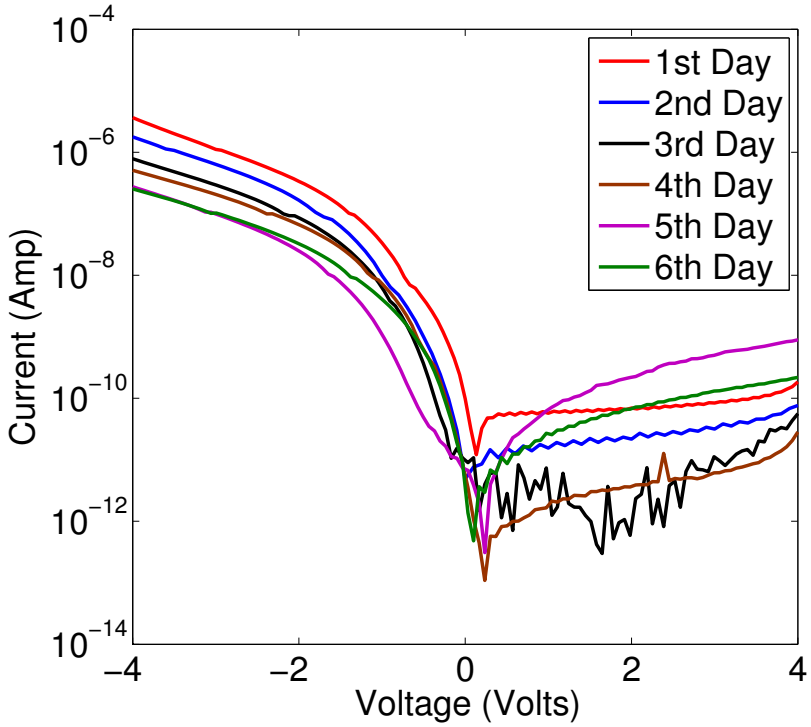

Figure 4.27: Current-voltage characteristic of a ring Schottky diode within 6 days. The sample was stored and characterized in air environment. The concentration of solution of P3HT/xylene was $0.5mg/ml$.

Day	1	2	3	4	5	6
Rectification	$\sim 10^4$	$\sim 10^4$	$\sim 10^4$	$\sim 10^4$	$\sim 10^3$	$\sim 10^3$
factor η	3.2	3.6	3.5	2.6	5.3	2.4
$T_0(K)$	960	1080	1050	780	1590	720
$T_c(K)$	436.4	415.4	420	487.5	369.8	514.3
Meyer Neldel Energy (meV)	37.6	35.8	36.2	42	31.9	44.4
Doping density N_A (m^{-3})	7.1×10^{20}	2.8×10^{21}	9.3×10^{24}	5.0×10^{22}	4.1×10^{23}	9.0×10^{22}

Table 4.3: Parameters extracted from $0.5mg/mL$, the parameters are extracted with standard methods.

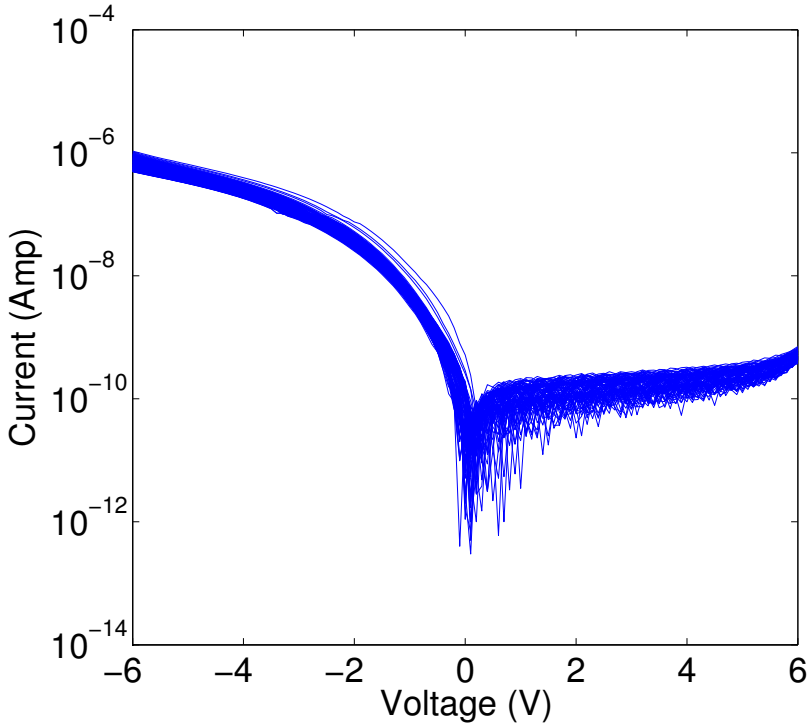

Figure 4.28: Current-voltage characteristics of a ring Schottky diode, with multiple voltage sweep carried out in dark condition.

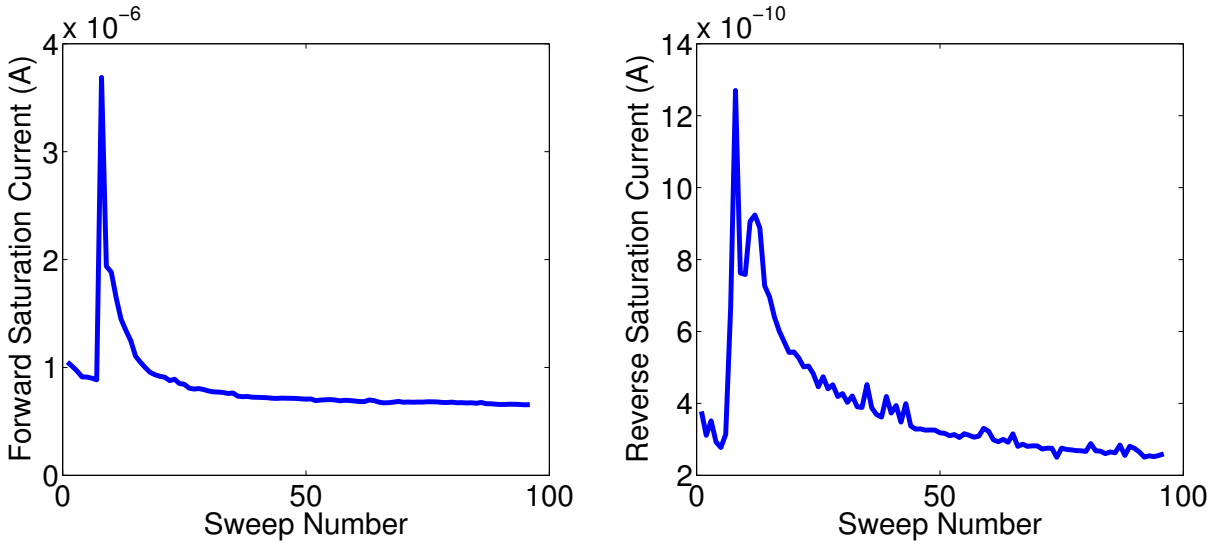

(a) (b)

Figure 4.29: Variation of the forward and reverse currents with respect to the number of sweeps.

Another improvement is about device bias stability, which is shown in *Figure*(4.28). The current-voltage characteristics was taken continuously 100 times. The variation of On/Off current against the sweep number is shown in *Figure*(4.29). Both figures show the stable performance of ring Schottky diode. The only sudden change of current value presented in *Figure*(4.29) may be caused by vibration of the probe station when someone is walk around the desk. In comparison to those of the lateral Schottky diode, the stability of ring Schottky diode's performance improve significantly.

4.6 Conclusion

Detailed analysis of the P3HT based Schottky diode is presented in this chapter, and three types of fabrication procedure and device structure designs are shown. The P3HT based diode was able to achieve a satisfactory rectification ratio of 10^4. Deposition of both the drop cast film and the spun cast film were carried out under clean ambient condition. It is thought that different film deposition methods give different thickness of the P3HT film. The air in-stability of P3HT Schottky barrier diode was also analysed by comparing the results measured in air at different times. The results indicate the significant effect of air expose to device performance and important parameters such as doping density and bulk mobility. However, further work needs to be done to understand the internal mechanism of bulk mobility change. For capacitance-voltage analysis of device, the presence of deep traps was not considered, which can cause overestimation of the doping density and built-in potential.

References

[1] S. M. Sze, Physics of Semiconductor Devices, Wiley, 2007.

[2] G. Güler, Ö. Güllü, Ş. Karataş and Ö. F. Bakkaloǵlu, "Analysis of the series resistance and interface state densities in metal semiconductor structures,"2009 Journal of Physics: Conference Series, 153, 012054, 2009

[3] S. K. Cheung, and N. W. Cheung,"Extraction of Schottky diode parameters from forward current-voltage characteristics", Applied Physics Letters, vol. 49, pp. 85-87, 1986.

[4] H. Norde, "A modified forward IV plot for Schottky diodes with high series resistance,"Journal of Applied Physics, vol. 50, pp. 5052-5053, 1979.

[5] M. Raja, and W. Eccleston, "The significance of Debye length in disordered doped organic devices,"Journal of Applied Physics, vol. 110, 114524, 2011.

[6] A. K. Mukherjee, A. K. Thakur, W. Takashima and K. Kaneto, "Minimization of contact resistance between metal and polymer by surface doping,"Journal of Physics D: Applied Physics, vol. 40, pp. 1789-1793, 2007.

[7] H. Bassler, "Charge Transport in Disordered Organic Photoconductors a Monte Carlo Simulation Study,"Status Solidi B, vol. 175, no. 1, pp. 15-56, 1993.

[8] S. V. Novikov, D. H. Dunlap, V. M. Kenkre, P. E. Parris, and A. V. Vannikov, "Essential Role of Correlations in Governing Charge Transport in Disordered Organic Materials,"Physics Review Letters, vol. 81, no. 20, pp. 4472-4475, 1998.

[9] N.F.Mott and R.W.Gurney, Electron Process in Ionic Crystals, UK, Oxford University Press, 1948.

[10] J. H. Werner, "Schottky barrier and pn-junction I/V plots Small signal evaluation,"Applied Physics A: Solids and Surfaces, vol. 47, no. 3, pp. 291-300, 1988.

[11] D. M. Taylor and H. L. Gomes, "Electrical characterization of the rectifying contact between aluminium and electrodeposited poly(3-methylthiophene),"Journal of Physics D: Applied Physics, vol. 28, pp. 2554-2568, 1995.

[12] Z. Chiguvare, J. Parisi, and V. Dyakonov, "Current limiting mechanism in indium-tin-oxide/poly3-hexylthiophene/aluminum thin film devices," Journal of Applied Physics, vol 94, no. 4, pp. 2440, 2003.

[13] S. Afzal, "A study of the electrical properties of polycrystalline biased organic devices", Phd Thesis, Univeristy of Liverpool, 2012

[14] M. Raja, "Metal-Oxide Conjugated Polymer Interface Property for Applications in polymer electronics", Phd Thesis, University of Liverpool, 2004.

[15] H. Bednarski, J. Gsiorowski, M. Domanski, B. Hajduka, J. Jurusik, B. Jarzbek and J. Weszka, "Stability of Diodes with Poly(3-hexylthiophene) and Polyazomethines Thin Organic Layer", ACTA PHYSICA POLONICA A, vol. 122, no. 6, 2012.

[16] I. Musa, and W. Eccleston, "Properties of Regioregular Poly(3-alkylthiophene) Schottky Diodes," Japan Journal of Applied Physics, vol.37, pp. 4288-4293, 1998.

[17] E. Orgiu, A. M. Masillamani, and Vogel, Jorn-Oliver and Treossi, Emanuele and Kiersnowski, Adam and Kastler, Marcel and Pisula, Wojciech and Dotz, Florian and Palermo, Vincenzo and Samori, Paolo, "Enhanced mobility in P3HT-based OTFTs upon blending with a phenylene-thiophene-thiophene-phenylene small molecule," Chem. Commun.2012, vol. 48, no. 10, pp. 1562-1564, 2012

[18] N. Sedghi, D. Donaghy, M. Raja, S. Badriya, S. J. Higgins, W. Eccleston, "Experimental observation of the density of localized trapping levels in organic semiconductors", Journal of Non-crystal Solids, vol. 352, pp. 1641-1643, 2006.

[19] A. Assadi, C. Svensson, M. Willander, and O. Inganäs, "Properties of the planar poly(3-octylthiophene)/aluminum Schottky barrier diode," Journal of Applied Physics, vol. 72, no. 7, pp. 2900-2906, 1992.

Chapter 5

Optical characteristics of conjugated polymer devices

In this chapter, a brief resume of photo-current generation basics and device operation mechanism are presented. Results of P3HT based diode and thin-film transistor under illumination are presented.

5.1 Introduction

Organic electronics is mostly dominated by light-emitting diodes, photovoltaic cells and optoelectronic applications.[1] Organic-based photo-active semiconductor materials combine effective light absorption in a wide spectrum from ultraviolet to near infra-red with good photo generation and cost-effective low temperature fabrication potential over large area flexible substrates, which might enable innovative optoelectronic systems that can be targeted in the fields of large area displaying, large area imaging sensors, optical communications and even biomedical sensing.

Generally speaking, the light-sensitive devices convert a photon flux (light) into a flux of free charge carriers. And with respect to application, those devices can be divided into two major types. One type is energy-harvesting devices such as the solar cell which delivers electrical power to a load. Another type of device is the photo-detector or image sensor which delivers a photo-current signal. Both of these areas gain considerable popularity among researchers. The solution process-ability of organic photovoltaic devices reduce cost, energy consumption and environmental impact during manufacturing, which makes the OPVs a promising alternative candidate for renewable energy. Moreover, its flexible feature and potential for cost-effective large-area fabrication makes imaging systems another interesting field of applications.

This chapter begins by discussing the fundamental of the theory of charge photo-generation in organic material and operating mechanism of such organic optoelectronic devices. The current-voltage characteristics of a ring structure P3HT Schottky barrier diode under illumination is presented. The performance of such a single layer device as an OPV and photodetector is investigated. The air instability of the device over time is also discussed.

In addition, the P3HT based thin film transistor transfer and output characteristics under illumination are also presented. The potential of using as the organic photo detector is discussed.

The devices mentioned in this chapter were fabricated and characterized under a clean ambient condition. The fabrication procedures of the device were explained in previous two chapters.

5.2 Operation Mechanism

5.2.1 Schottky barrier photodetector

There are various types of two terminal photodetectors: a simple photoconductor, a pn junction diode, a Schottky barrier diode and a metal/semiconductor/metal device.[12][13] Comparing the various detectors, the Schottky barrier diode has several advantages, including simple fabrication, high quantum efficiency, high response speed, low dark current, and

possible zero bias operation. The Schottky barrier photodiode is a two-terminal device where the active layer is contacted with metal electrodes. The most common topology is the vertical one, which is identical to a normal diode structure, but is optimized to work with a reverse applied field, with low dark-current and fast charge collection. While, the device configuration discussed in this part of the work is of a lateral topology, which offers a direct access to the photo active layer(polymer layer), but on the other hand is characterized by larger inter electrode spacings and hence lower operation bandwidth. It should be noted that the area of illumination is not equal to the cross-section area between the two electrodes, as shown in *Figure.*(5.1). Ignoring this distinction between vertical and lateral diodes may lead to the miscalculation of responsivity and conversion efficiency.

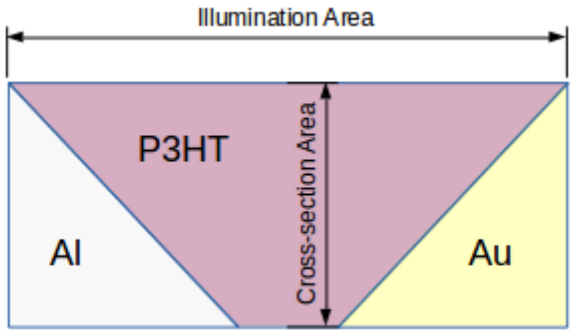

Figure 5.1: Cross section schematics of a lateral structure Schottky barrier photodiode.

The behaviour of a photo diode changes accordingly to the fate of photo generated charge carriers. Firstly, the charges are collected by the electrodes. Secondly, charge carriers recombination occurs before electrodes collection. For the first case, the lifetime of free charge carriers from the dissociation of exciton must be larger than the essential time for carriers reaching the electrodes.

$$\tau > \frac{L}{\mu E} \tag{5.1}$$

Where τ is the lifetime of charge carriers, μ is the mobility and E is the electric field strength between the electrodes, L is the diffusion length of charge carriers whose maximum length is equal to the spacing of inter-electrodes. The net photo generation rate G, takes into account both photon absorption and dissociation efficiency. If each photo-generated electron/hole pair is collected, the photodiode is working at highest efficiency, the photocurrent is $J_{ph} = qGL$, where q is the elementary charge. If the product of mobility-lifetime products are the same for holes and electrons, $\mu_p \tau_P = \mu_e \tau_e$, the photo-current I_{ph} can be written as *Equation*(5.2)

$$I_{ph} = qG(\frac{V\mu\tau}{L})A \tag{5.2}$$

Where A is the area.

5.2.2 Organic solar cell

The organic solar cell has the same configuration as a normal photo-diode. The results of single layer organic material based solar cells that use the conventional vertical topology has been disappointing. The first bilayer OPV device was reported in 1986[2], with the donor-acceptor interface found to be more efficient for the photo-generation than the semiconductor-metal contact. The bilayer interface is also known as the "planar interconnection structure". For operation of such devices, a thin semiconductor film (thickness $\sim 20nm$) is required to avoid recombination, however this is not a sufficient active film thickness for light absorption. Therefore, the improvement was still not satisfactory. The bulk heterojunction (BHJ) was proposed by Sariciftci and Heeger in 1992 [5]. Impressive achievements have been achieved on the device efficiency. The BHJ structure with vertical topology is the most commonly used structure in current OPV research.

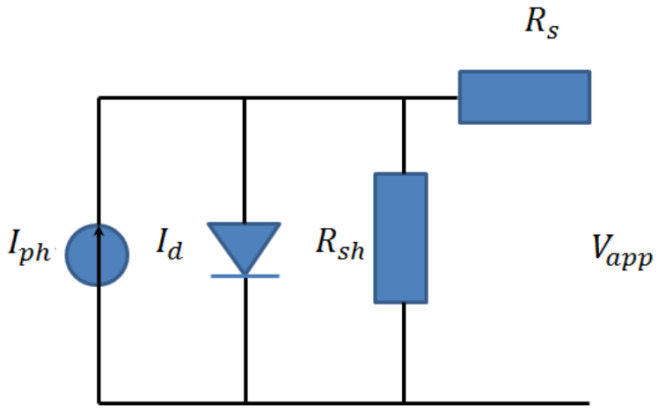

Figure 5.2: Equivalent circuit diagram of a solar cell, which consists of a current source J_{ph} representing photo-generated current, current through the device J_d, shunt resistance R_{sh} and series resistance R_s.

Regardless of different configurations, the current density for the solar cell is always written as :

$$I = \frac{R_{sh}}{R_{sh}+R_s}\{I_0\left[exp(\frac{q(V_{app}-IR_s)}{\eta k_B T})-1\right]+\frac{V_{app}}{R_{sh}}\}-I_{ph} \tag{5.3}$$

Here, I_0 is the saturation current density, η is the ideality factor of the photodiode, and V_{app} is the bias voltage. Based on the current density equation of a solar cell and the equivalent circuit diagram, the open-circuit voltage V_{oc} can be expressed quantitatively using:

$$V_{oc} = \frac{\eta k_B T}{q} ln(\frac{I_{ph}}{I_s}+1) \tag{5.4}$$

Where V_{oc} is the open circuit voltage, which is the largest voltage that the device is able to provide under the condition that the net current through the device is zero, I_{ph} is the

photogenerated current, and I_s is the reverse saturation current. The V_{oc} can be affected by the series resistance R_s and shunt resistance R_{sh}, in addition, the upper limit of V_{oc} is determined by the difference between the splitting of electron and hole quasi Fermi level (E_{Fn} and E_{Fp}), given as $V_{oc} \leq (1/q)(E_{Fn} - E_{Fp})$.

Another important parameter is the short circuit current I_{sc} under zero external load condition($V = 0$):

$$I_{sc} = I_{ph} - I_{sh} - I_d \tag{5.5}$$

Here, I_{sh} and I_d are the current through the shunt resistance and the diode respectively. In practice, both V_{oc} and I_{sc} are dependent on the shut resistance R_{sh} and series resistance R_s

5.2.3 Photo-transistor

Photo-transistors basically have the same configuration and similar characteristics with normally operated OTFTs. Whilst in the normal operation mode, the current flowing through the accumulated channel is controlled by the gate voltage bias at fixed drain/source voltage, and also, the channel conductance can be enhanced by the light absorption. Theoretically, there are two different effects typically occuring in the active polymer channel region under illumination for organic photo transistor. When the gate voltage $V_G < V_{th}$, the transistor operates in the accumulation region, and the so-called photovoltaic effect is dominant. And if $V_G > V_{th}$, than the photo-conductive effect is more significant.

Photovoltaic mode

In the photovoltaic mode, the illumination results in a shift in threshold voltage on the reverse side, for Co-channel device, such that the V_{th} becomes more positive. If the photon-energy absorption occurs among the channel polymer molecules, the excited holes easily flow to the drain electrode whereas electrons accumulate under the source electrode, where they effectively lower the hole injection barrier between the source and the channel. The lowered injected barrier induced by photon absorption may results in a significant increase in channel conductivity and a reverse direction threshold voltage V_{th} shift. The photo-generated current I_{ph} in this mode can be expressed as:

$$I_{ph} = g_m \Delta V_{th} \tag{5.6}$$

Here, g_m is the transconductance of transistor and ΔV_{th} is the shift of the threshold voltage.

Photo conductive mode

When the device is in the off-state ($V_G > V_{th}$ for p-channel), the photo-generated current I_{Ph} shows a linear increase with optical power due to a photo-conductive effect. The situation is similar to the two-terminal devices discussed in earlier chapters, but with the additional gate

terminal responsible for a transverse electric field enhancing photo-generation. The current can be modeled according to:

$$I_{ph} = (q\mu n\frac{dV_D}{dL})WD = BP_{in} \tag{5.7}$$

Where μ is the mobility of majority charge carriers, V_D is the drain voltage, n the charge carrier concentration, W the channel width, D the depth of absorption region (or the thickness of polymer film z_p),and B is a proportionality factor. In addition to the fundamental OFET characteristics, such as the field-effect mobility (μ), the threshold voltage V_{th}, and the subthreshold swing (SS), the figures of merit specific to organic photo transistor (OPTs) are responsivity (R) and photocurrent on/off ratio. The responsivity of OPTs (R) can be defined using the following equation:

$$R = E.Q.E\frac{\lambda q}{P_{in}} = \frac{I_{d,Ph} - I_{d,D}}{P_{in}} \tag{5.8}$$

Where, $E.Q.E$ is the external quantum efficiency, λ is the wavelenegth of light source, P_{in} is the incident optical power, $I_{d,D}$ and $I_{d,ph}$ are the drain current in dark and under illumination, respectively.

5.3 Illuminated IV characteristics of single layer solar cell based on P3HT

The single layer solar cell with a lateral topology is less popular due to the inter-electrode spacings of the lateral topology, which could be tens or hundreds time larger than that of a vertical topology. However, the lateral topology provides direct access to the light incident on the device active area. Using the fabrication method presented in Chapter 4, the inter-electrode spacing can be controlled to a sub-micron size. *Figure*(5.3) shows the effect of light irradiation on the I-V characteristics of a ring structure Schottky diode. The characteristic intersections with axes define the open circuit voltage (V_{oc}) and the short-circuit current (I_{sc}) respectively. The largest power output (P_{max}) is found by the point where the product of the voltage and current is maximum. The inset plot shows the illuminated IV characteristic on the fourth quadrant.

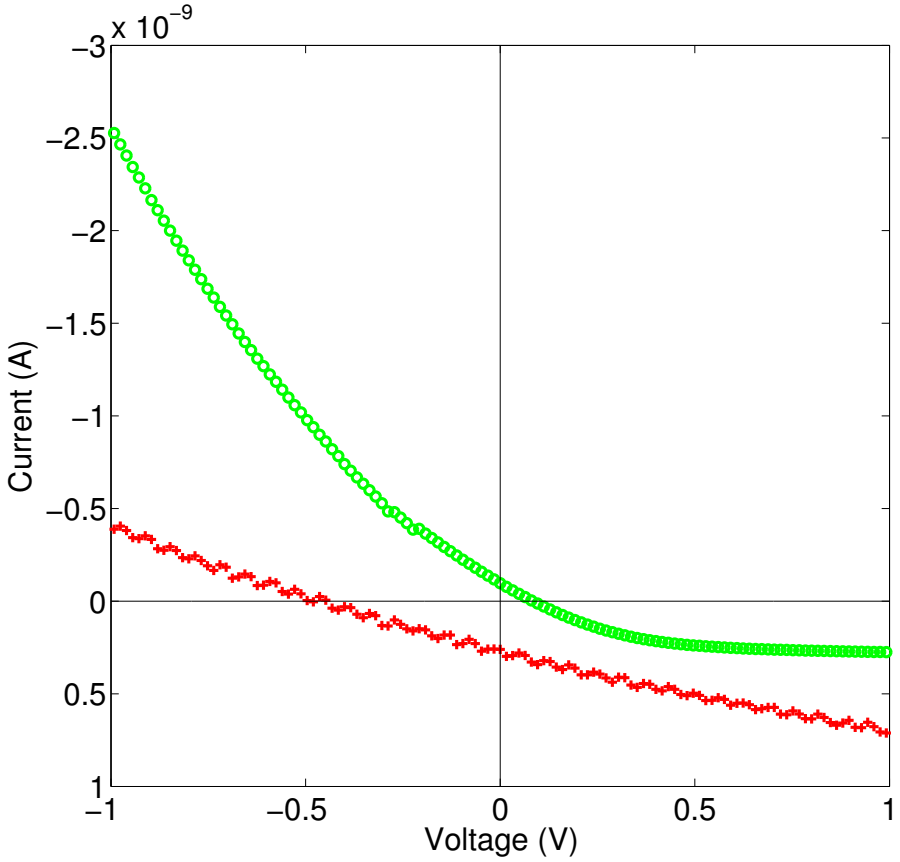

Figure 5.3: Current-voltage (IV) characteristics of a ring P3HT single layer two terminal solar cell (dark, green circle; illuminated, red cross).

Under illumination of a light source with wavelength $\lambda = 550nm$ and incident light power

$P_{in} = 1.38mW/cm^2$, a significant photovoltaic effect was observed as shown in $Figure(5.3)$. The device structure is shown in $Figure(4.12)$, the diameter of the ring is $300\mu m$, the area of illumination area is $1.88 \times 10^{-9}m^{-2}$. The short circuit current $I_{sc} = 2.9 \times 10^{-10}A$ and the open circuit voltage $V_{oc} = 0.42V$. The short circuit current I_{sc} is the current that flows without any external field applied, the charge carriers are drifting due to an internal field, and I_{sc} is determined by the number of photons absorbed, the quantum efficiency for free charge carriers separation, and the transport of the free charge carriers through the semiconductor. The open circuit voltage (V_{oc}) is the maximum voltage delivered by the solar cell. In this case, there is no net current through the device. The open circuit voltage V_{oc} is determined by the difference in the quasi-Fermi level of the metal electrode and semiconductor. As an energy harvesting device, the performance of device should be determined by the efficiency of energy conversion:

$$\eta_{eff} = \frac{P_{max}}{P_{in}} = FF\frac{V_{oc}I_{sc}}{P_{in}} \tag{5.9}$$

Where the P_{max} is maximum power output, the device produces in the photovoltaic mode, P_{in} is the incident power of the light source, and FF is the fill factor. The best efficiency obtained from the results of lateral P3HT single layer device is 0.15% with a fill factor of 39%.

The average fill factor obtained from results is $35\% - 40\%$. In order to obtain a high FF and η_{eff}, two factors are essential, firstly, the shunt resistance should be very large to prevent leakage currents, secondly, the series resistance should be low to get a sharp rise in the forward current. Based on the results presented in the previous chapter, the lateral P3HT based Schottky diode was found to have a large shunt resistance and large series resistance. The large series resistance comes is attributed to the large contact resistance between the polymer and metal. The best obtained efficiency and fill factor for the ring structure device are better than some of the recently published results for a vertical single layer OPVs using P3HT as listed in $Table.(5.1)$. It proves that, if the spacing between electrodes can be maintained in the range from several μm to sub-micron size, this topology can be applied to photovoltaic device. Compared to the vertical topology, the lateral topology has the main advantage of providing direct access to the active material, which may improve the light absorption efficiency. Althought, the ring structure Schottky barrier type solar cell has a better efficiency than the normal single layer solar cell. However, its efficiency is still much lower than that of the vertical bulk heterojunctions, whose efficiency exceeds 3%. This may be due to two factors: firstly, the contact resistance of the polymer is too large and significantly limits the photo-current, and secondly, the efficiency of the charge carriers dissociation at the metal-semiconductor interface is not high enough.

Efficiency (%)	$FF(\%)$	Device	Comments
3.3×10^{-5}	25	Al/P3HT/PEDOT:PSS/ITO	single layer polymer, vertical topology [6]
3.51	62	ITO/ PEDOT:PSS/P3HT:PCBM/LiF/Al	BHJ, P3HT:PCBM blend ratio: 1 : 1 [7]
3.39	49.3	PEDOT:PSS/P3HT:PCBM:ZNO	BHJ, P3HT:PCBM blend with ZnO particles [8]

Table 5.1: Survey of important performance parameters of various P3HT based solar cells.

Compared to the vertical topology, the other major differences is the effect of the polymer film thickness. In the vertical topology, thicker polymer film is used, which may result in a higher possibility of charge carrier recombination and lower efficiency. Whilst, in the lateral topology, the electrode spacing is independent of film thickness and the thicker the film, the better the light absorption efficiency and lower contact resistance (or series resistance). The best results in this chapter was obtained from a device deposited with solution of concentration $2mg/mL$. This topology may have potential for application on bulk heterojunction devices, and device may yield high efficiency of energy conversion.

5.4 IV characteristics of P3HT ring Schottky barrier photo-detector under illumination

Figure(5.4) to *Figure*(5.6) show the effect of illumination on devices. The devices have the same structure as in the previous section, but not identical to avoid the influence of device degradation. The current-voltage characteristics under illumination of the same devices were obtained continuously within 96 hours to investigate the device stability. The responsivity of a polymer photo-diode is a measure of the sensitivity to light, in other words, it is a measure of the effectiveness of the conversion of the light power into the electrical signal. The value is defined as the ratio of the photocurrent I_P to the incident light power P_{in} at a given wavelength:

$$R_\lambda = \frac{I_{ph}}{P_{in}} \tag{5.10}$$

The quantum efficiency (Q.E.) is defined as the fraction of the incident photons that contribute to photo current. It is related to responsitivity by:

$$Q.E. = \frac{R_{\lambda Observed}}{R_{\lambda Ideal}} = R_\lambda \frac{hc}{\lambda q} = 1240 \frac{R_\lambda}{\lambda} \tag{5.11}$$

All the diodes mentioned in this part use the ring structure mentioned in previous chapter, the active layer is single layer P3HT film, which is spin-coated onto devices. The xylene is used as polymer solvent, different diodes use different solution for film deposition, whose concentrations(polymer weight/ solvent volume ratio) range from $0.5mg/mL$ to $2mg/mL$. Those measurements have been made continuously for 4 days to investigate the stability of device performance. The devices are stored and characterized in normal air environment. In the solar cell, the effect of I_{dark} is not very significant. For example, based on the equation $V_{oc} = \frac{\eta k_B T}{den} ln(\frac{I_{ph}}{I_{dark}} + 1)$, a reduction of dark current by one order ($10\times$) only increases the V_{oc} by $\sim 58mV$. While in this case, the dark current I_{dark} plays a key role in determining the overall performance of photodiode as a photo-detector, which is discussed in chapter 2. With reduction in the dark current I_{dark}, the I_{ph}/I_{dark} and the detectivity D^* improve significantly. *Figure*.(5.7) shows 100 times DC bias sweep of device under the illumination, which proves the bias-stability of ring structure Schottky diode under illumination. Although, there some significant noise in the reverse bias region, the performance of the ring Schottky diode is stable. Full recovery of devices to the initial dark IV characteristics was observed after removing the light source.

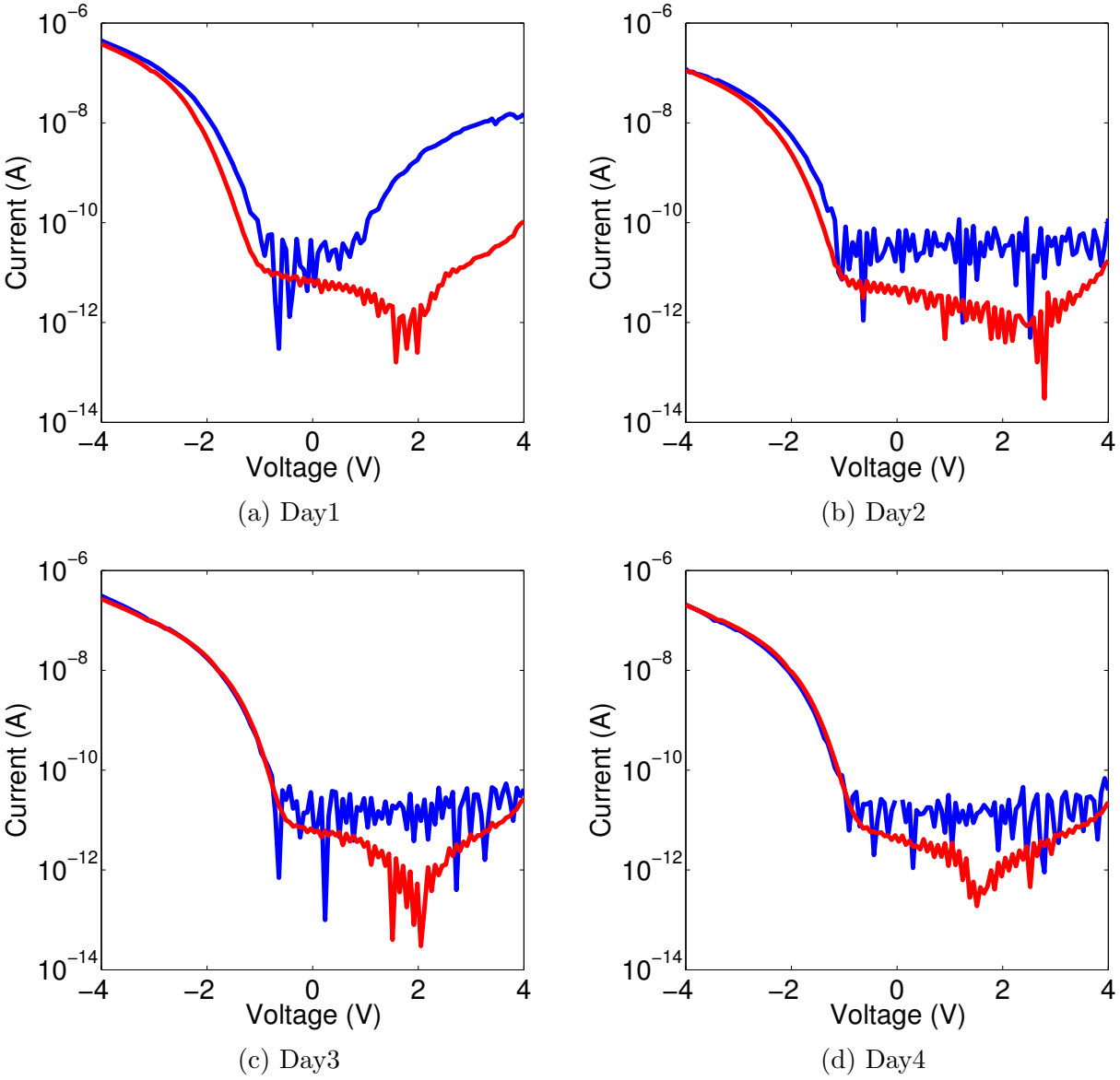

(a) Day1

(b) Day2

(c) Day3

(d) Day4

Figure 5.4: Current-voltage characteristics of P3HT ring structure photodiode, the concentration of the polymer solution was $0.5mg$ P3HT/mL xylene.(Blue, illuminated; Red, Dark).

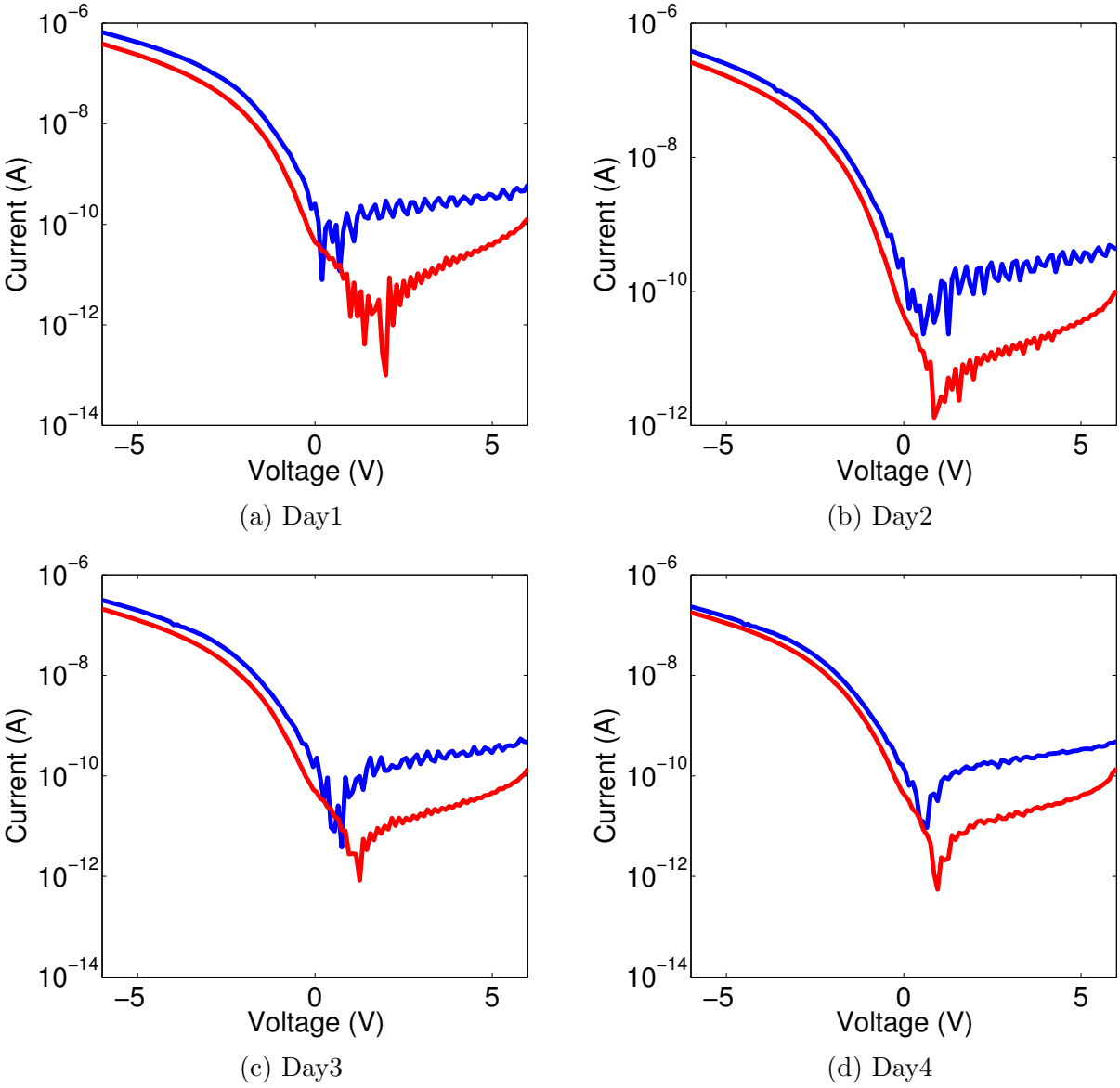

(a) Day1

(b) Day2

(c) Day3

(d) Day4

Figure 5.5: Current-voltage characteristics of P3HT ring structure photodiode, the concentration of the polymer solution was $1mg$ P3HT/mL xylene.(Blue, illuminated; Red, Dark).

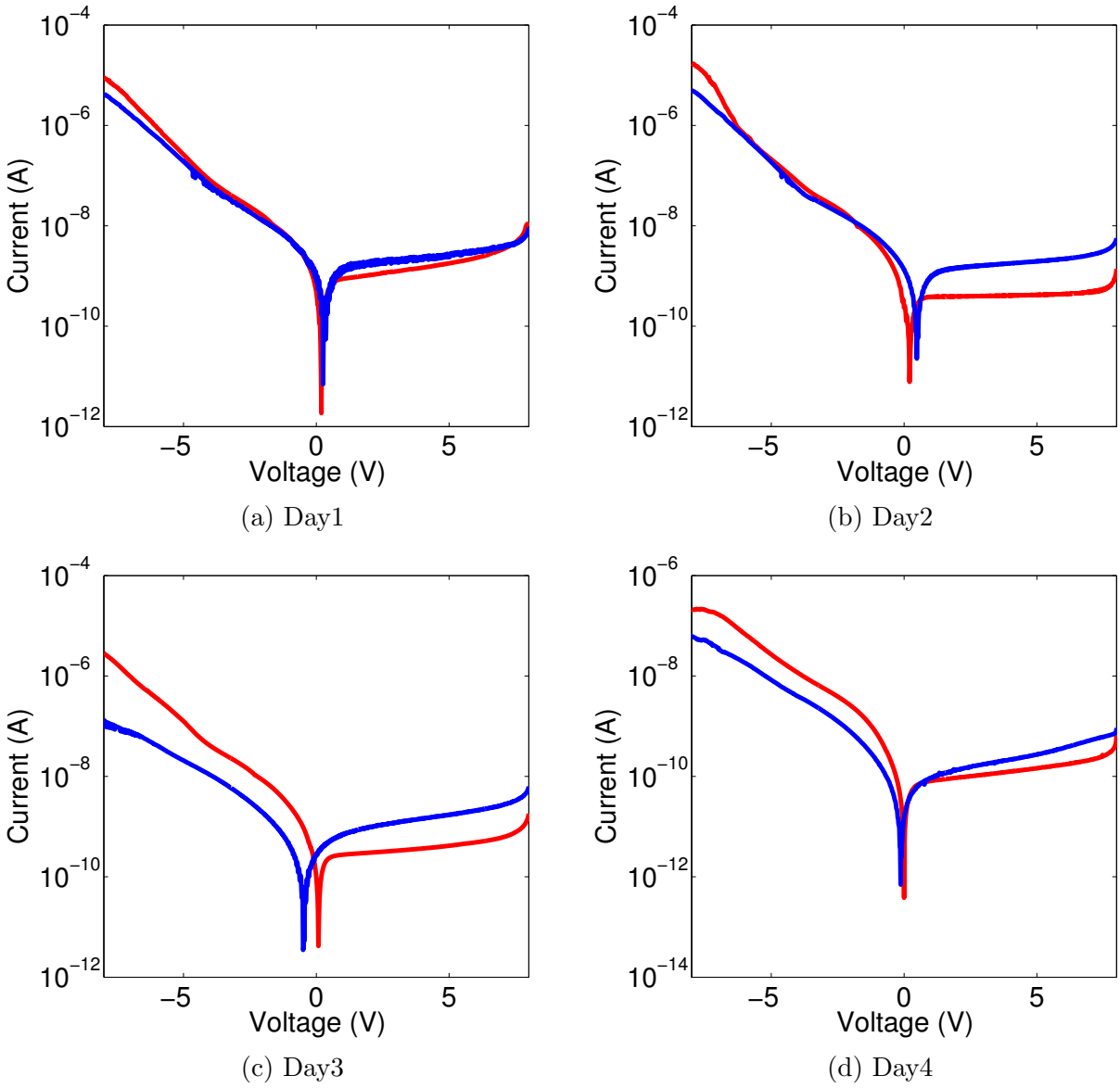

(a) Day1

(b) Day2

(c) Day3

(d) Day4

Figure 5.6: Current-voltage characteristics of P3HT ring structure photodiode, the concentration of the polymer solution was $2mg$ P3HT/ml xylene. (Blue line, illuminated; Red, Dark)

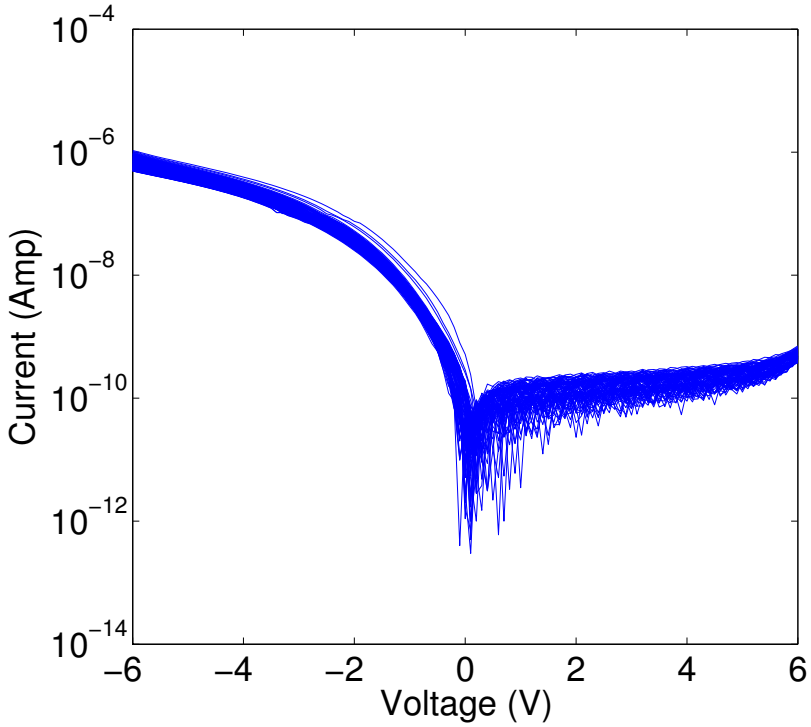

Figure 5.7: Current-voltage characteristics of a ring Schottky photo diode, with multiple voltage sweep carried out under illumination.

From the current-voltage characteristic presented in *Figure*(5.4) to *Figure*(5.6), significant noise can be observed in the reverse bias region. For the photodiode, several sources of the noise signal can be identified. Firstly, fluctuation in both dark current and photo current, which may be caused by the vibration of the probe station and background radiation. Shot noise [10], is dominated in the photo conductive mode (reverse bias under light irradiation). It can be expressed as:

$$I_{sn} = \sqrt{2q(I_{dark} + I_B)\Delta f} \tag{5.12}$$

Where I_{dark} is the dark current, I_B is the current due to the background irradiation, q is the elementary electron charge, and Δf is the bandwidth of noise measurement. Secondly, another source is the thermal noise, thermal noise occurs in any conductor or semiconductor device and is caused by the random thermal motion of the current carriers[10].

$$I_{tn} = \sqrt{\frac{4k_B T \Delta f}{R_{sh}}} \tag{5.13}$$

Where R_{sh} is shunt resistance of the device, k_B is the Boltzmann constant, and T is the absolute temperature. Based on *Equation*(5.12) and *Equation*(5.13), the noise level can be estimated, the shot noise is about $1pA$ and the thermal noise is about $10pA$. Due to the level of noise current, the thermal and shot noise have the significant influnce on the fluctuation in I-V curves, especially for the photodiode with lower polymer concentration.

The detectivity of photodiode (or photodetector) is a measure of the effectiveness of the photocurrent readout process. The unit of D^* is $cm \cdot Hz^{\frac{1}{2}} \cdot W^{-1}$. It can be written as:

$$D^* = R_\lambda \sqrt{\frac{R_0 A}{4k_B T}} \tag{5.14}$$

where R_0A is the resistance area product in the dark condition, which can be expressed as $R_0A = \frac{k_B}{qA^*T} exp(\frac{\phi_b}{k_B T})$ for a Schottky barrier diode following the thermionic emission model. However, based on analysis of Schottky barrier diode in previous chapter, the ideality factor η is greater than 3, which means that device do not follow the thermionic emission model perfectly. A more straightforward approach for estimation of the detectivity D^* is shown as below:

$$D^* = \frac{\sqrt{\Delta f \times A}}{NEP} = \frac{R_\lambda \times \sqrt{A\Delta f}}{\sqrt{2qI_{dark}\Delta f}} \tag{5.15}$$

where I_{dark} the dark current, A is the active area of diode, and R_λ is the responsivity. The shot noise dominates the total noise, and the noise equivalent power (NEP) can be approximated to $\frac{\sqrt{2qI_{dark}\Delta f}}{R_\lambda}$. The bandwidth Δf is defined by full width at half maximum of the light source spectrum, which is obtained by use of a spectrometer (ocean optic usb 2000+). Based on *Equation*(5.14) and *Equation*(5.15), it is clear that reducing the leakage current of the device can significantly lower the noise level and improve the detectivity.

D^* $(cm \cdot Hz^{\frac{1}{2}} \cdot W^{-1})$	$R_\lambda(A/W)$ @ $V_{bias} = -1V$	device	comments
3.15×10^{11}	0.17	P3HT/PCBM BHJ	green led is used as light source(575nm)[12]
3.0×10^{12}	0.27	P3HT/PCBM BHJ	TAZ interfacial layer [13]

Table 5.2: Survey of important performance parameters of various P3HT based BHJ photo detector.

Table(5.3) summarises all the P3HT ring structure Schottky barrier photodiode optical parameters extracted from *Figure*(5.4), *Figure*(5.5), and *Figure*(5.6). It is clear that the device with lower dark current yields a better light detectivity in the visible region. In addition, the device with a lower polymer solution concentration has a better light responsivity. The best obtained detectivity results are in the same order of magnitude as those obtained by using a vertical organic BHJ structure [14][15]. Compared to results presented in *Table*.(5.2), the results on detector properties aspect are similar. However, the fabrication procedures of ring structure P3HT photodiode are simpler and cheaper. Air-stability of the device on the optical characteristics was not that satisfactory, especially for the device with lower polymer solution concentration. For instance, after 96 hours since the D^* of the sample presented in *Figure*(5.4) decreased by 2 orders of magnitude.

Solvent concentration	Comments	R_λ@ V_{bias}	I_{ph}/I_{dark}	D^* $(cm \cdot Hz^{\frac{1}{2}} \cdot W^{-1})$
$0.5mg/mL$	Storage in air for 8 hours	$0.43A/W$@ 4V	166.2	4.02×10^{11}
..	Storage in air for 32 hours	$0.97mA/W$@ 2V	63.2	1.18×10^{10}
..	Storage in air for 56 hours	$0.803mA/W$@ 2V	55	1×10^{10}
..	Storage in air for 80 hours	$0.59mA/W$@ 2V	12.75	4.12×10^{9}
$1mg/mL$	Storage in air for 8 hours	$13.7mA/W$@ 4V	20	2.488×10^{10}
...	Storage in air for 32 hours	$8.4mA/W$@ 4V	11	1.447×10^{10}
...	Storage in air for 56 hours	$8.3mA/W$@ 4V	7.9	1.226×10^{10}
...	Storage in air for 80 hours	$7.9mA/W$@ 4V	8.2	1.215×10^{10}
$2mg/mL$	Storage in air for 8 hours	$26mA/W$@ 4V	0.4	5.2×10^{9}
....	Storage in air for 32 hours	$52.6mA/W$@ 4V	3.33	2×10^{10}
....	Storage in air for 56 hours	$42mA/W$@ 4V	3	1.6742×10^{10}
....	Storage in air for 80 hours	$4mA/W$@ 4V	0.7	2.64×10^{9}

Table 5.3: P3HT ring structure Schottky barrier photodiode optical parameters.

5.5 P3HT based photo transistor

The first polymeric photo transistor based on P3OT was reported in 2001 [11], and found to exhibit a large I_{Ph}/I_{dark} ratio under illumination. Compared to the results obtained on the lateral photodiode fabricated with the same polymer in the same condition and tested under the same light source, the responsivity and light/dark current ratio are much larger, which may be due to the influence of the gate dielectric field. The output and transfer characteristics of P3HT organic photo-transistor (OPT) are presented in figures from *Figure.*(5.8) to *Figure.*(5.11). The P3HT OPTs with bottom gate bottom contact (BGBC) structure are fabricated using SiO_2 as the gate dielectric with the various concentration of P3HT spin-coated on the device. As observed in figures below, the devices with thinner polymer film yield a better responsivity to light. As indicated in the *Equation*(5.8) of the organic photo transistor responsivity, the off-state drain current of the OPTs increases due to the light illumination. In addition, a significant shift of the V_{th} can be observed, which can be seen from *Figure.*(5.8)(*a*).

Solution concentration (mg/mL)	Figure number	Responsivity (A/W)	I_{ph}/I_{dark}
0.5	5.8	34.1	253
1	5.9	7.4	35
2	5.10	2.74	8.9
3	5.11	8.8	5.2

Table 5.4: Summary of the parameters extracted from a BG/BC P3HT based photo transistors with different concentrations of the polymer solution.

Table.(5.4) summaries the optical parameters extracted from OPTs results presented in figures from *Figure.*(5.8) to *Figure.*(5.11). It seems that the OPTs with a lower polymer solution concentration has a better light responsivity, which may result from their lower level of the dark current.

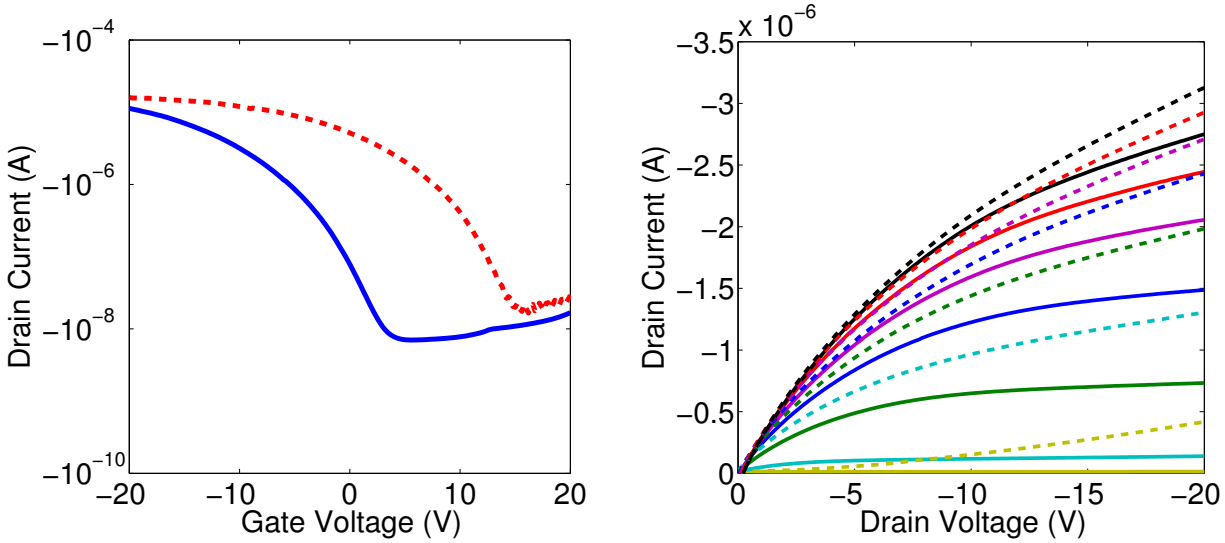

(a) $0.5mg/mL$ Transfer Characteristics (b) $0.5mg/mL$ Output Characteristics

Figure 5.8: Output and transfer characteristics of P3HT based organic photo-transistors under dark (line) and illuminated condition (dot).

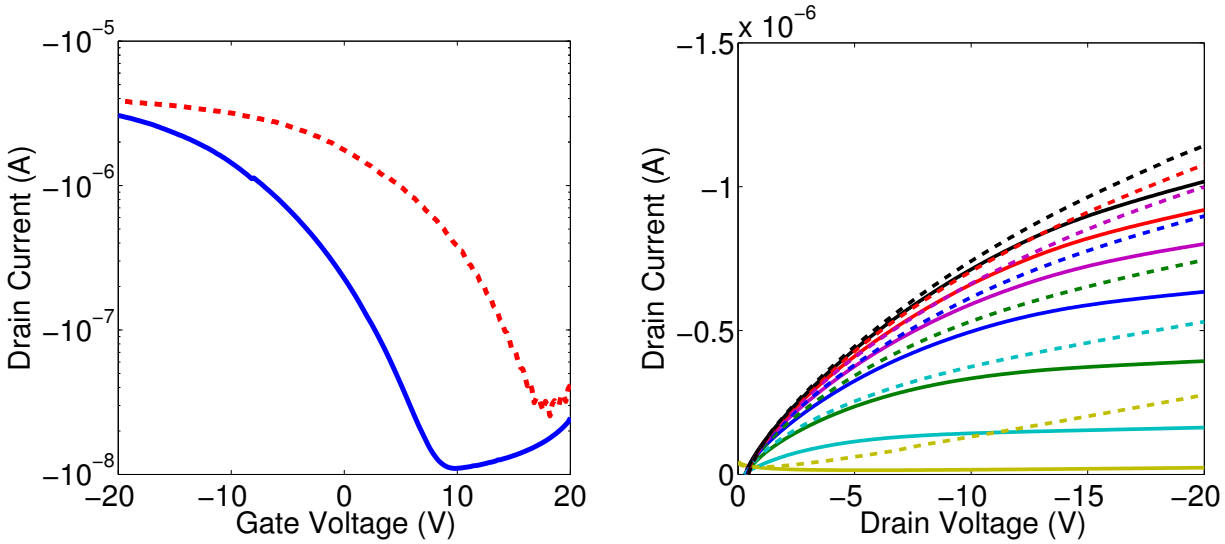

(a) $1mg/ml$ Transfer Characteristics (b) $1mg/ml$ Output characteristics

Figure 5.9: Output and transfer characteristics of P3HT based organic photo-transistors under dark (line) and illuminated condition (dot).

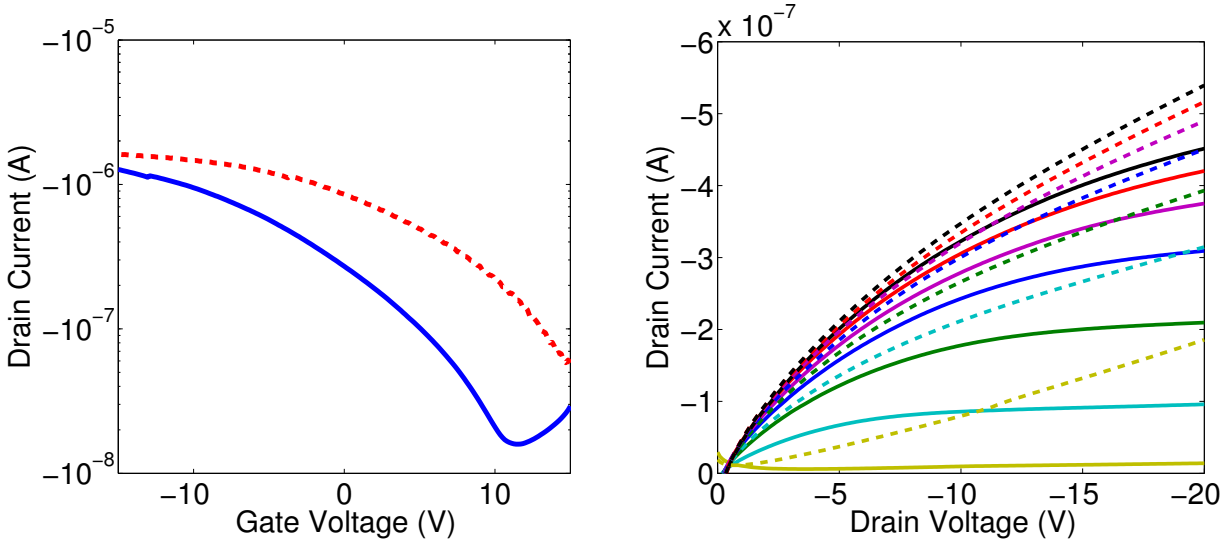

(a) $2mg/ml$ Transfer Characteristics (b) $2mg/ml$ Output Characteristics

Figure 5.10: Output and transfer characteristics of P3HT based organic photo-transistors under dark (line) and illuminated condition (dot).

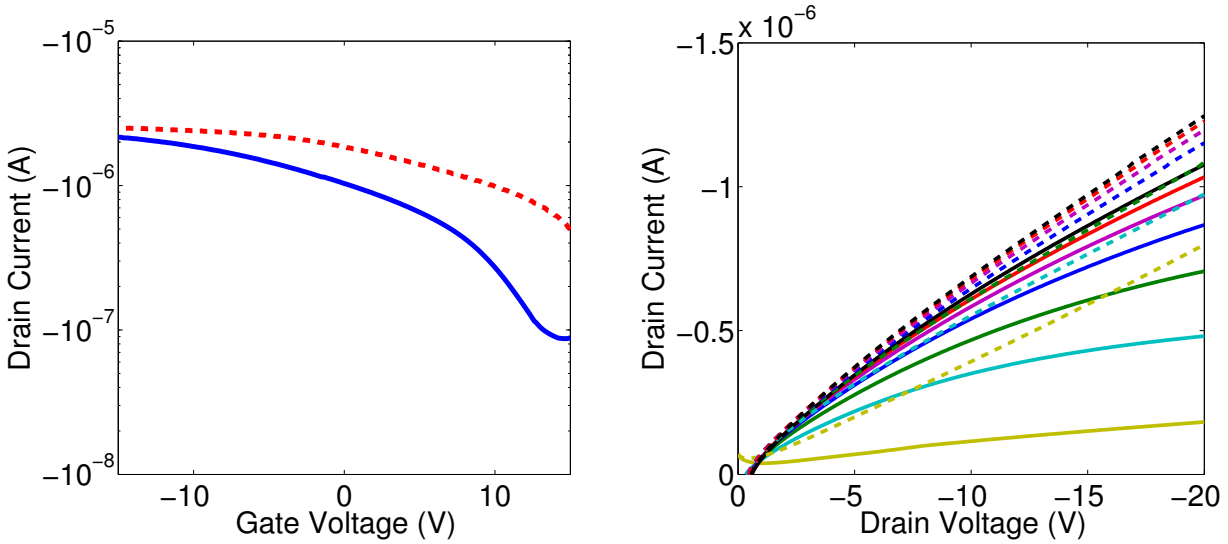

(a) $3mg/ml$ Transfer Characteristics (b) $3mg/ml$ Output Characteristics

Figure 5.11: Output and transfer characteristics of P3HT based organic photo-transistors under dark (line) and illuminated condition(dot).

5.6 Conclusions

The current-voltage characteristics of P3HT lateral Schottky barrier diodes were tested under illumination. The best energy conversion efficiency of a single layer Schottky barrier type solar cell achieved was 0.15% with a fill factor of 39%. Compared to the literature, mean efficiency of P3HT single layer solar cell with vertical topology, the lateral topology indeed improves efficiency of energy conversion. However, its efficiency is still much lower compared to recently published P3HT:PCBM BHJ solar cells. The lateral single layer Schottky barrier diode may improve the light absorption efficiency, however, the efficiency for separation of the excitons was low and is dependent on the nature of the electrode. The performance of the ring structure Schottky barrier diode as a photo detector in visible light shows sensitivity comparable to similar devices with BHJ structure. For the lateral topology device, the active layer is directly exposed to light and air. Therefore, in order to eliminate the influence of oxygen to the polymer film and achieve satisfactory air stability, a transparent passivation or encapsulation layer should be applied on the top the polymer film to block the oxygen and moisture, especially for those air sensitive materials like P3HT.

References

[1] K. J. Baeg, M. Binda, D. Natali, M. Caironi, and Y. Y. Noh, "Organic Light Detectors: Photodiodes and Phototransistors,"Advanced Materials, vol. 25, no. 31, pp. 4267-4295, 2013.

[2] C. W. Tang, "Two layer organic photovoltaic cell,"Applied Physics Letters, vol. 48, no. 2, pp. 183, 1986.

[3] A. J. Heeger, N. S. Sariciftci, "Conjugated polymer-acceptor heterojunctions; diodes, photodiodes, and photovoltaic cells,"U.S. Patent 5331183 A, 19 July 1994.

[4] B. Kippelen, and J. L. Bréads,"Organic Photovoltaics,"Energy& Environmental Science, vol. 2, no. 3, pp. 251-261, 2009.

[5] S. E. Sean, B. J. Christoph, S. N. Serdar, P. Franz, F. Thomas, and H. C. Jan, "2.5 % efficient organic plastic solar cells ,"Applied Physics Letters, vol. 78, no. 6, pp. 841-843, 2001.

[6] Y. T. Chang, J. H. Su, Y. T. Shih, and Y. L. Shih, "Study of Al/Organic/ITO Polymer Solar Cell on Glass Substrate,"Applied Mechanics and Materials, vol. 448-453, pp. 1446-1451, 2013.

[7] D. D. S. Fung, L. F. Qiao, C. C. H. Wallace, C. D. Wang, W. E. I. Sha, F. X. Xie and S. L. He, "Optical and electrical properties of efficiency enhanced polymer solar cells with Au nanoparticles in a PEDOTPSS layer", Journal of Materials Chemistry, vol. 21, no. 41, pp. 16349-16356, 2011.

[8] S. H. Oh, S. J. Heo, J. S. Yang and H. J. Kim, "Effects of ZnO Nanoparticles on P3HT:PCBM Organic Solar Cells with DMF-Modulated PEDOT:PSS Buffer Layers,"ACS Applied Materials & Interfaces, vol. 5, no. 22, pp. 11530-11534, 2013.

[9] K. S. Narayan, and N. Kumar, "Light responsive polymer field-effect transistor, "Applied Physics Letters, vol. 79, no. 12, 1891, 2001.

[10] S. M. Sze, Physics of Semiconductor Devices, Wiley, 2007.

[11] M. Razeghi and A. Rogalski, "Semiconductor ultraviolet detectors,"Journal of Applied Physics, vol. 79, no. 10, pp. 7433, 1996.

[12] B. Arredondo, B. Romero, J. M. S. Pena, A. Fernández-Pacheco, E. Alonso, R. Vergaz, and C. D. Dios, "Visible Light Communication System Using an Organic Bulk Heterojunction Photodetector,"Sensors, vol. 13, no. 9, pp. 12266-12276, 2013.

[13] S. Valouch, C. Hönes, S. W. Kettliz, N. Christ, H. Do, M. F. G. Klein, H. Kalt, A. Colsmann, and U. Lemmer, "Solution processed small molecule organic interfacial layers for low dark current polymer photodiodes,"Organic Electronics, vol. 13, no. 11, pp. 2727-2732, 2012.

Chapter 6

Conclusions

This chapter summarises the main conclusion in the thesis. Future work needed in improving device performance are suggested.

6.1 Conclusion

- Detailed analysis of organic P3HT based Schottky diode is presented in this thesis, and three type different device structures and associated fabrication processes are presented. The ring P3HT Schottky diode achieved a satisfactory rectification ratio under ambient condition. Deposition of the P3HT solution were carried out using drop-cast and spin-coating methods under clean ambient condition. The air instability of P3HT Schottky barrier diodes were also analysed by comparing the results measured in air at different times. The results show significant effect of air expose to device performance and important parameters such as doping density and bulk mobility. However, further work needs to be done to understand the internal mechanism of bulk mobility change.

- From the current-voltage characteristics of P3HT lateral Schottky barrier diodes under illumination, the best energy conversion efficiency obtained in this thesis for a single layer Schottky-barrier type solar cell was 0.15% with fill factor of 39%. Compared to the literature, the mean efficiency of P3HT single layer solar cell with vertical topology, it seems the lateral topology indeed improve efficiency of energy conversion, however, its efficiency are still much lower compared to recently published P3HT:PCBM BHJ solar cell results. The lateral single layer Schottky barrier diode may improve the light absorption efficiency, however, the separation of excitons still has low efficiency and is dependent on the nature of the electrode. For the lateral topology device, the active layer is directly exposed to light and air. Therefore, in order to eliminate the influence of oxygen in the polymer film and achieve satisfactory stability, a transparent encapsulation layer should be applied on the top the polymer film to block the oxygen and moisture, especially for those air sensitive material like P3HT.

- Thin film transistors using P3HT were fabricated with BGBC and BGTC configurations. The mobility and threshold voltage obtained from transconductance and channel conductance plots were different. The mobility extracted from the transconductance was higher than that value extracted from channel conductance, while the threshold voltage extracted from the transconductance was lower. The channel conductance was obtained in the linear region where the drain field dependency is small and significantly affected by the polymer bulk conductivity unlike the transconductance plots obtained in the saturation region. The effect of the solution concentration has been investigated to optimise the device performance.

6.2 Future work

- The goal of fabricating two lateral electrodes whose spacing is around $1\mu m$ has been achieved by using undercut and photo resist lift-off processing. The gap between two electrodes is not very uniform, which may affect the performance of the lateral diode. Some investigations concerning edge of photo resist after development must be done. Apart from those factors that have already been considered such as development time and soft bake time, there are still many other factors that may affect the outcome of the lithography, such as strength of UV light, exposure time, chemical treatment before/after the UV light exposure, control of metal etch time and even selection of the photo resist. If the uniformity of the gap is improved, the result of lateral structure diode should be more reliable.

- Some modification of the fabrication of P3HT TFT should be made in future to improve its performance, the most important ones are reducing the threshold voltage. The future work should focus on adjusting the carrier concentration.

- Encapsulation is definitely an important area that should be studied with P3HT. Seen from all air-stability results, the electrical and optical characteristic of the device were affected by the photo-oxidation effect.

- The study of optical characteristics of photo sensitive devices using P3HT is not sufficient. The illuminated IV characterization is conducted under a fixed wavelength and fixed power light source only. A power adjustable light source should be used to investigate the dependency of their detectivity and responsivity on the irradiation power. In addition, a set of LEDs with different colour can also be used as a light source to explore the relationship between the light wavelength and device performance, and assessing the spectral response range. Another important parameter that was absent from this optical characteristic study is response time, which looks at the photocurrent transient response and rise and fall time of the photocurrent.

Appendix

A	Area(m^2)
A^*	Richard constant $120A/cm^2K$
E_F	Extrinsic Fermi level (eV)
E_{Fn} E_{Fp}	Quasi Fermi level for electrons and holes(eV)
η	Ideality factor of diode
J	Current density
$Q.E.$	Quantum Efficiency
I_{ph}	Photocurrent
I_d	Dark current
R_{sh}	Shunt Resistance
R_s	Series Resistance
R_λ	Responsivity
V_{oc}	Open circuit voltage
V_G	Gate Voltage (V)
V_D	Drain voltage (V)
V_{th}	Threshold voltage
W	Width of the TFT channel(μm)
I_{sc}	Short circuit current
k_B	Boltzmann constant
K_{UML}	Constant in Universal Mobility Law
μ	Mobility
z_p	Thickness of the polymer film in TFT
D^*	Detectivity (jones)
E_T	lowest energy level for significant current
E_{th}	Thermal energy
N_G	Gaussian DOS
ε_0	Permittivity in free space
ε_s	Relative permittivity for semiconductor
FF	fill factor
P_{in}	incident light source power
R_λ	Responsivity
m	Exponential index in Universal Mobility Law
L	Length of the TFT channel
ϕ_{bi}	built-in potential
T_0	Characteristics temperature for the distribution of carriers
T_C	Characteristics temperature of the distribution of traps
I_D	Drain Current
Δf	Bandwidth of the light source
NEP	Noise equivalent power
R_0	Resistance of photo-diode in dark condition
I_{sn}	Shot noise in the optical test
I_{tn}	Thermal noise in the optical test
P_{in}	Incident light power per unit area
λ	Wavelength of the light source
P_{max}	Maximum solar cell power output
I_s	Diode reverse bias saturation current

W_d	Width of the depletion region
C_d	Capacitance of the depletion region
ϕ_b	Barrier height of Schottky barrier diode
G	Conductance
R_{dr}	Differential resistance in the werner's method
J_0	Saturation current density
C_0	Gate insulator capacitance
σ	Conductivity of polymer film in OTFT
S	Sub-threshold swing of Thin Film Transistor
g_m	Transconductance of TFT
g_D	Channel conductance of TFT
N_{ex}	Exponential DOS

Image charge force effect

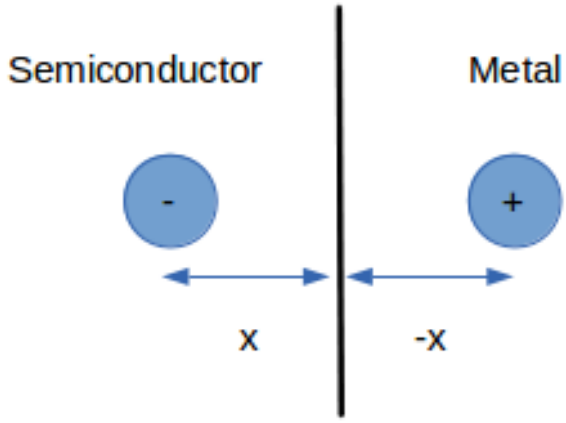

Figure 1: Image charge present in the metal due to an identical opposite charge present in semiconductor, two charges have got same distance to x the semiconductor/metal interface.

The semiconductor contains both a depletion region and a neutral region. The image-force-induced lowering of the barrier energy for charge carrier emission occurs in the presence of electric field. This positive charge is referred to as the image charge. The attractive force toward the metal, called the image force,is given by

$$Force = \frac{-q^2}{4\pi\varepsilon_0\varepsilon_p(2x)^2} = \frac{-q^2}{16\pi\varepsilon_0\varepsilon_s x^2} \tag{1}$$

where ε_0 is the permittivity of free space, ε_s the relative permittivity of P3HT($\varepsilon_p = 2.7$)[5], x is the distance between the charge and the interface. The work done to an electron in the course of its transfer from infinity to the point x is given by:

$$E(x) = \int_{\infty}^{x} Force \cdot dx = \frac{q^2}{16\pi\varepsilon_0\varepsilon_s x} \tag{2}$$

This energy corresponds to the potential energy of an electron placed at a distance x from the metal surface, which is measured downwards from the x-axis. When an external field F is applied in the $-x$ direction, the total potential energy $E_{potential}$ is given by the sum of both:

$$E_{potential} = \frac{q^2}{16\pi\varepsilon_0\varepsilon_s x} + qFx \tag{3}$$

based on above equation, the distance x where maximum height of barrier reached, hence where $dE_{potential}/dx = 0$:

$$\frac{dE_{potential}}{dx} = \frac{d}{dx}\left(\frac{q^2}{16\pi\varepsilon_0\varepsilon_s x_{max}} + qx_{max}F\right) = 0 \tag{4}$$

The rearrangement giving an expression for x_{max}:

$$x_{max} = \sqrt{\frac{q}{16\pi\varepsilon_0\varepsilon_s F}} \tag{5}$$

The resulting image-force lowering $\Delta\phi_B = 2x_{max}F$. From Poisson's equation, the maximum field strength F_{max} can be obtained as below:

$$\frac{d^2\phi}{dx^2} = -\frac{qN_A}{\varepsilon_0\varepsilon_s} \tag{6}$$

Here N_A is the dopant concentration. Multiplying $\frac{d\phi}{dx}$ on both sides of the equation:

$$\frac{d^2\phi}{dx^2}\frac{d\phi}{dx} = -\frac{qN_A}{\varepsilon_0\varepsilon_s}\frac{d\phi}{dx} \tag{7}$$

And integrating over the limit from 0 to F_{max}:

$$\int_{F_{max}}^{0} F dF = -\frac{qN_A}{\varepsilon_0\varepsilon_s}\int_0^{\phi} d\phi \tag{8}$$

The maximum field strength F_{max}can be expressed as below:

$$F_{max} = \sqrt{\frac{2qN_A\phi}{\varepsilon_0\varepsilon_s}} \tag{9}$$

Subtituting the expression of maximum depletion region field strength into the equation, the expression for distance X_{max} where the highest barrier reaches.

$$x_{max} = \sqrt[4]{\frac{q}{512\pi^2\varepsilon_0\varepsilon_s N_A V}} \tag{10}$$

The lowering of the potential barrier due to the image charge force:

$$\Delta\phi_b = 2x_{max}F_{max} = 2\sqrt[4]{\frac{q}{512\pi^2\varepsilon_0\varepsilon_s N_A V}}\sqrt{\frac{2qN_A\phi}{\varepsilon_0\varepsilon_s}} \tag{11}$$

Lateral Structure Diode Fabrication

1. Rinsing of the substrate and aluminium evaporation

   The glass is thoroughly rinsed using Decon 90, acetone, propanol and de-ionized water to remove any dirt on the substrate, and dried in the furnace. Secondly, 220 nm metal layer is formed by evaporating aluminium wire at a rate around 4.5 A/s under pressure of 10^{-6} mbar.

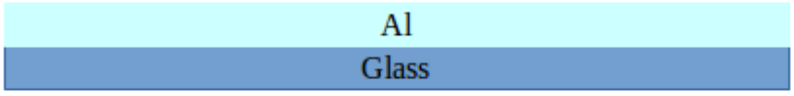

Figure 2: Deposition of the aluminium layer.

2. Aluminium layer photo-lithography

   Two different photoresist layers are spin coated onto the aluminium layer. The underlying photo resist layer is LOR 3A. The LOR 3A layer is dehydrated by a 2 minutes soft bake at temperature of 179°C. The overlying photo resist is HPR 504; the HPR 504 layer is dehydrated by a 90 seconds soft bake at 110°C. Both layers are spin coated under a speed of 3000 rpm. The cross-section of the sample after photoresist deposition is shown in *Figure*.3. Due to the property of LOR 3A, which is ideal for the bi-layer undercut; the undercut rated is defined by the soft bake temperature and time. After UV exposure, the exposed portion of the photo resists layer is weakened and dissolved by the developer solution and the LOR 3A layer will be undercut. This step is followed by 2-minutes 140°C hard bake and 10 minutes aluminium wet etch.

Figure 3: Deposition of the photoresist layers.

3. Gold layer evaporation and layer patterning

   The cross-section diagram of the sample after finishing previous step is shown in *Figure*.4. A 50 nm thickness gold layer is formed onto the top, which is shown in

Figure.5. The microstrip 2001 will lift off the photoresist remaining and the gold layer over remaining layers of photoresist, as shown in *Figure*.6. The gap between two electrodes is formed in this way. Due to limitation of the negative photoresist used in the photo lithography and undercut, the minimum gap is in the um order, which limits the on current of device. In addition, another photo-lithography step is taken to divide the gold strips into several parts on sample, as shown in *Figure*.7.

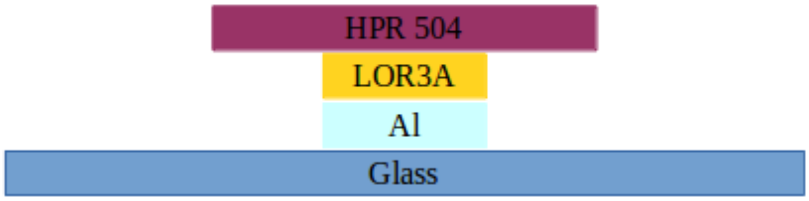

Figure 4: Aluminium photo lithography.

Figure 5: Deposition of the gold layer.

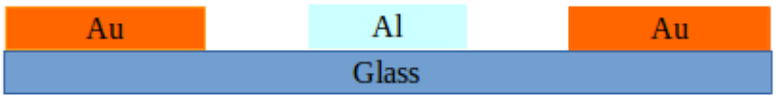

Figure 6: Lift-off of the unwanted gold layer.

4. OSC film deposition and patterning

   The polymer P3HT is dissolved in xylene, the solvent is heated on the hotplate at 80°C and ultrasonic bath is given in the middle of heating to make sure the solvent is fully mixed. Then the organic semiconductor is spin-coated onto the sample twice followed by 2 minutes bake on the 80°C hotplate. After the OSC film is deposited on the sample, negative photo resist is spin-coated on the top of the OSC film. UV light

makes the exposed part of the photo-resist layer harden, so as not be dissolved by the developer solution. At the last stage, the sample is soaked in the developer solution and the uncovered OSC is etched. Finally the photo-resist layer on the top of the patterned OSC film is lift-off, the top view of finished sample is shown *Figure*.8. All of the fabrication procedures are finished, and the sample can be stored in a Glove box to allow the polymer solvent evaporate and make the polymer film stable. The advantage of this structure and fabrication technique is that the quality of organic semiconductor film is improved as the film is spin-coated onto the sample, which gives a more uniform film than the drop-cast method. One major drawback in the lateral structure device fabrication is that the aluminium electrode is attacked by gold etchant solution during the patterning of gold electrode, which may affect the interface of the Schottky metal and the semiconductor.

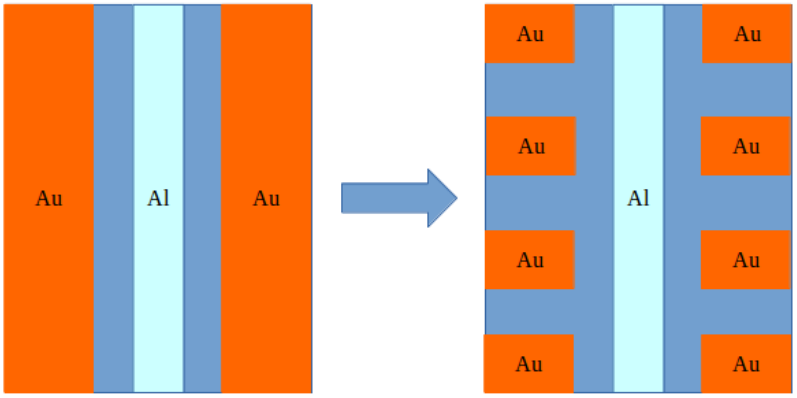

Figure 7: Gold layer photo lithography. (Top view)

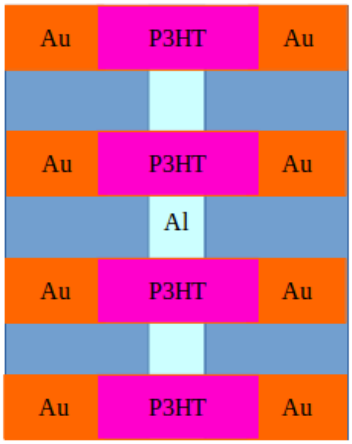

Figure 8: Top view of the finished lateral structure Schottky diode.